

University of Naples Federico II

Ph.D. Program in
Structural Engineering, Geotechnics and Seismic Risk

THESIS FOR THE DEGREE OF DOCTOR OF PHILOSOPHY

# Fire behaviour of underground structures: damage states and spalling modelling

by

Enrico Cardellino

Advisor: Prof. Emidio Nigro

Co-Advisors: Dr. Donatella de Silva and Dr. Marco Andreini

2024

SCUOLA POLITECNICA E DELLE SCIENZE DI BASE

DIPARTIMENTO DI STRUTTURE PER L'INGEGNERIA E L'ARCHITETTURA

FRIDERICVS DEI GRATIA ROMANORVM IMPERATOR SEMPER AVGVSTVS

# Fire behaviour of underground structures: damage states and spalling modelling

Ph.D. Thesis presented

for the fulfilment of the Degree of Doctor of Philosophy

in Structural Engineering, Geotechnics and Seismic Risk

by

Enrico Cardellino

2024

Approved as to style and content by

_____

Prof. Emidio Nigro, Advisor

_____

Dr. Donatella de Silva, Co-advisor

_____

Dr. Marco Andreini, Co-advisor

University of Naples Federico II

Ph.D. Program in Structural Engineering, Geotechnics and Seismic Risk

XXXVI cycle - Chairman: Prof. Iunio Iervolino

www.dist.unina.it/dottorati-di-ricerca/dottorati

**Candidate's declaration**

I hereby declare that this thesis submitted to obtain the academic degree of Philosophy Doctor (Ph.D.) in Structural Engineering, Geotechnics and Seismic Risk is my own unaided work, that I have not used other than the sources indicated, and that all direct and indirect sources are acknowledged as references.

Parts of this dissertation have been published in international journals and/or conference papers.

Naples, 2024

Enrico Cardellino

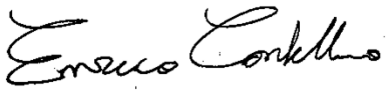

*“La più bella e profonda emozione che possiamo provare*
*è il senso del mistero; sta qui il seme di ogni arte, di ogni vera scienza”*
*Albert Einstein*

FRIDERICVS DEI GRATIA ROMANORVM IMPERATOR SEMPER AVGVSTVS

# Abstract

The thesis explores the critical issue of fire resistance in tunnels and underground infrastructures, which are becoming increasingly crucial in modern society for overcoming significant physical obstacles and advancing technological capabilities. Historically, tunnel excavation relied on manual labour and rudimentary mechanical aids until the mechanization of the mid-1800s, leading to modern advanced construction techniques using Tunnel Boring Machines (TBMs). Ensuring the safety of these structures, particularly their fire resistance, is fundamental due to the high-risk activities often associated with them. Recently, the EU has established directives to standardize safety requirements for road tunnels, highlighting the importance of structural integrity during fires to ensure safe evacuation and post-incident functionality. The main aim of this thesis is to contribute with a new methodology, to the structural fire assessment of tunnels, by using performance-based approaches.

In the scientific literature, the fire resistance of tunnel linings is a widely discussed topic, particularly focusing on two main aspects: fire modelling and thermomechanical modelling of structures. In this work, the definition and quantification of damage states and performance levels of underground infrastructures subjected to fire were proposed, in deep understanding and modelling the very common concrete spalling phenomenon due to fires.

In started with studying the existing literature, analysing both prescriptive and performance-based approaches to fire safety. Next, it addresses the definition of damage levels, performance levels and especially their qualitative and quantitative specification. Within this framework, significant importance is given to spalling, which was find very frequent event in tunnel fires. The theory of the phenomenon and modelling

are considered to simulate its effects and accurately predict the resulting damage on the structural elements. The result of this work phase is a new spalling model integrated with a probabilistic correction based on experimental data, useful to predict the concrete spalling in case of fire, linked also to the proposed damage levels and their quantification.

The final part of the thesis is dedicated to apply the developed methodologies to a specific case study: an underground structure used for nuclear physics research, at CERN in Geneva, Switzerland. Advanced fire models and thermomechanical analyses were conducted to evaluate the structure's performance under fire conditions, optimizing the simulation of structural behaviour with the application of the proposed methodologies, by including also the spalling phenomenon.

In conclusion, the thesis contributes to the field of fire resistance in underground infrastructures by offering new models and methodologies for evaluating structural performances and the spalling effect. The practical application of these models to real scenarios demonstrates their effectiveness and potential to enhance the safety and resilience of underground structures against fire incidents.

**Keywords**: underground structures, tunnels, fire resistance, performance levels, spalling, reliability.

# Sintesi in lingua italiana

Il presente lavoro di tesi tratta la resistenza al fuoco dei rivestimenti delle gallerie e delle infrastrutture sotterranee. Dette strutture ed infrastrutture stanno diventando sempre più indispensabili nella società moderna per superare ostacoli fisici significativi legati alla viabilità ferroviaria e stradale ed alla ricerca sulla fisica nucleare. Storicamente, lo scavo delle opere sotterranee si basava sul lavoro manuale e su ausili meccanici rudimentali. La meccanizzazione della metà del 1800 ha portato alle moderne tecniche di costruzione avanzate basate sull'utilizzo di macchine perforatrici definite TBM, le quali hanno reso più rapida ed agevole la costruzione di dette opere. Tuttavia, queste strutture presentano diversi aspetti critici legati anche al loro esercizio, tra questi di particolare rilievo è il rischio incendio ed i danni ad esso associati. La resistenza al fuoco dei rivestimenti delle gallerie è pertanto un requisito fondamentale al fine di abbattere il rischio incendio ed i danni legati ad esso. Recentemente, infatti, l'UE ha stabilito direttive per standardizzare i requisiti di sicurezza per le gallerie stradali, sottolineando l'importanza dell'integrità strutturale durante gli incendi per garantire una evacuazione sicura e la funzionalità dopo detti eventi.

Nella letteratura scientifica, la resistenza al fuoco dei rivestimenti delle infrastrutture sotterranee è un tema ampiamente discusso ed attuale. I principali aspetti studiati legati a detto possono essere sintetizzati in: la modellazione dell'incendio e la modellazione del comportamento termomeccanico delle strutture. Nel presente lavoro vengono trattati degli argomenti legati soprattutto all'aspetto di modellazione del comportamento termomeccanico, ovvero la definizione e la quantificazione degli stati di danno, l'attribuzione dei livelli di prestazione, e la comprensione e mo-

dellazione del fenomeno dello spalling. Innanzitutto, viene riportato un approfondimento dei temi tratto dalla letteratura scientifica esistente, analizzando sia l'approccio prescrittivo che quello prestazionale legati alla sicurezza antincendio. Successivamente, viene trattata la definizione dei livelli di danno, con particolare riferimento alla loro quantificazione. In tale trattazione viene inoltre posta l'attenzione sul fenomeno dello spalling, data la sua particolare influenza sul comportamento termomeccanico dei rivestimenti in cemento armato delle gallerie. Vengono trattati innanzitutto gli aspetti teorici alla base del fenomeno, poi vengono studiate le risultanze sperimentali ed infine viene trattata la modellazione del fenomeno di natura deterministica e probabilistica per simularne gli effetti sulle strutture. Viene infatti sviluppato un nuovo modello di spalling integrato da una correzione probabilistica basata su dati sperimentali.

La parte finale del lavoro di tesi è dedicata all'applicazione delle metodologie sviluppate da un particolare caso studio di struttura sotterranea adibita alla ricerca sulla fisica nucleare. Nello specifico si tratta di una caverna realizzata in cemento armato all'interno della quale è localizzato uno dei rivelatori di particelle più grandi al modo chiamato ATLAS, presso il CERN di Ginevra, in Svizzera. Sono stati studiati i documenti progettuali di detta struttura ed i materiali combustibili presenti al suo interno al fine di arrivare alla modellazione termofluidodinamica dei possibili incendi verificabili ed alla modellazione termomeccanica avanzata tridimensionale della struttura di sostegno. Dai risultati di dette modellazioni è stato possibile risalire agli stati di danneggiamento ed ai livelli di prestazione tenendo in conto anche dell'occorrenza dello spalling, attraverso le metodologie proposte.

In conclusione, la tesi contribuisce al campo della resistenza al fuoco nelle infrastrutture sotterranee offrendo nuovi modelli e metodologie per valutare le prestazioni strutturali e lo spalling. L'applicazione di questi modelli a scenari reali dimostra la loro efficacia e il potenziale utilizzo al fine di migliorare la trattazione della

sicurezza e la resilienza delle strutture sotterranee contro soggette al fuoco.

**Parole chiave**: strutture sotterranee, gallerie, resistenza al fuoco, livelli di prestazione, spalling, affidabilità.

# Aknowledgements

This work encapsulates intense years of study, cultural and professional growth, filled with both positive and negative moments. The doctoral years coincided with pivotal periods in my life, marked by significant changes. What has been accomplished to this day is the result of hard work, made possible especially by the presence of people who played a key role in this journey, and whom I would therefore like to thank.

First and foremost, I must thank dear Professor Emidio Nigro, who initiated this path and, with his knowledge, experience, and patience, has been a constant guide. Thanks to his brilliant insights, it was possible to overcome even the most difficult obstacles, turning them into opportunities for profound growth.

I would like to thank Donatella de Silva, whose tenacity and patience helped and guided me through the most critical moments of the work.

I am grateful to my friend and colleague Margherita Autiero, whose spirit of sharing and friendship significantly lightened the load throughout the journey.

I also thank all my colleagues, professors, and students at DIST whom I met along the way, as their small contributions fostered my personal and cultural growth.

I would also like to thank the entire HSE section and the FSE group at CERN, led by the kind Saverio La Mendola, who welcomed me during the fantastic research experience in Geneva.

A special thanks goes to Marco Andreini, for his tireless contribution, dedication, and kindness, which were essential in overcoming the most complex challenges. He played a significant role as a constant guide, from the very first steps taken during the CERN experience to the completion of this work.

The valuable support of the people closest to me has also been of great importance. I especially thank my life partner, Ida, who, with great love and care, accompanied me through every phase of this journey, proving to be my greatest supporter. Her constant presence gave me strength and courage, believing in me more than I did during the most challenging moments of this path.

A special thanks goes to my parents, who provided the foundation that made all this possible, and once again managed to support and encourage me throughout the process.

Finally, I would like to thank all the friends, relatives, and colleagues who, even with just a word or a gesture, fueled my desire to continue and complete this journey.

# Contents

# List of acronyms

The following acronyms are used throughout the thesis.

| | |
|---|---|
| **FRC** | Fiber Reinforced Concrete |
| **TERN** | Trans-European Road Network |
| **TBM** | Tunnel Boring Machine |
| **LANL** | Los Alamos National Laboratory |
| **LLNL** | Lawrence Livermore National Laboratory |
| **ITER** | International Thermonuclear Experimental Reactor |
| **HC** | Hydrocarbon fire curve |
| **HCM** | Hydrocarbon Modified fire curve |
| **HRR** | Heat Release Rate |
| **CFD** | Computational Fluid Dynamic |
| **AST** | Adiabatic Surface Temperature |
| **MZ** | Multi Zone |
| **MLZ** | Multi Layer Zone |
| **LES** | Large Eddy Simulation |
| **RANS** | Reynolds-averaged Navier-Stokes |
| **FDM** | Finite Difference Method |
| **FEM** | Finite Element Modelling |
| **HC** | HydroCarbon fire cure |
| **CERN** | Conseil Européen pour la Recherche Nucléaire |
| **FSE** | Fire Safety Engineering |

| | |
|---|---|
| **RC** | Reinforced Concrete |
| **PC** | Plain Concrete |
| **PL** | Performance level |
| **RHR** | Rate of Heat Release |
| **CSTB** | Scientific and Technical Centre for Building |
| **IHC** | Increased Hydrocarbon Curve |
| **DS** | Damage State |
| **FORM** | First Order Reliability Method |

# List of symbols

The following symbols are used throughout the thesis.

| | |
|---|---|
| $\boldsymbol{K\,(T)}$ | Reduction factor |
| $\mathbf{T_{avg}}$ | Average temperature |
| $\mathbf{T}$ | Temperature |
| $\mathbf{t_{start}}$ | Starting time of salling |
| $\mathbf{t_{end}}$ | End time of spalling |
| $\mathbf{F_{Ed}}$ | Demand force |
| $\mathbf{F_{Rd}}$ | Capacity force |
| $\mathbf{F_{ext}}$ | External force |
| $\mathbf{F_{\Delta t}}$ | Thermal force |
| $\mathbf{F_b}$ | Buckling force |
| $\boldsymbol{\sigma_{ext}}$ | Stress in the structural elements in cold conditions |
| $\boldsymbol{E_c(T)}$ | Concrete Young modulus affecting by temperature |
| $\boldsymbol{\epsilon_c(T)}$ | Thermal deformations |
| $\boldsymbol{l_b}$ | Buckling length |
| $\boldsymbol{B}$ | Base of RC sections |
| $\boldsymbol{d_s}$ | Spalling depth |
| $\boldsymbol{\Theta}$ | Denotes a set of parameters introduced to ''fit'' the model to observed data and |
| $\boldsymbol{C}$ | Is the capacity quantity of interest |
| $\boldsymbol{\theta = (\theta_1, \theta_2, \ldots)}$ | Denotes the set of unknown model parameters |

| | |
|---|---|
| $c(x) =$ | Selected deterministic model |
| $\gamma(x, \theta)$ | Correction term for the bias inherent in the deterministic model |
| $\varepsilon$ | Random variable with zero mean and unit variance |
| $\sigma$ | Represents the standard deviation of the model error |
| $f_{ctk,fi}$ | Characteristic axial tensile strength of concrete eroded by fire |
| $f_{ck,fi}$ | Characteristic compressive cylinder strength of concrete at 28 days eroded by fire |
| $M_{Ed,fi}$ | Bending Moment affected by fire |
| $N_{Ed,fi}$ | Normal forces affected by fire |
| $M_{Rd,fi,red}$ | Bending moment capacity in fire conditions for spalling reduced section |
| $t_{s,ini}$ | Initiation spalling time |
| $t_{s,fin}$ | Final spalling time |

# List of figures

The figure present in the thesis are:

# List of tables

The tables present in this thesis are:

Chapter 1

# Introduction

## 1.1 General overview

Among the structures and infrastructures increasingly used by today's society to facilitate the evolutionary process are tunnels and underground infrastructures. These infrastructures are becoming increasingly important for modern society, and the main reason lies in their ability to overcome significant physical obstacles, primarily in the field of mobility, but also in other sectors, such as nuclear research and experimentation. The increasingly widespread use of underground structures and infrastructures is also due to the significant technological and mechanical advancements achieved in their construction. Consider that until the early 1800s, the excavation of tunnels and underground structures in general was primarily done by hand or with the help of partially mechanical equipment. From the mid-1800s, following the Industrial Revolution, the mechanization of excavation operations and the construction of tunnel linings began to spread increasingly. Nowadays, the construction techniques for these structures and infrastructures are entirely based on the mechanization of processes, especially through the use of Tunnel Boring Machines (TBMs). Given the increasing and extensive use of tunnels, scientific knowledge about all the aspects necessary to ensure their safety is also growing accordingly. When we talk about the safety of structures and infrastructures, one of the most important aspects is to consider, during the design phase, all the scenarios that could compromise it throughout their useful life. On one hand, the most frequent actions are

those exerted by the self-weight of the structures and the loads they are required to bear in ordinary use. On the other hand, there are those actions that the history of events has taught us to recognize, such as actions resulting from seismic events, explosions, and, no less importantly, fires. It is precisely on the latter that this thesis aims to focus.

The fire resistance of tunnels is a crucial aspect because these structures are highly confined by the surrounding ground and are used for activities associated with a significant fire risk. The issue of tunnel safety is highly significant today, regardless of their intended use. In Europe, an important step forward has been made with the issuance of the EU Directive on minimum safety requirements for tunnels in the *Trans-European Road Network (TERN)* [1]. For railway tunnels, the European regulatory commission has issued guidelines to ensure safety requirements for these infrastructures [2]. An important requirement is the structural integrity of the tunnel for the entire duration needed to safely evacuate the occupants. Equally important is ensuring fire safety in major underground infrastructures dedicated to nuclear physics research. Such underground facilities are widespread worldwide, among the most prominent being CERN (European Organization for Nuclear Research) - located in Geneva, Switzerland; LANL (Los Alamos National Laboratory) - situated in New Mexico, USA; Fermilab (Fermi National Accelerator Laboratory) - located near Chicago, Illinois; LLNL (Lawrence Livermore National Laboratory) - situated in California, USA; ITER (International Thermonuclear Experimental Reactor) - located in Cadarache, France; it is the world's largest and most advanced nuclear fusion project, etc. Numerous studies have already been conducted to enhance the safety of these facilities and have yielded significant results.

In order to ensure the safety of underground infrastructures, regardless of their intended use, the structural strength in case of fire is particularly crucial. The partial collapse of tunnel linings during a fire could compromise all other aspects related to safety (evacuation of occupants, spread of harmful and/or radioactive fumes, intervention of

rescue teams, etc.). These underground facilities structures are typically made of reinforced/plane concrete and in Fiber Reinforced Concrete (FRC), constructed with two distinct linings known as primary lining and secondary lining. The fire resistance of reinforced concrete structural elements, including tunnel linings, is regulated in Europe by Eurocode 2 part. 1-2 [3]. This standard provides the general principles and two different approaches that can be used to ensure the fire resistance of structures: the prescriptive approach and the performance-based approach. From the analysis of the current regulations and the study of scientific literature, it emerges that many advances have been made in terms of material [4] and structural [5] modelling under fire conditions , definition of fire scenarios and their modelling [6] and the development of innovative active protection systems [7]. However, the main topics of study regarding the fire resistance of underground structures are the methodology for evaluating structural performance under fire conditions, the modelling of a very frequent phenomenon in tunnel fires known as spalling, and how to consider most of the uncertainties that characterize the problem.

## 1.2 Objectives

The main aim of this thesis is to contribute with a new methodology, to the structural fire assessment of tunnels, by using performance-based approaches and by including some detail aspect of the concrete behaviour in case of fire, such as the spalling effect. The thesis work was carried out by addressing four main phases.

The first phase starts with an in-depth study of the state of the art in terms of fire resistance of tunnel linings. This discussion reaches two crucial aspects: the first concerns the methodologies of fire modelling, and the second involves the thermomechanical modelling of structures. In this phase, the main gaps in scientific literature and regulations were identified, which then drove the subsequent research phases.

The second phase involves studying a methodology that could address the regulatory gaps in defining performance levels for tunnels exposed to fire. To this end, the definition of damage states is first addressed through the analysis of post-fire findings present in the scientific literature. Subsequently, a quantification of these damage states is proposed, along with correlating them to performance levels. This phase further highlights the significance of the spalling phenomenon and its modelling.

The third phase concerned the study of the phenomenon starting on the existing scientific literature, evaluating both experimental and numerical activities, with the aim of formulating a new model capable of predicting it. Having developed the spalling model, and aware of the high randomness of the parameters involved in the phenomenon, a probabilistic model was refined and applied to correct the results of the deterministic one. The probabilistic approach, combined with the statistics related to experimental data available in the literature, allowed for a reliability study of tunnel linings under fire conditions concerning the spalling phenomenon.

The fourth phase concerned the application of the proposed methodology on a particular type of underground infrastructure dedicated to nuclear physics research. The application also involved advanced fire modelling within a performance-based approach, advanced thermomechanical modelling of the entire structure, and the development of methods for defining the performance level of the construction.

Essentially, this work has made it possible to implement a methodology for the quantification of damage states, which allows for the identification of performance levels of tunnels exposed to fire, also considering their intended use. Furthermore, the spalling phenomenon has been studied, leading to the proposal of a deterministic spalling model enhanced by a probabilistic correction, which allows for the simulation of the time and depth of spalling.

## 1.3 Organization of the thesis

This PhD dissertation work is organized in the following 6 chapters:

- *Chapter 1*: this chapter presents the introduction of the current work, starting from the motivations that generated it, the objectives that were set, and then moving on to the description of the structure in which it is organized;
- *Chapter 2*: this chapter reviews the state of the art regarding fire resistance of structures in general, and then specifically for underground structures. In particular, it revisits the concept of fire resistance of structural elements, starting from the study of fire modelling methods within both the prescriptive and performance-based approaches, highlighting those used for tunnels. Subsequently, it examines the thermomechanical modelling methods of structures, first analysing their thermal modelling and then their structural modelling;
- *Chapter 3*: this chapter addresses the problem of defining performance levels for underground structures exposed to fire. First, it examines the definition of damage states for tunnels, which is achieved through the analysis of the consequences of past fires. Subsequently, it provides relationships related to the quantification of the defined damage states. Finally, it outlines the potential corresponding performance levels and the relevant assignment criteria;
- *Chapter 4*: this chapter extensively addresses the phenomenon of spalling, first by analysing the main experimental tests conducted and reported in the scientific literature, and then by studying some of the fire models available in the literature. One of the studied models is then selected to evaluate its reliability by applying it to samples for which experimental results are available, and comparisons are made. Subsequently, by analysing the shortcomings of the model and based on the principles underlying the phenomenon, a spalling model is proposed, which is further enhanced with a probabilistic correction model. The proposed model is then studied and applied to cases of experimental relevance, and its reliability is

assessed using the most sophisticated probabilistic methods available in the literature;

- *Chapter 5*: in this chapter, the methodologies and principles studied in the previous chapters are applied to a real case of an underground structure. First, the specific structure of the tunnel under examination and the possible fire scenarios are described. Subsequently, the thermomechanical study of the tunnel is conducted, and the potential damage state of the structure resulting from the design fires is defined;
- *Chapter 6*: at the end, the conclusions of the work are drawn by analysing the main aspects of each individual chapter and outlining potential future developments.

Chapter 2

# State of the art

The check of a structures under fire conditions is necessary when the risk of fire is not negligible, and structural damage can have unacceptable consequences for the safety of occupants or firefighting teams. It may also lead to the loss of functionality of the structure or incur excessive expenses for potential recovery. Fire prevention technical regulations aim to achieve safety in the event of a fire in buildings. In the first part of this chapter, an introduction to the fire phenomenon will be provided, addressing the general issue for structures and referring to the historical and current regulatory framework on which fire prevention is based. The second part will specifically address the problems caused by a fire in a tunnel, considering the specific regulations in force to deal with this phenomenon. Reference will be made to the possibility of performing the verification of structural safety in the event of a fire through prescriptive and performance-based approaches, introducing specific fire curves typical for tunnels and the Advanced thermofluid dynamics models to predict the fire.

Structural design in the event of a fire can follow two fundamentally different methodologies. The first approach is called *prescriptive approach* and is based on the use of prescriptive standards, resulting in a design characterized by extreme cases. However, it has the drawback of being more restrictive to regulatory prescriptions. The second approach is called *performance-based approach* which exploits the principles of Fire Safety Engineering (FSE.) and, starting from most probably fire scenarios, analyzes the struc-

ture's performance to verify the achievement of safety requirements. National and international regulations impose a minimum period of stability for load-bearing structures in buildings for specific activities, measured in the temporal resistance to the action of a conventional fire. This approach, known as *the prescriptive approach*, ensures that the current regulations define the sufficient conditions to ensure safety in the event of a fire, within the limits attributed to the role of load-bearing structures. Fire Safety Engineering is a complex discipline that addresses, through scientific methods, the issue of selecting the most appropriate safety measures aimed at protecting people, property, and the environment from the effects of fire. The use of a prescriptive approach is generally simpler for both designers and inspectors (regulatory bodies). In this case, the regulations impose compliance with minimum safety requirements through the adoption of prescriptive measures. However, these measures can lead to significant constraints and limitations, especially for complex projects (such as underground works), innovative structures, historical buildings, etc. Performance-based models, on the other hand, require greater expertise from both designers and inspectors, making their application more challenging. Nevertheless, they offer the possibility of freeing oneself from the significant constraints of prescriptive measures, by engineering the most probable actual consequences of a fire for the specific case under consideration, thereby reducing excessive caution and optimizing interventions.

Below we will see how in general the evaluation of the fire resistance of the structures is addressed with the two approaches and in particular for the structures in concrete (the greater type of construction characterizing the underground structures). The two most important aspects to fully evaluate the fire resistance of the structures will be discussed: the modelling of the fire and the thermomechanical modelling of the structure invested by it.

## 2.1 Fire modelling

A fire is an extremely dynamic and potentially destructive phenomenon, characterized by the rapid oxidation of combustible material accompanied by the production of heat and light. Its origin can vary, from natural causes such as lightning to human factors such as negligence or criminal activities. Once initiated, the fire can progress through different stages, involving the combustion of surrounding material and the production of gas and smoke. The effects of a fire are manifold and often devastating; the generated heat can cause direct and indirect harm to nearby individuals. On one hand, the heat and combustion by-products can be severely harmful to people, while on the other hand, they can cause structural damage to buildings and objects in the affected area, thereby endangering lives. Flames can spread rapidly, fuelled by flammable materials, creating a hazardous environment for anyone in the vicinity. Additionally, the resulting smoke can be toxic and harmful to human health, complicating rescue operations.

The consequences of fires can also extend to the surrounding environment and, from a structural standpoint, may affect adjacent structures. Noteworthy is the dispersion of chemical substances in the air and soil following a fire, which can have long-term impacts on environmental quality. On the human front, fires can lead to loss of life, injuries, and the displacement of entire communities. Rescue operations are complex and require the coordination of human resources, firefighting equipment, and emergency vehicles. In many situations, fires demand significant efforts to be contained. Firefighting teams employ various strategies, including the use of water, foam, or other extinguishing agents, as well as controlled extinguishing techniques. However, the size and intensity of a fire can sometimes surpass available resources, leading to widespread emergency situations. In summary, fires pose a serious threat to human safety, the environment, and resources. Prevention, preparedness, and prompt response are crucial to mitigate the impacts of such events and protect communities.

For these reasons, thermal action modelling is crucial to simulate exceptional events characterized by fire and estimate the expected damage it could cause.

The thermal action refers to the impact of fire on a structure, and the [8] outlines various options for considering it. One approach involves time-temperature relationships, which depict the temperature's evolution over time in the environment surrounding the structure. This temperature, along with appropriate boundary conditions, helps determine the heat flux transmitted from the surroundings to the structure. Another option involves relationships that directly provide the heat flux incident on the structure. This incident heat flux is then combined with the flux reemitted by the structure to ascertain temperature changes within the structure.

The [8] distinguishes between nominal temperature-time curves, including the standard temperature-time curve, hydrocarbon curve, and external fire curve, and natural fire models. The applicable thermal action is typically a legal requirement specified by the country or region where the building is situated, considering factors like size, use, and occupancy.

Certain countries prescribe requirements specifying both the time-temperature curve and the time (referred to as fire resistance) that the structure must endure when exposed to the curve. For instance, a hotel in Country A may need to withstand the standard curve for 60 minutes, while a railway station in Country B might require a resistance to the hydrocarbon curve for 30 minutes. In such cases, the designer must ensure compliance with the stipulated requirements and employ the prescribed time-temperature curve.

In more flexible legal environments of certain countries or regions, designers may adopt a performance-based design approach. In such instances, the designer assumes responsibility for choosing a suitable representation of the fire, with the Eurocode offering guidance on the application limits of some natural fire models. Ideally, these models

should align with performance-based requirements related to evacuation or intervention times. Approval from the relevant authority overseeing fire safety and design scenarios is recommended before initiating any performance-based design.

### 2.1.1 Nominal fires

Temperature-time curves are mathematical functions of time that provide a temperature value. The term "curve" is used because these functions are continuous and can be graphically represented on a time-temperature plane. They are termed "nominal" because they are not intended to replicate an actual fire. Instead, they should be viewed as conventional or arbitrary functions. The use of the term "fire curve" might be misleading, as it could suggest that the temperature corresponds to that of a real fire. In reality, the temperature is within the same order of magnitude as temperatures observed in fires. Because these relationships are conventional, they are best suited for application in a prescriptive regulatory framework. Any requirement specified in terms of a nominal curve is therefore prescriptive and somewhat arbitrary. It's essential to recognize that the resistance of a structure to a nominal fire should not be equated with the time needed for evacuation or intervention. These nominal curves are not designed to represent real-world fire scenarios, and comparisons based on such durations may lead to misconceptions.

The [8] introduces three distinct nominal temperature-time curves, the standard, the external and hydrocarbon temperature-time curves.

***The standard time- temperature curve***, historically employed and still in use for standard fire tests assessing structural and separating elements, is designed to depict a fully developed fire within a compartment. Commonly known as the ISO curve, it derives its expression from the standard [9]. The formulation for this standard curve is provided by Eq. ( 1 ).

$$T_g = T_0 + 345 \cdot log_{10}(8 \cdot t + 1) \quad (1)$$

Where $T_g$ is the gas temperature in °C, $T_0$ is the ambient temperature of the compartment (conventionally 20°C) and $t$ is the time in minutes.

***The external time-temperature curve*** is specifically employed for evaluating the outside surface of external walls that act as separations in a building. These walls are exposed to a fire originating outside the building or to flames emanating through windows from a compartment either below or adjacent to the external wall. It's important to note that this curve is not suitable for calculating the impact of a fire on external load-bearing structures, such as steel beams and columns, positioned outside the building envelope. The thermal assault on external structural steel elements is detailed in Annex B of [8]. The formulation for the external curve is provided by Eq. ( 2 ).

$$T_g = T_0 + 660\,(1 - 0.687 \cdot e^{-0.32 \cdot t} - 0.313 \cdot e^{-3.8 \cdot t}) \qquad (2)$$

Where $T_g$ is the gas temperature in °C, $T_0$ is the ambient temperature of the compartment (conventionally 20°C) and $t$ is the time in minutes.

***The hydrocarbon time-temperature curve*** is utilized to model the impact of a fire involving hydrocarbon fuels. Its formulation is provided by Eq. ( 3 ).

$$T_g = T_0 + 1080\,(1 - 0.325 \cdot e^{-0.167 \cdot t} - 0.675 \cdot e^{-2.5 \cdot t}) \qquad (3)$$

Where $T_g$ is the gas temperature in °C, $T_0$ is the ambient temperature of the compartment (conventionally 20°C) and $t$ is the time in minutes.

The three different curves are compared in the Figure 1. The graph illustrates that the hydrocarbon and external curves exhibits a rapid ascent, reaching a constant value respectively of 1100 °C and 680 °C, after half an hour, whereas the standard curve

demonstrates a more gradual increase that persists over time.

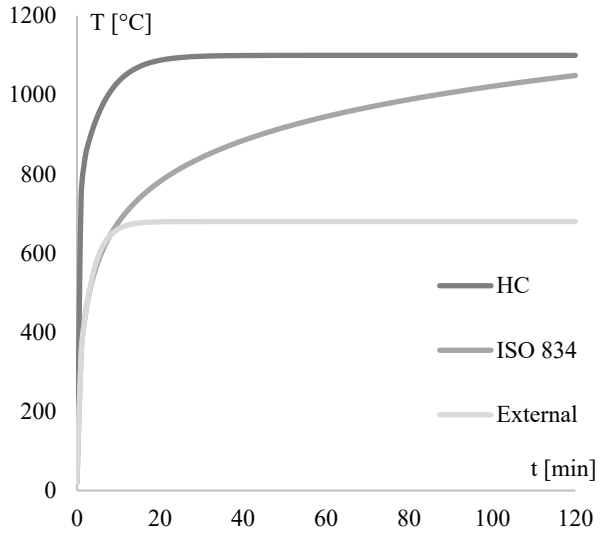


*Figure 1: Nominal fire curves [8].*

When discussing the fire resistance of structures and infrastructures, it is necessary to introduce additional nominal fire curves that can be used and have been introduced by other European country standards.

***The Modified Hydrocarbon time-temperature curve*** was derived from the standard Hydrocarbon curve by the French regulation that requires an enhanced version known as HCM. The maximum temperature of the HCM curve is increased to 1300°C, as opposed to the 1100°C used in the standard Hydrocarbon curve. However, the temperature gradient in the initial minutes of an HCM fire remains as severe as in all hydrocarbon-based fires (RWS, HCM, HC), potentially leading to a temperature shock to the underground concrete structures and consequent concrete spalling. This HCM curve has primarily been used in France since the Mont Blanc tunnel disaster, as described in [10].

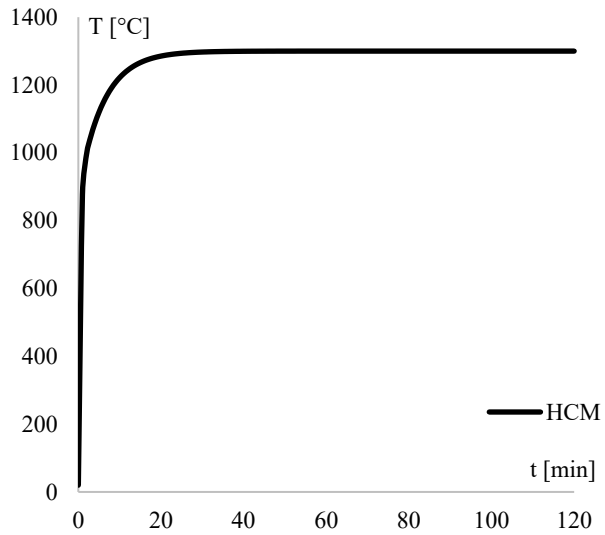


*Figure 2: The Modified Hydrocarbon time-temperature curve.*

The time-temperature curve HCM was described by the equation ( 4 ) and represented in the Figure 2.

$$T_g = T_0 + 1280\,(1 - 0.325 \cdot e^{-0.167 \cdot t} - 0.675 \cdot e^{-2.5 \cdot t}) \qquad (4)$$

Where $T_g$ is the gas temperature in °C, $T_0$ is the ambient temperature of the compartment (conventionally 20°C) and $t$ is the time in minutes.

***The RABT time-temperature curves*** originated in Germany through a series of testing programs, including the Eureka project. In the RABT ZTV curves, the temperature rises rapidly, reaching 1200°C within 5 minutes. However, the duration of exposure to 1200°C is shorter compared to other curves, with the temperature starting to decline after 30 minutes for car fires and 60 minutes for train fires.

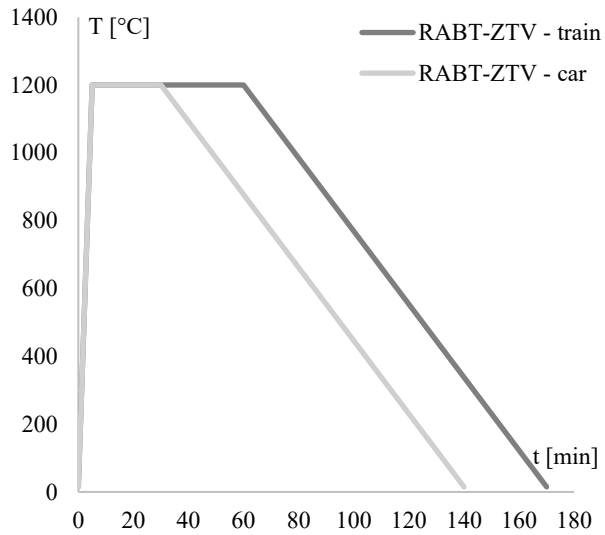


*Figure 3:The time-temperature curves RABT-ZTV for train and car.*

Both fire curves undergo a 110 minutes of cooling period. For the time-temperature curve development of the RABT-ZTV there is not analytically relation but only the recorded point as showed in the Figure 3. These curves are used to simulate the fire in the tunnels induced by cars and trains.

***The RWS time-temperature curve*** was developed by the Rijkswaterstaat, Ministry of Transport in the Netherlands. It is formulated based on the assumption that in a worst-case scenario, a tanker fire with a capacity of 50 m³ of fuel, oil, or petrol and a fire load of 300MW could occur, lasting up to 120 minutes. The RWS curve is derived from the results of testing conducted by *TNO Centre for Fire Safety* in the Netherlands in 1979, after a fire in the Velser Tunnel in the Netherlands in 1978. The reliability of the RWS fire curve as a design reference for road tunnels was reaffirmed through full-scale tests conducted in the Runehamar tunnel in Norway.

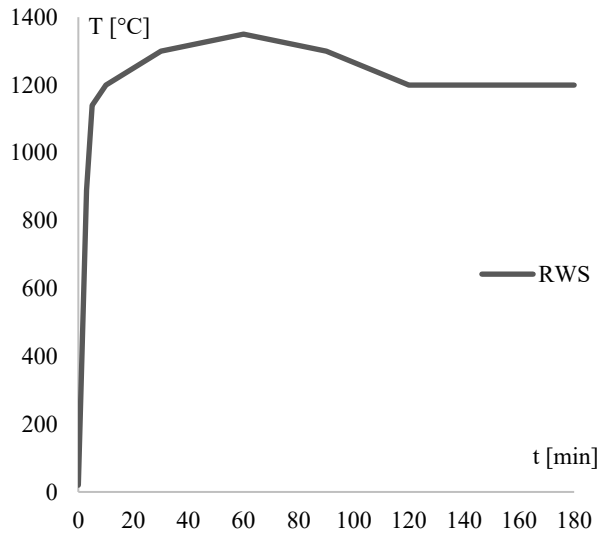


*Figure 4: The time-temperature RWS curves.*

In 2003, Efectis (formerly TNO) was involved in the European research project UPTUN, which involved conducting full-scale tunnel fire tests using a variety of non-hazardous materials such as timber, plastic, furniture, and paper. The results of these fire tests affirmed that the temperature rise, and peak observed in the RWS fire curve are distinctive not only for pool fires, as demonstrated in 1979 and 1980, but also for solid fuel fires. The temperature evolution of the RWS fire curve is characterized by the values showed in the Figure 4, without analytical relations.

All the fire curves seen earlier have been developed in scientific literature through the interpolation of experimentally recorded data. We have seen that we are dealing with nominal fire curves calibrated based on temperatures recorded on-site or in the laboratory during experimentation with real fires. Through these curves, it will be possible to assess the fire resistance of underground structures using prescribed approach.

### 2.1.2 Natural fire

The relationship between temperature and time within a fire compartment depends on factors such as compartment size, compartment type, the combustible materials present, and the availability of air for combustion. The fire model that takes to account the previous mentioned parameters is commonly described as a *natural fire*.

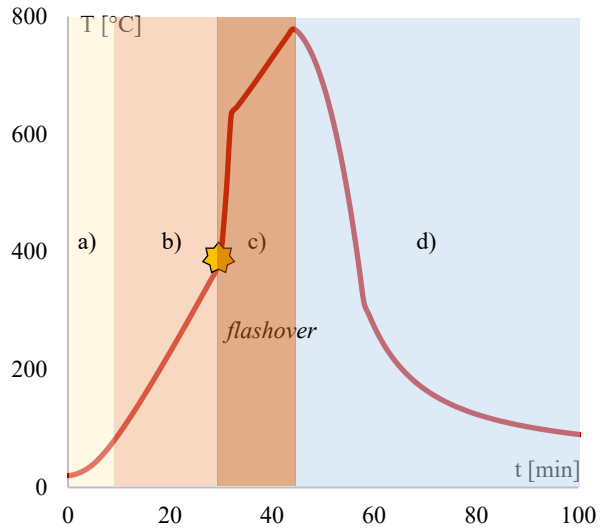


*Figure 5: An example of a fire curve and its different phases a) Ignition, b) Growth c) Burning; d) Decay.*

The progression of compartment fires could be divided into four stages, around the *flashover* point (this represents a transition phase during which flames, from a localized fire, rapidly propagate throughout the volume of the compartment, transforming into a fully developed fire), as reported below and showed in the Figure 5:

a) *The ignition*, which represents the beginning of the fire from one of the combustible materials present in the compartment;

b) *The fire growth,* which represents the spread of fire through the combustible materials present in the compartment;

c) *Fully developed phase*, which represents the fire extended at all combustible materials post *flashover*;

d) *Decay period*, which represents the temperature decreasing phase due to the depletion of combustible material.

If there is sufficient oxygen and combustible materials inside the compartment, a flashover may occur. After the flashover, a phase of sustained combustion begins, until reaching a decay phase when the fuel is depleted.

The natural curve effectively traces what physically occurs during a fire in terms of temperature evolution, taking into account all the thermophysical factors involved in a fire, such as the compartment dimensions and geometry, the materials of walls and ceilings, the openings and the type, position and quantity of combustible materials. Natural wildfires can be simulated through various models outlined in scientific literature, which fall into two main categories, the *simplified models* and *advanced models* exposed below.

The *simplified models are:*

1) Parametric fire curves: the temperature-time equation as a function of specific parameters that describe the generalized fire (The curves describe the evolution of the average temperature within the compartment as described in [8]);

2) Localised fire models: these models are used when the compartment is very big with respect to the combustible quantity. These allow to calculate the temperature evolution due to a localised fire in a specific point trough the analytical relation of heat propagation and flame shape;

The *advanced models are:*

3) Zone models: These models are based on applied thermos-fluid dynamics

to simplified volumes (zones) that discretize the compartment. There are the one-zone models and two-zone models in which the temperature in time is described by a set of ordinary differential equations derived from the fundamental laws of mass and energy conservation;

4) Computational Fluid dynamics models: These are the most sophisticated and advanced fire models currently available. They provide an estimation of the fire evolution in a discretized space through grids, numerically solving the fundamental equations of fluid flow resulting from a fire.

Before delving into the detailed analysis of all the aforementioned types of natural fire models, the principal required input parameters need to be defined: The *fire load density* and the the *Heat Release Rate curve* (HRR curve).

The *fire load density* is the first input necessary to carry out the fire action and the fire resistance design of structures. This can be determined for a specific project by performing a fire load survey in terms of typologies and quantity of combustible materials. In this scenario, both the composition and combustible components of the structure should be considered. The net calorific values of combustible materials need to be considered and adjusted for the influence of moisture if applicable. The characteristic fuel loads $q_{fk}$ $[MJ/m^2]$ can be calculated as shown in the ( 5 ).

$$q_{fk} = \frac{\sum_{i=1}^{n} g_i \, H_i \;\; m_i \; \psi_i}{A} \qquad (5)$$

Where:

- $g_i$ $[kg]$ is i-th combustible material mass;
- $H_i$ $[MJ/kg]$ is the calorific value of the i-th combustion material;
- $m_i$ $[-]$ is a combustion factor, the value of which [0 ; 1];

- $\psi_i$ $[-]$ is the limiting factor of participation in combustion;
- $A$ $[m^2]$ is the floor area of the compartment.

Frequently, the characteristic fire load density is derived from the classification of the compartment's occupancy, typically provided by the national standards. Additionally, Informative Annex E of [8] offers a table containing characteristic fire load densities for various occupancies. The 80th percentile value from this table is adopted as the characteristic fire load density for the contents. If applicable, fire loads stemming from the building's construction materials should be included in these values. In the assessment of fire resistance of structures, it's necessary to consider the design value of fire load $q_{fd}$ which could be assessed starting from the characteristics value trough the relations ( 6 ).

$$q_{fd} = \delta_{q1}\delta_{q2}\delta_n q_{fk} \qquad (6)$$

Where:

- $\delta_{q1}$ $[-]$ is the factor that considers the risk of fire occurrence related to the compartment size;
- $\delta_{q2}$ $[-]$ is the factor that considers the risk of fire occurrence related to the type of occupancy;
- $\delta_{qn}$ $[-]$ is the factor that considers the risk of fire occurrence related to every active firefighting measures.

For the application of advanced fire models, such as zone models or computational fluid dynamics models, it is essential to define another important parameter: the *Heat Release Rate* (HRR) density. The fire load defines the available energy, while the HRR determines the gas temperature trend during the fire. Indeed, it is well known that the same fire load, burning very quickly or slowly, results in completely different gas temperature curves. In general, fires can be divided into two categories: fuel-controlled

or ventilation-controlled. During the fire propagation phase, two scenarios can occur depending on whether there is sufficient oxygen to sustain combustion. In one case, once the fire has reached maximum development without any oxygen limitation, the HRR is limited by the available fuel load (fuel-controlled fire). In the other case, if the openings in the compartment are too small to allow sufficient air intake, available oxygen limits the HRR, and the fire is ventilation-controlled. Both types of fire, fuel-controlled and ventilation-controlled, can escalate until reaching flashover. The HRR could be determined experimentally or analytically, using the procedure provided by the National [11] or International Standards [8] as reported below.

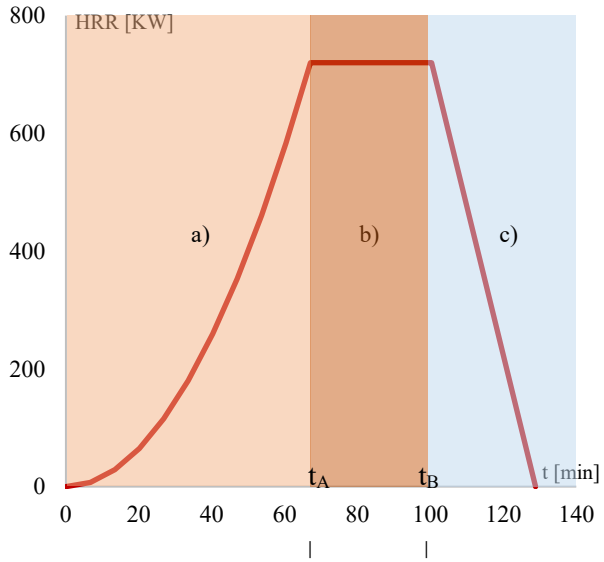


*Figure 6: Phases of HRR curve; a) Growth phase; b) plateau phase; c) decay phase.*

The power released by the fire, denoted as Q and often referred to as the HRR [kW], can be determined as a function of time using the equation ( 7 ).

$$Q = 10^3 \left(\frac{t}{t_\alpha}\right)^2 \leq A_{fi}\, HRR_f \qquad (7)$$

Where:

- $t_\alpha$ is the time needed to reach a HRR of 1 MW, in [s];
- $HRR_f$ is the maximum HRR produced by 1 $m^2$ of fire in case of fuel-controlled conditions, $[kW/m^2]$;
- $A_{fi}$ is the maximum area of the fire, which is the fire compartment in case of uniformly distributed fire load, but which may be smaller in case of a localised fire, in $[m^2]$.

The parameters $t_\alpha$ and the maximum rate of heat release $HRR_f$, could be given by the national and European codes for different occupancies. The HRR is generally characterized by a *growth phase* (ignition - propagation - flashover), followed by a subsequent peak or *plateau phase*, and then by a subsequent *decay phase*, as showed in Figure 6.

The calculation of the HRR curve can be done based on the aforementioned parameters and phases, considering the expressions provided below.

During the *growth propagation* phase, the HRR as a function of time can be described by the equation ( 7 ) until the time $t_A$ at which the maximum value occurs.

The *plateau phase* begins at the time $t_A$ at which corresponds the maximum rate of heat release value $HRR_{max}$, and it finish at the time $t_B$, the start time of the decay phase, in which 70% of the initially available thermal energy has been released in the fire compartment. The time $t_A$ was performed trough the equation ( 8 ).

$$t_A = \sqrt{HRR_{max} \cdot \frac{t_\alpha^2}{10^3}} \qquad (8)$$

In the previous relationship, when the fire is fuel-controlled the $HRR_{max}$ is calculated as reported in the equation ( 9 ). In other case, when the fire is ventilation-controlled, the $HRR_{max}$ must be reduced due to the amount of available oxidizer that can

flow through the ventilation surfaces present in the post-flashover phase. When openings in compartments are also located on horizontal surfaces, it is necessary to evaluate the reduced HRR through advanced CFD models, while, if the compartment walls only have vertical openings, the reduced value of $HRR_{max}$ can be determined using the simplified expression ( 10 ).

$$HRR_{max} = HRR_f \cdot A_{fi} \quad (9)$$

$$HRR_{max} = 0.10 \cdot m \cdot H_u \cdot A_v \cdot \sqrt{h_{eq}} \quad (10)$$

Where:

- $m$ is the combustion participation factor;
- $H_u$ is the lower calorific value of wood (17 500 kJ/kg);
- $A_v$ total area of vertical openings presents in the compartment walls;
- $h_{eq}$ is the equivalent height of the vertical openings, which can be calculated using the following relationship ( 11 )

$$h_{eq} = \frac{\sum_i A_{v,i} \cdot h_i}{\sum_i A_{v,i}} \quad (11)$$

- $A_{v,i}$ is the area of the i-th vertical opening [$m^2$];
- $h_i$ is the height of the i-th vertical opening.

When the initial available thermal energy is enough for obtain that the fire progress beyond the propagation phase, the time $t_B$ could be calculated as expressed in ( 12 )

$$t_B = t_A + \frac{70\%\, q_{f,d} \cdot A_f - \frac{1000}{3t_\alpha^2} t_A^3}{HRR_{max}} \qquad (12)$$

The *Decay Phase* starts at the time $t_B$ and finish at the time $t_C$ and, conventionally, represents the phase in which the residual 30% of initial available thermal energy consumed. Starting from this consideration the time $t_C$ could be calculated as exposed in the equation ( 13 ), and considering that in the decay phase the $HRR$ curve is linear, the function $HRR(t)$ can be expressed with the function ( 14 ).

$$t_c = t_C + \frac{2 \cdot 30\%\, q_{f,d} \cdot A_f}{HRR_{max}} \qquad (13)$$

$$HRR(t) = HRR_{max} \cdot \frac{t_C - t}{t_C - t_B} \qquad fot \quad t_B \leq t \leq t_C \qquad (14)$$

Once the main parameters necessary for calculating natural fire curves are defined, we can move on to analysing the main types of natural fire curves currently used, starting from the simplest ones and progressing to the most complex ones.

#### *2.1.2.1 Parametric fires*

Parametric temperature-time curves are mathematical functions that describe the evolution of gas temperature within a compartment over time. These functions rely on parameters that symbolize the critical physical phenomena influencing the progression of a compartment fire. The [8] provides details about a specific parametric curve in Annex A. The parametric curve describe the evolution of temperature during the heating phase trough the relation ( 15 ).

$$T_g = T_0 + 1325\left(1 - 0.324 \cdot e^{-0.2 \cdot t^*} - 0.204 \cdot e^{-1.7 \cdot t^*} - 0.472 \cdot e^{-19 \cdot t^*}\right) \qquad (15)$$

Where:

- $t^* = \Gamma \cdot t$ ;
- $\Gamma$ is the expansion coefficient and it is equal to ( 16 )

$$\Gamma = \left( \frac{O}{\frac{0.04}{\frac{b}{1160}}} \right)^2 \quad (16)$$

The curve ( 15 ) is applicable to fire compartments with a floor area of up to 500 m², no openings in the roof, and a maximum compartment height of 4 meters.

The parameters that affect the curves are presented following.

A parameter $b$ is introduced to consider the thermal properties of the enclosure. This parameter is associated with the effectiveness of the compartment boundaries in absorbing a portion of the energy released by the fire. The value of $b$ is determined using the relation ( 17 ), when the walls are made of only one material, and ( 18 ) when confinement elements are made of different materials.

$$b = \sqrt{c\rho\lambda} \quad (17)$$

$$b = \frac{\sum b_i A_i}{\sum A_i} \quad (18)$$

where:

- $c$ is the specific heat of the material forming the boundaries in $\frac{J}{KgK}$;
- $\rho$ is the density of the material, in $\frac{Kg}{m^3}$;
- $\lambda$ is the thermal conductivity of the material, in $\frac{W}{mK}$;
- $b_i$ is the value of the factor for part $i$ and $A_i$ is the area of part $i$, openings are

not included.

When a surface comprises multiple layers of materials, only the parameter b associated with the material of the innermost layer is taken into consideration, assuming that its value is lower than the corresponding value of the second layer. However, if the b value of the inner layer exceeds that of the second layer, the b value of the inner layer may be utilized, provided the inner layer is sufficiently thick. In the [8] there is the procedure to determine, in the cases where the inner layer is thin, the influence of the second layer.

A parameter $O$ is introduced to consider the openings in the vertical walls, with higher values indicating increased ventilation within the compartment. The permissible range for this parameter is set between 0.02 and 0.20. In the presence of a single rectangular opening within the compartment, the opening factor is determined using ( 19 ).

$$O = \frac{A_v\sqrt{h}}{A_t} \qquad (19)$$

Where:

- $A_v$ is the area of the opening;
- $h$ is the height of the opening;
- $A_t$ is the total area of the enclosure, including the openings.

This equation ( 19 ) is derived from the integration of the Bernoulli equation, capturing the pressure differential between the exterior and interior of the compartment, which varies linearly based on the vertical position. The previous equation demonstrates that, for a constant area, a vertically oriented opening is more effective in ventilating the compartment compared to a horizontally oriented one. In cases where multiple rectangular openings exist within the compartment, the opening factor is determined using the equation ( 20 ).

$$O = \frac{A_v\sqrt{h_{eq}}}{A_t} \quad (20)$$

Where:

$$h_{eq} = \frac{\sum_i A_{vi} h_i}{A_v} \quad (21)$$

In the previous mentioned equation, it's possible to see that a vertically oriented opening is more efficient inventing the compartment than a horizontally oriented opening.

The final parameter is the design fire load density, denoted as $q_{t,d}$ which is associated with the total area of the enclosure, including the floor, ceiling, walls, and openings. Annex E of [8] provides a method to establish the design value concerning the floor area, $q_{f,d}$ taking into account the compartment's occupancy type and the presence of active fire protection measures. These two values are interlinked through Equation ( 22 ).

$$q_{t,d} = \frac{q_{f,d} \cdot A_f}{A_t} \quad (22)$$

Where:

- $A_f$ is the floor area;
- $A_t$ is total area of the enclosure;

The parametric fire curve model, descripted above, is valid for value of $q_{t,d}$ between 50 and 1000 $\frac{MJ}{m^2}$.

The parameter $t^*$ further indicates that when the parameter Γ exceeds a value of $1^1$, the temperature increase in relation to real time $t$ occurs more rapidly compared to situations where Γ is lower. The heating phase duration $t_{max}$ is given by ( 23 ).

$$t_{max} = \frac{0.0002\ q_{t,d}}{O} \quad (23)$$

This value has to be compared with a limit value $t_{lim}$ that depends on the growth rate associated to the occupancy of the compartment, as reported in the [8]. The comparison between the calculated value for $t_{max}$ and the value of $t_{lim}$ lead to two distinct situations:

a) If the time range falls within the condition where $t_{lim} \leq t_{max}$, and the fire is under ventilation control, a specific procedure is employed to address this scenario. The calculation process for determining the gas temperature at the conclusion of the heating phase $T_{max}$ involves substituting the value of $t_{max}$ into $t^*$ and equation ( 15 ). This step allows for a precise determination of the maximum gas temperature. Subsequently, the expanded time, corresponding to the maximum time, is computed using the relation of $t^*_{max}$. This calculation is integral to obtaining a comprehensive understanding of the fire dynamics during the ventilation-controlled phase. The derived values and parameters from these calculations contribute significantly to the overall analysis of the thermal behavior and control measures within the given context. In this case the cooling phase of time-temperature curve could be calculated as below in the equations ( 24 ),( 25 ) and ( 26 ).

$$T_g = T_{max} - 625(t^* - t^*_{max}) \qquad for\ t^*_{max} \leq 0.5 \quad (24)$$

$$T_g = T_{max} - 250(3 - t^*_{max})(t^* - t^*_{max}) \qquad for\ 0.5 < t^*_{max} < 2.0 \quad (25)$$

$$T_g = T_{max} - 250(t^* - t^*_{max}) \qquad for\ 2.0 \leq t^*_{max} \quad (26)$$

b) When the $t_{max} < t_{lim}$ and the fire is fuel, the procedure for evaluate the gas temperature is this:

$$t^* = \Gamma_{lim} \cdot t \quad (27)$$

Where:

$$\Gamma_{lim} = \left( \frac{\frac{O_{lim}}{0.04}}{\frac{b}{1160}} \right)^2 \quad (28)$$

$$O_{lim} = \frac{0.0001 q_{t,d}}{t_{lim}} \quad (29)$$

In this case if $O > 0.04$ and $q_{t,d} < 75$ and $b < 1160$, $\Gamma_{lim}$ has to be multiplied for the factor given by Equation ( 30 ). The expanded time corresponds to the time of maximum temperature and is calculated from:

$$t^*_{max} = \Gamma_{lim} \cdot t_{lim} \quad (30)$$

When the heating phase finish, the value of the gas temperature is equal to $T_{max}$ which could be calculated by inserting the value of $t^*_{max}$ in equation ( 15 ). The last part of the curve is the cooling phase that could be evaluated by:

$$T_g = T_{max} - 625(t^* - \Gamma t_{lim}) \qquad for\ t^*_{max} \leq 0.5 \quad (31)$$

$$T_g = T_{max} - 250(3 - t^*_{max})(t^* - \Gamma t_{lim}) \qquad for\ 0.5 < t^*_{max} < 2.0 \quad (32)$$

$$T_g = T_{max} - 250(t^* - \Gamma t_{lim}) \qquad or\ 2.0 \leq t^*_{max} \quad (33)$$

A minute variation in a parameter can result in two time-temperature curves that diverge significantly. Essentially, when $t_{max} = t_{lim}$ the equations governing a ventilation-controlled fire yield a distinct fire curve compared to the one derived from the equations characterizing a fuel-controlled fire. This phenomenon underscores the sensitivity of the fire dynamics to even the smallest changes in input parameters. In simpler terms, the distinction in fire behavior arises from the subtle differences in conditions and control

mechanisms between a ventilation-controlled scenario and a fuel-controlled one. This emphasizes the need for precision and accuracy in determining these parameters, as they play a pivotal role in shaping the temporal and thermal aspects of the fire progression. The significance of these variations becomes particularly pronounced when analyzing the intricate interplay of factors influencing fire development and response strategies.

The parametric fire curves presented were treated by Eurocode but in the scientific literature other parametric fire curves were studied, in function of the specific buildings of infrastructures and based on the fire test results. For example, one of this is the parametric natural fire model for the structural fire design of multi-storey buildings presented in [12]. This parametric natural fire model was developed through simulations using heat balance models for realistic natural design fires. This model considers the typical compartment conditions found in residential and office buildings. The curve is called *iBMB parametric fire curve* and it was derived using simplified empirical equations, facilitating their integration into structural fire design within a performance-based natural fire design framework. Validation of the *iBMB parametric fire curves* involves comparing them with results from various heat balance models and published fire tests conducted in different fire research facilities. Additionally, a natural fire test conducted in a room furnished as an ordinary office space further supports the presented parametric natural fire model. To illustrate their utility, an example demonstrating the application of the *iBMB parametric fire curves* is provided. Unlike other simplified natural fire models, such as the parametric fire curves of Eurocode [8], the *iBMB parametric fire curves* offer two significant advantages. Firstly, they can account for actual ventilation conditions, and secondly, they are based on a realistic design fire that aligns temporally with the rate of heat release. This linkage to the rate of heat release allows for the consideration of changes in fire boundary conditions caused by phenomena like flashover, compartmentation failure, or firefighting efforts.

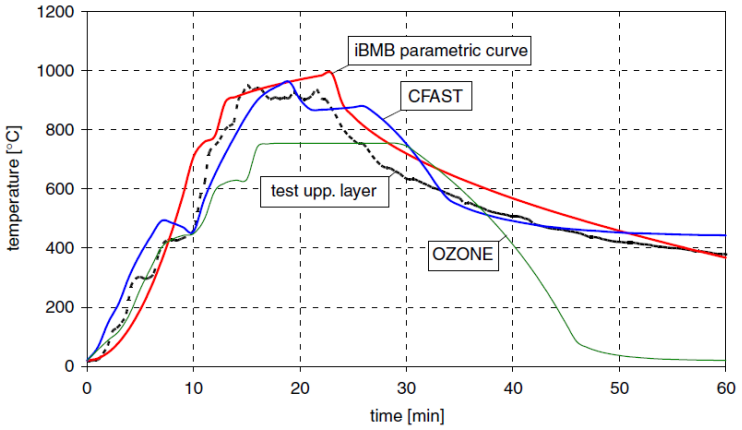


*Figure 7: Comparison of iBMB parametric fire curves with fire curves measured and those calculate by zone models [12].*

### *2.1.2.2 Localised fire models*

When the compartment volume is very big compared to the combustible materials and its position or the ventilation is very low generating the ventilation-controlled fire, a localized fire could be initiated. The localised fires can be simulated with advanced fire models such as CFD or zone models (which we will see later on). Nevertheless, various simplified localized fire models are present in the literature and below are the most relevant ones.

***The Heskestad model*** is implemented in Annex C of the Eurocode EN1991-1-2 [8] and could be applicable for open air fire or for the compartment fire when the flame is not impacting the ceiling. The method allow to calculate the temperature variation along the vertical line passing through the centre of the plume using the equations ( 34 ) and ( 35 ).

$$T_f(z) = \min\left(900°C;\ 20 + 0.25 Q_c^{2/3} (z - z_0)^{-5/3}\right) \quad (34)$$

$$z_0 = -1.02\, D + 0.00524\, Q^{2/5} \quad (35)$$

Where:

- $Q_c$ is the convective part of the *HRR;*
- $Q$ is the *HRR;*
- $z$ is the vertical distance from the fire source;
- $D$ is the diameter of the fire in [m].

To verify the applicability of the model the *flame length* has to be evaluated by the relation ( 36 ).

$$L_f = -1.02\,D + 0.0148\,\mathrm{Q}^{2/5}) \qquad (36)$$

The procedure to calculate the heating of structural members starting from the temperature of the plume evaluated by Heskestad's method is not specified in the Eurocode, but there are some methods to use the results of equation ( 37 ) to evaluate the incident radiative heat flux on structural elements based on the theory of radiation with computation of view factors, such for as the equation ( 37 ).

$$\dot{q}_{inc} = \sigma \cdot \varepsilon \cdot (T_f(z) + 273)^4 + h_c \cdot T_f(z) \qquad (37)$$

Where:

- $\sigma$ is the *Stefan-Boltzmann* constant;
- $\varepsilon$ is the emissivity of the fire;
- $h_c$ is the convective heat transfer coefficient.

***The Hasemi model*** can be used to calculate the heat flux received by the structural member at the ceiling level when the flame impacts the surface of the ceiling. The model was presented in [13] and reported in the Annex C of Eurocode [8]. The heat flux $\dot{q}$ $(W/m^2)$ aforementioned is given by the equations

$$\dot{q} = 100000 \qquad if\ y \leq 0.3 \qquad (38)$$

$$\dot{q} = 136300 - 121000y \qquad if\ 0.3 < y < 1.0 \qquad (39)$$

$$\dot{q} = 15000y^{-3.7} \qquad if\ y \geq 1.0 \qquad (40)$$

Where:

$$y = \frac{d - H + z'}{L_h + H + z'} \qquad (41)$$

- $d$ is the horizontal distance between the centerline of the fire plume and the section of interest along the ceiling where the flux is calculated in [m];
- $H$ is the ceiling height calculated in [m];
- $z'$ is the vertical position of the heat source in [m];
- $L_h = (2.9 \cdot H \cdot (Q_H^*)^{0.33}) - H$ is the horizontal flame length;
- $Q_H^* = \frac{Q}{1.11 \cdot 10^6 \cdot H^{2.5}}$ With Q equal to the HRR.

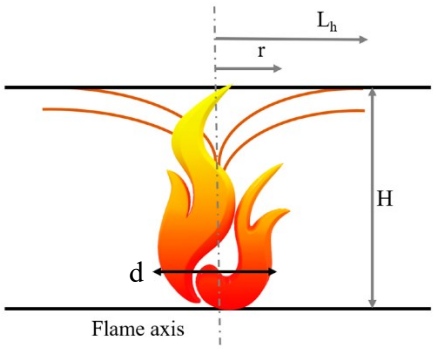


*Figure 8: Hasemi model scheme [13].*

The relations seen, as reported in the Eurocode [8], are valid also for fire diameter up to 10 m and HRR up to 50 MW. The Hasemi flux ( 38 )( 39 )( 40 ) is an absorbed heat flux. The net heat flux received by unit area of exposed surface could be computed by subtracting the re-emitted flux such as in ( 42 ).

$$\dot{q}_{net} = \dot{q} - h_c(T_s - T_{amb}) - \phi \cdot \varepsilon_s \cdot \sigma((T_s + 273)^4 - (T_{amb} + 273)^4) \qquad (42)$$

Where:

- $h_c$ is the convection coefficient;
- $\varepsilon_s$ is the emissivity of the exposed surface;
- $\phi$ is the configuration factor;
- $T_s \; and \; T_{amb}$ respectively the member and ambient temperature in [°C].

***The LOCAFI model*** is a localized fire model and it allow to evaluate the radiative heat flux resulting from the fire impacting a structural element located away from the flame, considering that the surrounding gas is at ambient or close to ambient temperature, neglecting the convective part of heat flux. The model was developed in the [14] and is based on the virtual solid flame, taken as either a cylindrical or conical shape as shown in Figure 9.

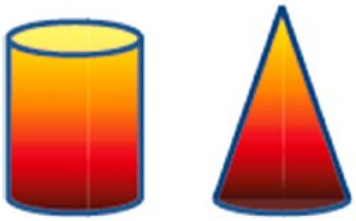

*Figure 9: Cylindrical and conical solid flame models [14].*

Radiative heat flux is emitted from the surface of the flame discretized in the several cylinders characterized by different diameters in function of the height. The analytical model is based on the relation above mentioned regarding Heskestad model, in fact, the flame height is calculated by the equation ( 36 ). To determine the flame temperature along its height, it is assumed that the temperature in each individual cylinder, in which the flame is discretized, is uniform and equal to that of the vertical centerline. This assumption allows for the evaluation of different flame temperatures through equation ( 34 ). Once the geometric and thermal features of the flame are defined, the radiative heat

flux emitted from it (surface A) and directed towards the surface of a structural element (surface B) can be calculated as shown in equation ( 43 ).

$$\dot{q}_{inc,AtoB} = \phi_{AtoB} \cdot \sigma \cdot \varepsilon_A \cdot (T_A + 273)^4 \quad (43)$$

Where:

- $\phi_{AtoB}$ is the configuration factor calibrated in [14];
- $\varepsilon_A$ is the emissivity of the fire surface A;
- $T_A$ is the temperature of the fire surface calculated with the equation ( 34 ).

The relation ( 44 ) is used for every cylinder in which the fire flame is discretized, and the total incident heat flux received by the external surface B is the sum of the radiative heat flux emitted by all fire surface visible to the external surface B, calculated as shown in the equation

$$\dot{q}_{inc,flametoB} = \sum_{i=1}^{n} \phi_{itoB} \cdot \sigma \cdot \varepsilon_i \cdot (T_i + 273)^4 \quad (44)$$

Where $n$ is the number of cylinders.

This model has the same limitations as Hasemi and Heskestad models in terms of fire diameter and *HRR*.

***The CFD model*** is a numerical method implemented in the several software as such as the Fire Dynamics Simulator (FDS) developed by the NIST. It solves the Navier-Stokes equations numerically for low-speed thermally driven fluid flow and models the thermal radiation through the radiation transport equation for grey gas. The model will be further described in a subsequent dedicated paragraph. For now, the two main methods to transfer the results of thermos-fluid dynamics analysis to the FEM model for thermo-mechanical analysis are reported. As studied and described in the work [15] there are two different methods studied, the use of Adiabatic Surface Temperature (AST) and the use of dedicated FDS-FEM interface. The use of AST is based on recording the variation of

AST through specific virtual devices present in the FDS software and subsequently, these temperature curves are applied as thermal boundary conditions to the structural elements. The other model allows avoiding the modelling of AST devices in FDS by directly transferring radiative heat fluxes to the individual sections of the structural elements. This is made possible only by the perfect matching of the discretization of the computational volume of the CFD model with that of the FEM model for thermomechanical analyses. Essentially, FDS generates a transfer file containing gas temperatures and radiant intensities at different positions and from various directions within the compartment. These values can be output at every grid point of the FDS model or only at selected intervals of the grid points. The transfer file can then be read by FEM software, which interprets the values as heat transfer boundary conditions.

In [15] the authors perform the benchmark among different aforementioned models of localized fires demonstrating that the:

- The Heskestad model is suitable for structural members within fire areas but outside smoke layers, although it tends to overestimate temperatures;
- The Hasemi model is appropriate for members under ceilings and within smoke ceiling jets, offering conservative temperature predictions. However, it does not consider member geometry or thermal properties' effects on received flux;
- The LOCAFI model accurately predicts temperatures of structural members outside fire areas and smoke layers, incorporating the geometry to consider shadow effects on received flux;
- FDS-FEM AST method demonstrated versatility and accuracy for the studied case studies, enabling precise temperature predictions in structural elements exposed to localized fires. Structural members must be included in FDS if their presence affects fire development; otherwise, they may be excluded. However, large structures pose modelling challenges due to the effort required to evaluate

thermal boundary conditions;

- The FDS-FEM interface method provides accurate results for structural members with minimal influence on localized fire development, such as distant columns or beams. In this method, structural members should not be modelled in FDS, and slabs, walls, and ceilings should be included.

#### *2.1.2.3 Zone models*

In the field of fire resistance of structures, one of the models most used to simulate the fire scenario is the zone model. Zone models based on differential equations of mass and energy balance, compute temperature development within fire compartments. This type of model can be useful in small to medium size rooms. Parameters influencing temperature include those in parametric fire models but, unlike parametric models, zone models represent individual openings with their dimensions and positions, accounting for openings in walls and ceilings. Some may open over time or at temperature thresholds. Zone models also consider forced ventilation and energy absorption by compartment boundaries. Unlike parametric models, each wall in zone models can be represented individually, with precise calculation of energy absorbed and transmitted through conduction and radiation. Fuel quantity and HRR are crucial for this type of model and to determine these in function of the occupancy, the Annex E.4 of the Eurocode [8] provides guidance. If user-input rates exceed airflow capacity, the model adjusts data, extending fire duration or shifting combustion outside the compartment. Zone models lack predefined time-temperature curves, adapting to introduced rate curves. Compartments are divided into zones assumed uniform. Common models include one-zone (post-flashover) and two-zone (pre-flashover), with some transitioning based on criteria, called Control Volumes as showed schematically in the Figure 10.

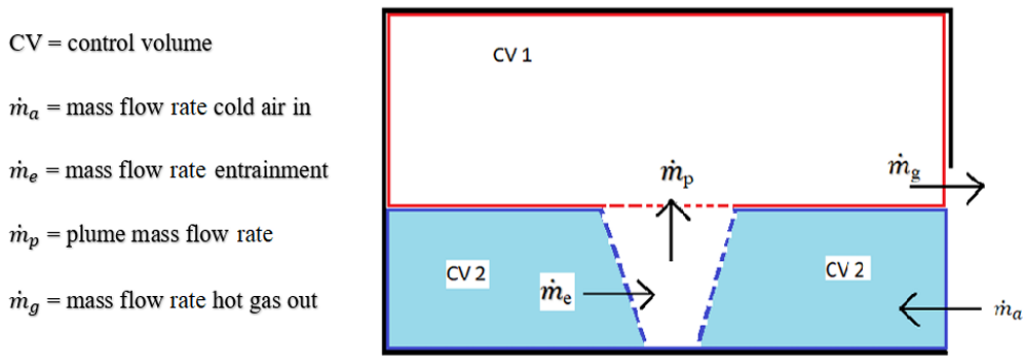


*Figure 10: control volumes of a zone models [16].*

In order to overcome the limitation regarding the application of the model to medium-small compartments, Multi-Zone (MZ) and Multi-Layer Zone (MLZ) models have been studied over the years. These models have allowed achieving the same simulation capabilities as CFD models but with lower computational burden [17]. The MLZ model was developed for this purpose by dividing the area into multiple layers instead of just two, allowing the smoke to rise through the layers to the ceiling. The MLZ model assumes uniform temperature and substance concentration in each layer, resulting in a two-dimensional model of the enclosed area. Later, the model was modified to calculate horizontal variations in temperatures and substance concentrations while maintaining its two-dimensional structure [18], are showed in the Figure 11. However, in environments with high depth-to-height ratios, the uniformity of horizontal temperature may not be accurate. The flow between different zones is driven by temperature differences and calculated based on Bernoulli's equation principles, without considering turbulence.

The Multi-Zone (MZ) model shares the basic principles of the MLZ model but has some significant differences. Specifically, the MZ divides an enclosed area into multiple three-dimensional cells, while the MLZ divides the area into vertical layers. Additionally, while the MLZ uses the Zukoski smoke column model to calculate smoke column mass flow, the MZ uses the Heskestad smoke column model. Although both models

share similar principles and some parts of the MZ are based on the MLZ, it is not possible to establish the exact similarities between the two since the MLZ code has not been made public. Therefore, the MZ and MLZ are considered separate models. The goal of the MZ is to combine the ability to divide the room into multiple zones, similar to a CFD model, with the ability to perform simulations on large enclosed areas without requiring significant computing power.

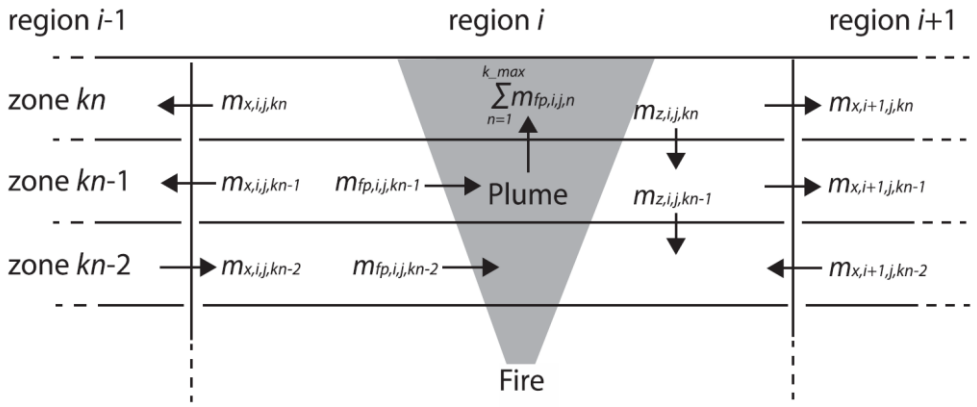


*Figure 11: Principles of the MLZ concept [18].*

Users have the flexibility to decide on zone sizes, but it is advisable to use the largest zones possible while maintaining reasonable values. A recommended option is a size of 4 x 4 x 0.5 meters (length x width x height), ensuring that the fire and smoke column remain within the zone's area. As the smoke column expands with air entrainment while rising, it is important for the zone to have sufficient area relative to the fire surface [19].

To simulate a fire using the zone model, it is possible to use the CFAST software from NIST in the United States [20] and OZone from the University of Liège in Belgium [21]. Both are extensively tested and validated software for the correct application of zone fire models.

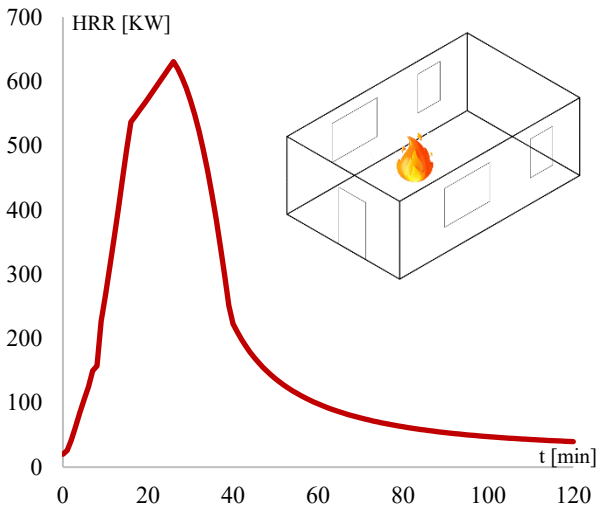


*Figure 12: example of natural fire curve by Ozone software.*

In the Figure 12 an example of fire curve performed by OZone software regarding the compartment with dimensions 5 m x 8 m x h = 3 m with openings on three sides and the fire estimated thanks to the Annex E (EN 1991-1-2) for occupancy: *school*.

### *2.1.2.4 Computational Fluid Dynamics Models*

In recent years, Computational Fluid Dynamics (CFD) models have gained significant popularity in fire safety engineering. CFD refers to the set of numerical and non-numerical techniques used for the approximate solution of fluid motion and associated phenomena such as heat exchange, mass transfer, combustion, chemical reactions, etc.. Essentially, these models are designed to solve the fundamental equations that preserve the basic principles of thermodynamics and fluid dynamics, namely:

- the principle of conservation of mass;
- the principle of conservation of energy;
- the balance of momentum.

With CFD techniques, the solution of the differential equations governing the phenomena is approximated through the discretization of the spatial and temporal domain of

interest, transforming the problem from continuous to discrete.

CFD originated within large research centres, both public and private, between the 1950s and 1960s [22] [23] [24]. Initially, it was primarily used in the aeronautical and aerospace fields. However, with the continuous improvement in computing platforms, the reduction of associated costs, and the development of commercial CFD packages, it gradually expanded into academic and professional realms. It also found applications in Fire Safety Engineering.

The techniques of CFD are increasingly used in research to study phenomena that, following an experimental approach, would require a high level of resources, which may not always be sustainable (such as studying specific fire scenarios in extended areas). This does not mean that CFD can entirely replace experimental methods, but through their simultaneous use, it is possible to significantly reduce the number of experimental campaigns and consequently, costs.

The CFD technique could be characterized by several components which can be summarized in: mathematical model, discretization method, coordinate system, computational grid, approximation methodology, solution method and convergence criterion. This involves dividing the compartment into numerous cells where the Navier-Stokes equations are formulated and solved in both space and time. These models provide detailed results such as pressure, temperature, velocity, chemical composition, and optical obstruction for every cell and selected time step.

Tunnel fires exhibit intricate three-dimensional flows, primarily driven by the release of energy, resulting in buoyant forces that govern the fire's development. Turbulence and heat transfer, influenced by the tunnel's geometry and ventilation conditions, further complicate this process. These interrelated factors contribute to the complexity of understanding and modelling tunnel fires.

To address this complexity, CFD techniques have been developed. CFD software

enables the study of fire and smoke behaviour concerning the safety assessment of tunnel infrastructures, a common practice in Performance Based Design within the industry. CFD software solves the Navier-Stokes equations, which comprise partial differential equations describing mass, energy, and momentum conservation laws [25]. These equations are solved over a finite number of control volumes, requiring the definition of boundary conditions. Discretization of the tunnel under consideration is achieved through proper mesh volume definition and boundary condition specification.

Various CFD packages employ different solution methods, each with its own set of assumptions and potential inaccuracies. These software tools are designed to model specific aspects of fluid dynamics problems, emphasizing different features [25].

CFD software utilization encounters fundamental limitations due to the procedures employed to average the model equations. Typically, two main approaches are utilized: the time-averaged form of the Navier-Stokes equations (RANS) and Large Eddy Simulation (LES). RANS necessitates a finer mesh but permits the application of symmetry conditions. However, both approaches require making assumptions during the solution of the equation system, and the obtained results must be rigorously verified and validated for each specific application.

Verification ensures the accurate solution of the equation system, while validation often entails comparing and confirming the agreement between results obtained from full-scale tests and those derived from CFD models [25]. There are most commercial and in house codes implemented to apply the CFD, the most used ones are:

- FLUENT, developed in the UK and commercialized by ANSYS, it is a software is a CFD solver from the Ansys family capable of accurately modelling turbulent flows, heat transfer, and chemical reactions;
- STAR CD, developed by Computational Dynamics Ltd. in UK, is a CFD program used to perform multi-physics simulations. It provides a solution to engineering

problems for industrial users in the automotive, power generation, turbomachinery, aerospace, civil and offshore structures, safety, environment, marine, etc.;

- CFX, developed by ANSYS in the UK, is widely regarded as the premier CFD software when it comes to turbomachinery applications;
- FDS, Developed by the National Institute of Standards and Technology (NIST) in USA in collaboration with the VTT Technical Research Centre of Finland, is a computational code specializing in Large-Eddy Simulation (LES) for low-speed flows [25], with a primary focus on simulating smoke and heat transport originating from fires.

The FDS software is the most utilized ones in the field of Fire Safety Engineering and the pertinent aspects are:

*Hydrodynamic model:* FDS offers both Large Eddy Simulation (LES) and Reynolds-averaged Navier-Stokes (RANS) averaging techniques. LES is the default option due to its lower computational time compared to RANS while maintaining comparable accuracy.

*Combustion model:* Three combustion models are available in FDS. The first is a single-step reaction model that determines the mass fraction of burned and unburned fuel, considering the efficiency of the reaction affected by oxygen availability. The second model involves a two-step combustion process, including the oxidation of fuel to carbon monoxide and subsequent oxidation to carbon dioxide. Additionally, users can define a multiple-step model. FDS allows prescribing fire by specifying the Heat Release Rate on a surface, modelling it as gas-phase combustion using the one-step combustion model. It also enables modelling of both solid-phase pyrolysis and gas-phase combustion when employing the multi-step model and specifying thermophysical properties of fuel materials.

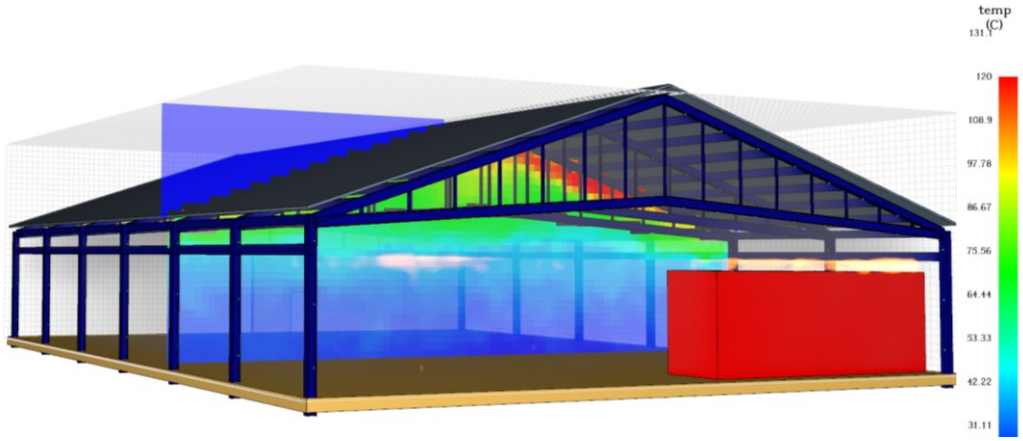


*Figure 13: Example of fire scenario modelled by FDS.*

*Radiation model:* FDS employs a grey gas transport equation solution to simulate radiative heat transfer. Fire radiation is modelled as a fraction of the chemical energy released in a mesh cell by the flames.

Thanks to the increasing spread of increasingly powerful hardware, computational fluid dynamics (CFD) models have become the most widely used tools for realistically modelling specific fire scenarios, both localized and generalized. In the chapter dedicated to applications, an example of modelling specific fire scenarios in underground structures is presented.

## 2.2 Thermomechanical modelling

The behaviour of structures exposed to fire is influenced by many factors, such as the loss of strength and stiffness of structural elements due to thermal degradation of materials, the structural scheme including any hyperstatic conditions, the relative stiffness of various parts composing the structure, load paths, and the fire exposure itself. Equally important are the fire scenarios, their severity, flame spread, and growth rate. All these factors affect the structure's response differently, adding numerous variables to an

already complex problem.

The Eurocode 2-1-2 [3] pertains to the design of concrete buildings as outlined in Eurocode 2-1-1 [26] and necessitates meeting the load-bearing, separation, integrity, and insulation requirements. This standard addresses the accidental situation of fire exposure and is intended to be used alongside Eurocode 2-1-1 [26]. Therefore, applying the Eurocode 2-1-2 [3] to tunnels may require significant adaptations, especially concerning the required level of reliability.

The Eurocode 2-1-2 [3] addresses the fire design of buildings considering standard fire exposure, hydrocarbon fire exposure, and physically based fire exposure. Thermal and mechanical actions are derived from Eurocode 1-1-2. Generally, partial factors for materials are set at 1.0 unless specified otherwise in the National Annex. The applicable design methods include:

- *Tabulated design data for specific types of members* is available for typical structural elements in buildings, such as columns, walls, tensile members, beams, and slabs. The design values indicated in the tabulated data are considered to be conservative, or even more conservative, compared to those obtained using simplified or advanced design methods. The minimum dimensions specified in the tables apply to buildings with the corresponding reliability level. Modifications are necessary to apply tabulated design to tunnels, for example, to account for different fire curves;
- *Simplified design methods for specific types of members* can be employed to determine a temperature field in a section, a temperature in a part of it, or the load-bearing capacity of a section or structural element. This method can be applied to verify the effects of bending, bending with axial force, shear, and torsion. Provisions for determining the capacity of elements must be adapted to account for higher reliability levels (and different fire curves) applicable

to tunnels;

- *Advanced design methods* must be based on fundamental physical principles, using local equilibrium equations that are satisfied at every point in the structure. They can be employed in conjunction with any thermal action, provided that the material properties are known for the relevant thermal history. The accuracy of the method must be validated based on relevant test results. Provisions for determining member capacity must be modified to account for higher reliability levels applicable to tunnels.

As an alternative to design by calculation, fire design can be based on fire tests or a combination of fire tests and calculations. For tunnels, higher reliability levels (higher reliability indices) can be considered by modifying the partial factors as indicated in Annex A of [26] and using them together with either simplified design methods or, preferably, advanced design methods.

In order to assess all the effects of fire on structures, it is necessary to simulate two important phenomena that determine them: Heat transfer, through a thermal analysis of the structural element starting from the flow of thermal energy derived from the fire; The variation in stress state within the structure, through mechanical modelling of any hyperstatic effects of the fire and the erosion of resistances dictated by material heating.

In the following paragraphs, an overview of thermal and mechanical modelling of structural elements will be discussed.

### 2.2.1 Thermal analysis

When a structure is subjected to thermal action, the temperature of its elements rises. This phenomenon, known as "thermal response," may trigger thermal expansions in the structural elements and diminish the mechanical properties of the heated parts of the load-bearing structure. Depending on the structure's geometry and the heating type,

thermal expansions can result in additional stresses if resisted. Thus, conducting a precise analysis of the structure's thermal response is imperative to assess its performance under fire conditions. Determining the temperature distribution inside a structural element generally requires solving a nonlinear heat transfer problem. For a generic structural element, there is a transient regime of internal conduction following a radiative-convective exposure on its outer surface. From a numerical standpoint, solving the problem involves solving the energy balance equation along with the corresponding boundary conditions.

It is important to remember that heat transfer occurs through three fundamental mechanisms:

- *Conduction*: This mechanism occurs between two or more bodies in contact. The temperature difference between the bodies generates a transfer of internal energy in the form of heat. The energy transferred between the bodies is kinetic energy of the particles (internal energy), which, being at a higher energy state, are more mobile than the corresponding particles at lower temperatures.
- *Convection*: This is a mechanism of energy transfer determined by the combined action of conduction and the transport of matter. It enables the transfer of energy between two fluids or between a fluid and a body. Convection can be defined as free convection when convective motions in the fluid are solely due to heat exchange, or forced convection when convective motions are enhanced by external actions (e.g., fans, pumps, etc.);
- *Radiation*: This mechanism allows heat transfer between bodies through mutual exposure. According to Maxwell's wave theory, every body is a source of electromagnetic waves, and wave emission is a form of internal energy dissipation. These waves strike exposed bodies, providing them with thermal energy.

The main parameters of heat transfer involved in the thermal model of a structural element are:

- *Convective heat transfer coefficient* $\alpha_c$: Convective heat flux on the element relative to the difference between the gas temperature that impinges on the element's surface and the surface temperature itself;
- Flame emissivity $\varepsilon_f$: Amount of radiant flux emitted by the flame relative to the radiant flux emitted by the *"blackbody"* at the same temperature;
- Surface emissivity $\varepsilon_m$: Ratio of the radiant heat absorbed by a given surface to that absorbed by the surface of the blackbody.

To determine the temperature of structural elements, it is also necessary to know the thermal characteristics of their materials and their variation laws as a function of temperature. In particular, it is necessary to know: *density* $[kg/m^3]$, *specific heat* $[J/(kgK)]$, *thermal conductivity* $[W/(mK)]$. Both thermal conductivity and specific heat of most construction materials are strongly dependent on temperature, for this reason in Figure 14 and Figure 15, these typical variations as a function of temperature are plotted for concrete and steel bars [3].

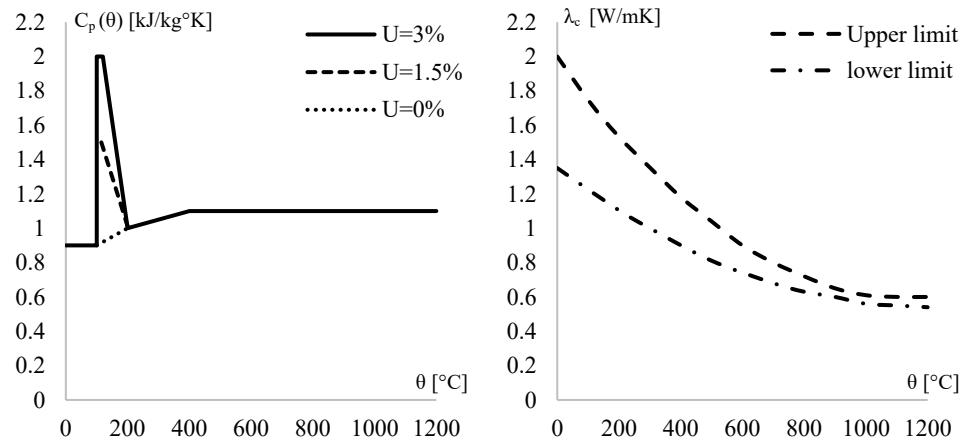


*Figure 14:* a) *specific heat* and b) *thermal conductivity* of concrete in function of temperature *[3]*.

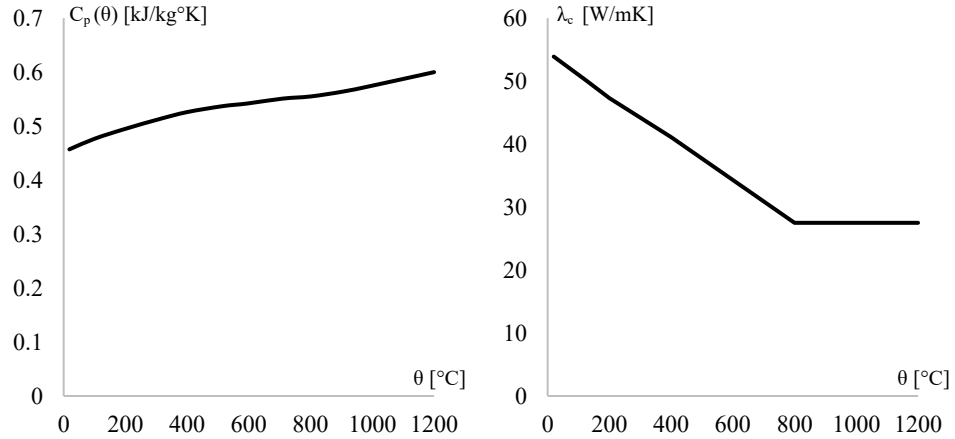


*Figure 15:* a) *specific heat* and b) *thermal conductivity* of steel in function of temperature *[27]*.

Once the aforementioned parameters are known, it is possible to determine the temperature of the structural elements. Based on the specific design conditions, particularly the materials involved, different methods of modelling the thermal response can be utilized.

Thermal analyses on structural elements could be performed using two main types of calculation procedures, according to Eurocodes, they can be either advanced or simplified. Advanced models are based on the finite element method: the members or their cross-sections are discretized into a certain number of 3D or 2D elements. Thermal action due to fire, in the form of thermal flux or fire curve, and boundary conditions are applied to them, obtaining the temperature in each element. Simplified methods are calculation procedures based on simple equations that allow for an approximate determination of temperature.

The examination of temperature response within a structural member can be divided into two main components. Firstly, there's the heat transfer across the boundary from the fire to the surface of the structural member, typically involving a combination of convection and radiation. This aspect is usually addressed as boundary conditions.

Secondly, there's the heat transfer within the structural member itself, predominantly through conduction, which is governed by the Fourier equation ( 45 ) of heat transfer.

$$\mathrm{q} = -\lambda \nabla \mathrm{T} \qquad (45)$$

Where:

- q is the vector of heat flux per unit area;
- λ is the thermal conductivity tensor;
- T is the temperature.

Heat conduction refers to the movement of thermal energy from one location to another within a solid or fluid, driven by temperature disparities between the two locations. This transfer of thermal energy occurs at the molecular and atomic levels without significant material displacement.

The heat conduction equation is described in ( 46 ) and it is solved subject to an initial condition and appropriate boundary conditions.

$$\rho c \frac{\partial T}{\partial t} = \nabla \cdot (\lambda \nabla \mathrm{T}) + \mathrm{Q} \qquad (46)$$

Where:

- $\rho$ is the density;
- $c$ is the specific heat;
- $t$ is the time;
- Q is the internal heat generation rate per unit volume.

The initial condition involves defining the temperature distribution across the solid at the beginning of the analysis. Boundary conditions can manifest in various forms, including:

a) *The net heat flux* to the exposed surfaces of structural members expressed ( 47 )

$$\dot{h}_{net} = \dot{h}_{net,c} + \dot{h}_{net,r} \quad (47)$$

Where:

- $\dot{h}_{net,c} = \alpha_c(T_g - T_m)$ represents convective heat flux; ( 48 )
- $\dot{h}_{net,r} = \Phi\varepsilon_m\varepsilon_f\sigma[(T_g + 273)^4 - (T_m + 273)^4]$ represents radiative heat; ( 49 )
- $\alpha_c$ is the coefficient of heat transfer by convection;
- $T_g$ is the gas temperature in the vicinity of the fire exposed surface;
- $T_m$ is the surface temperature of the structural member;
- $\Phi$ is the configuration factor;
- $\varepsilon_m$ is the surface emissivity of the structural member;
- $\varepsilon_f$ is the emissivity of the fire;
- $\sigma = 5.67\ x\ 10^{-8}\ W/m^2k^4$ is the Stephan–Boltzmann constant.

b) *The no heat-flow surface* is a thermal symmetric plane or has a large degree of insulation and thus can be assumed as thermally insulated having no heat flow through it. Therefore, the net heat flux to the surface of the structural member can be simply expressed as ( 50 );

$$\dot{h}_{net} = 0 \quad (50)$$

c) *The ambient exposed surface* is exposed to ambient conditions and thus can be treated similarly to that exposed to a fire but replacing the fire temperature with the ambient temperature $\theta_a$ using ( 51 );

$$\dot{h}_{net} = \alpha_c(T_a - T_m) + \Phi\varepsilon_m\varepsilon_f\sigma[(T_a + 273)^4 - (T_m + 273)^4] \quad (51)$$

d) *The fixed temperature surface* – The surface temperature of the structural member remains constant or varies according to a specified function of boundary coordinates and time.

The boundary conditions referred to the surface type d) are also called *Dirichlet* boundary conditions which defines the functions of the temperature $\theta_m = \bar{\theta}(t)$ considering that $\bar{\theta}(t)$ is the function of temperature at the boundary. This type of boundary conditions is used in the case of AST devices implemented in the CFD analyses to assign the temperature distribution recorded. The boundary conditions for the surface type a) and c) are also called *Neumann* boundary conditions in terms of derivative of the temperature as ( 52 ).

$$\lambda \frac{\partial T_m}{\partial n} = \dot{h}_{net} \qquad (52)$$

The relations ( 46 ) and boundary conditions ones composed a nonlinear relation solved in closed form for only simple cases. For this reason the numerical methods are usually required to solve the heat transfer problems. There are several methods to obtain the numerical formulation of a heat conduction problem, such as the *Finite Difference Method* (FDM), the *Finite Element Method* (FEM), the Boundary Element Method (BEM), and the Energy Balance (or Control Volume) method (EBM or CVM). The most used ones in the conductions problems for structural elements implemented in the commercial software is the FEM method. Several FEM computer codes are available for solving the nonlinear heat transfer equations with fire boundary conditions. For this reason the numerical methods are usually required to solve the heat transfer problems. There are several methods to obtain the numerical formulation of a heat conduction problem, such as the *Finite Difference Method* (FDM), the *Finite Element Method* (FEM), the Boundary Element Method (BEM), and the Energy Balance (or Control Volume) method (EBM or CVM). The most used ones in the conductions problems for structural elements implemented in the commercial software is the FEM method. Several FEM computer codes are available

for solving the nonlinear heat transfer equations with fire boundary conditions.

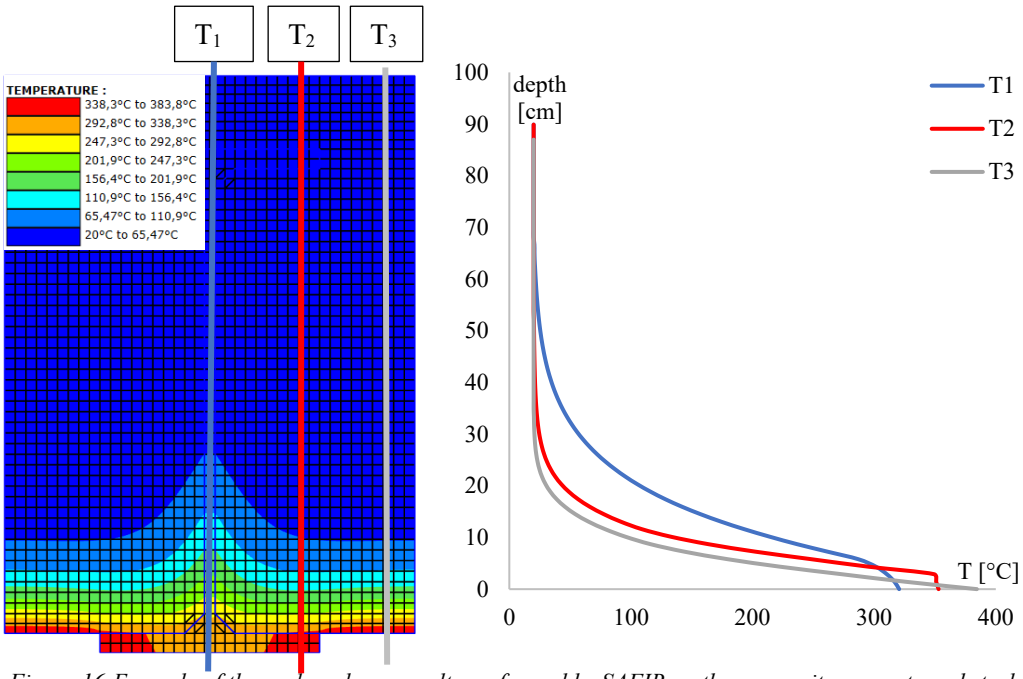


*Figure 16:Example of thermal analyses results performed by SAFIR on the composite concrete and steel structure subjected to fire curve 450°.*

Three commonly used ones include FIRES-T3 from the National Institute of Standards and Technology, USA [28], SAFIR from the University of Liège, Belgium [29], and TASEF from Lund Institute of Technology, Sweden [30]. Besides these specialized codes developed for structures exposed to fire, there are also general finite element programs like ABAQUS, ANSYS, DIANA, and Comsol Multiphysics, which can be used for heat transfer analysis.

In addition to the rigorous calculation of heat transmission, within the scope of fire resistance of reinforced concrete structures, some current standards, such as [3], provide temperature profiles applicable to slabs, beams, and columns in various fire expo-

sure configurations. These temperature profiles are calculated considering specific thermophysical properties of the material, such as certain moisture content values. In Annex B of [3], various temperature profiles are provided based on the fire resistance requirement, ranging from R30 to R240, as shown for slabs in the figure.

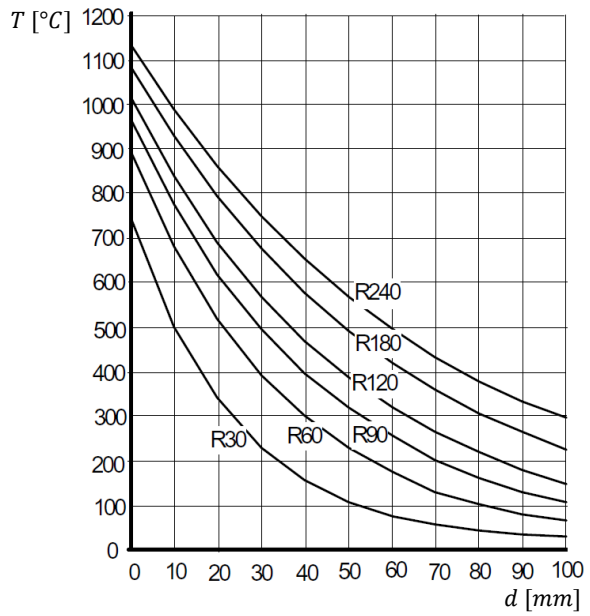


*Figure 17: Temperature profiles for slabs (height h = 200) for R60 - R240 by Annex A of [3].*

The temperature profiles reported in the Annex A of [3] can be used, for example, to evaluate the temperature of the individual reinforcing bar.

### 2.2.2 Mechanical analysis and verification procedures

As provided by Eurocode 2-1-2 [3], the Concrete structures subjected to fire could be analysed trough three different types of analyses:

- *Member analysis* is based on the effect of fire actions determined for time t=0 using combination factors according to [8]. Alternatively, it's possible to

determine the effect of fire actions starting from structural analysis for normal temperature design and applying on it's the fire reduction factor $\eta_{fi}$

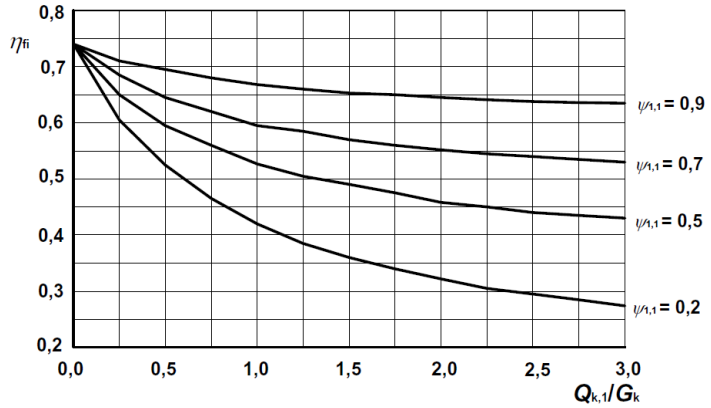


*Figure 18: fire reduction factor in function of load ratio [3].*

The effects of thermal deformations caused by thermal gradients across the cross-section need to be considered, while the axial or in-plane thermal expansions effects and the changes in boundary conditions can be neglected;

- *Substructures analysis* is an alternative method to simulate the structures in fire considering the directly exposed substructure with other parts of the structure can be approximated by time-independent support and boundary conditions during fire exposure. The analysed substructure takes into account of temperature-dependent material properties, member stiffnesses, effects of thermal expansions and deformations, assuming that the boundary conditions remain unchanged during the fire;
- *Global analysis* global analysis allows the overall behaviour of the structure to be considered, taking into account all the variations due to the thermal transient (strength, stiffness, stress characteristics, changes in boundary con-

ditions, etc.). It is certainly the most refined and effective analysis methodology for capturing all the structural consequences of a fire, but it remains costly when the model dimensions are significant.

In order to evaluate the mechanical behaviour of structures, it is necessary to clarify how the mechanical properties of the materials they are composed. In the case of underground structures and tunnels, the most used structural material is RC.

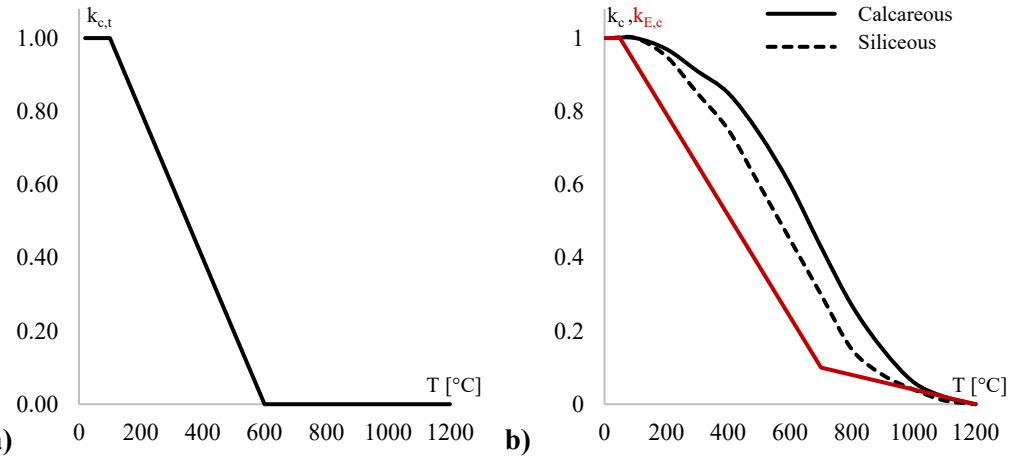


*Figure 19:The temperature-dependent reduction coefficients of concrete strength in tension $k_{c,t}$ a), in compression $k_c$ and of Young modulus $k_E$ b) [27].*

The variation in concrete properties at high temperatures depends on the type of coarse aggregate used. The paragraph 3 of Eurocode 2-1-2 provides the strength and deformation properties of concrete at elevated temperature. The aforementioned parameters may be used for normal weight concrete with siliceous or calcareous aggregates, and they are shown below in Figure 19. As shown in the aforementioned figure, in addition to strength, the stiffness of the material also decreases with increasing temperature, being reduced by half at temperatures around 500°C. Although tensile strength of concrete is typically neglected, it should be noted that it also decreases due to the increase in temperature, as shown in Figure 19 a).

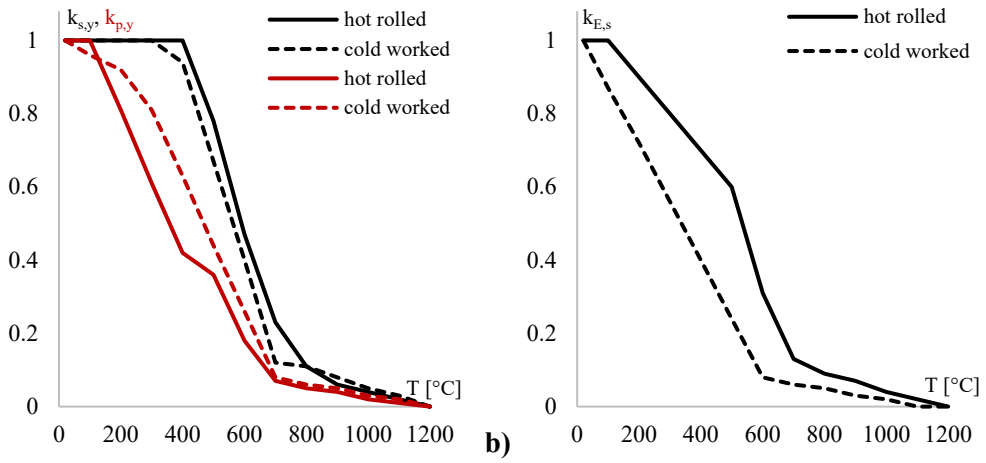


*Figure 20:The temperature-dependent reduction coefficients of reinforcing steel strength $k_{s,y}$ and prestressing steel strength $k_{p,y}$ a) and of Young modulus $k_E$ b) [27].*

Experimental results have allowed defining the laws governing the reduction coefficients of strength and stiffness for reinforcing steel. Concerning the reduction of strength, as depicted in Figure 20, there are different functions depending on the type of steel element manufacturing technique and the type of steel. From Figure 20 a), it can be observed that the reduction in strength is less pronounced for reinforcement bars compared to prestressing bars. It's important to emphasize that steel stiffness also decreases, and the reduction coefficient, as seen for strength, has a greater influence on cold-formed steel sections.

Having defined the various structural analysis methodologies according to the scale of the object under analysis, it is also necessary to outline the three different levels of methods present in the literature and codified by national and international standards (EC and NTC). Essentially, these methods can be summarized as follows:

1. Tabulated data or testing;
2. Simplified calculation methods, generally used for specific types of members;

3. Advanced calculation methods;

**Tabulated data** consist of a series of codified and tabulated solutions that provide the geometric parameterization of structural elements related to their fire resistance for specific types of elements and materials exposed to prescriptive fire curves at list for 240 minutes. In the Eurocode 2-1-2 the tabulated data are provided for concrete structural elements with siliceous aggregates and in order to extend the application to calcareous ones the reduction sections could be used (more or less 10% of reduction). The tabulated data are then classified and distinguished based on the load configuration to which the structural element is subjected and boundary conditions. The minimum axis distance for any individual bar is provided by the table to to achieve the predetermined resistance class ( for example R 30 ). It's important to underline that the tabulated data are different for types of structural elements. For assessing the fire resistance of columns there are two different tabulated methods, *Method A* and *Method B*, applicable only in the case of braced structures with circular or rectangular columns section; For both method there are some limit parameters.

*Method A* allow to evaluate the fire resistance of reinforced and prestressed concrete columns, mainly subjected to compression in braced structures, based on the degree of utilization in the fire situation and the number of exposed side. The provided parameters related to the fire resistance are the minimum base dimension and the depth of main bars from exposed surface. The method present in the section 5 of the [3] provides also the relation to interpolate the tabulated value of fire resistance (R).

*Method B* evaluates the fire resistance of reinforced and prestressed concrete columns using the mechanical reinforcement ratio and degree of utilization in the fire situation regardless the exposed sides.

For walls the tabulated data method, knowing the required resistance degree, allow to estimate the wall thickness and the cover of reinforcement bars.

For beams the code provides, for different types of beam section and the different type o static scheme of it, the standard fire resistances of R 30 to R 240 related to the load, and scheme of support. The same procedure is valid also for flat and ribbed slabs.

The **simplified calculation methods** permit to calculate the fire resistance of structural elements in presence of standard fire and other time heat regimes. In agreement with the Eurocode 2-1-2 the simplified calculation methods are *500°C isotherm method*, *Zone method* and *Curvature estimation method.*

The *500°C isotherm method* is applicable to a standard fire exposure and any other time heat regimes (only if it cause similar temperature fields) for structural elements

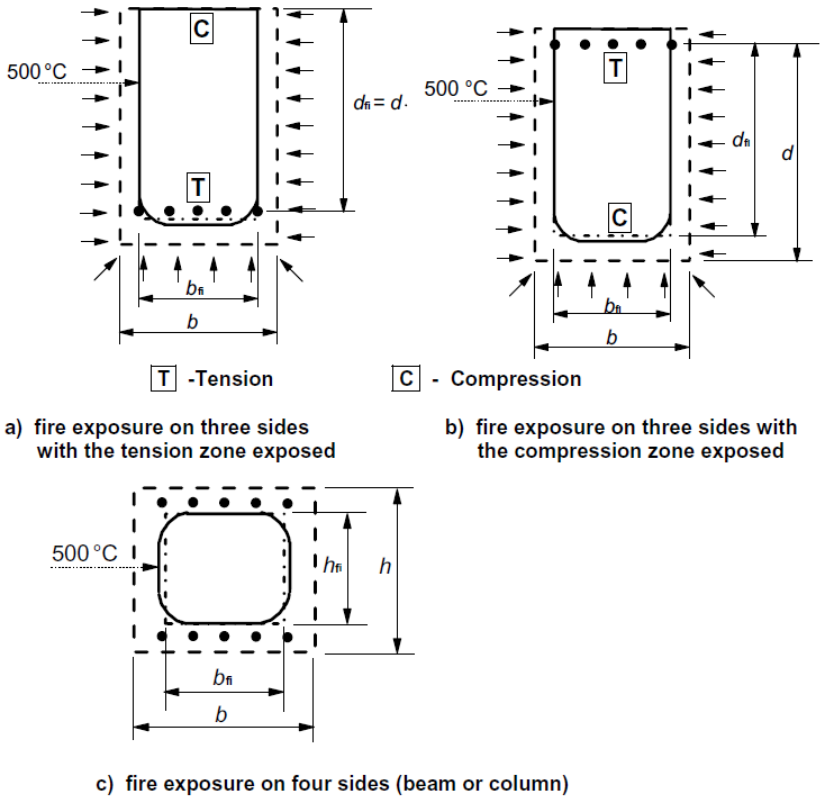


*Figure 21: Reduced cross-section of reinforced concrete beam and column by [3].*

characterized by a minimum with of cross-section related to require fire resistance (in the case of standard fire curve) or fire load density (in the case of natural fire curves). This method allow to calculate the fire resistance of structures considering the resistance of reduction reinforced concrete section in ambient temperature conditions. The reduction in section corresponds to the thickness at which an average temperature of 500°C is reached. The reduction is applied to all sides exposed to the fire but is limited to the portion of the section subjected to compression. As regarding the reinforced bars the temperature could be determined using the standard temperature profile in the Annex A of [3] or other scientific documents. At list, the ultimate load bearing capacity could be compared with the design load effect.

The *Zone method* involves subdividing the section into several zones and is applicable when the thermal load is described by a standard fire curve. The discretization of the section must be done in at least three elements, for which the average temperature and the corresponding reduction coefficients for strength and stiffness are determined. The method is applicable also in case of second order effect.

The *Curvature estimation method* is applied for the more accurate evaluation of the load-bearing capacity of reinforced concrete elements subjected to fire and more affecting by second order effect. It involves assessing the ultimate curvature of the section under fire conditions by applying a reduced section, particularly in terms of stiffness. The procedure consist in the calculation of isotherm curves in the r.c. section and then in the discretization of this in different elements characterized by men temperature varying from 20°C to 1100°C. For every single pieces the reduction factors can be calculated and then the corresponding curvature could be derived.

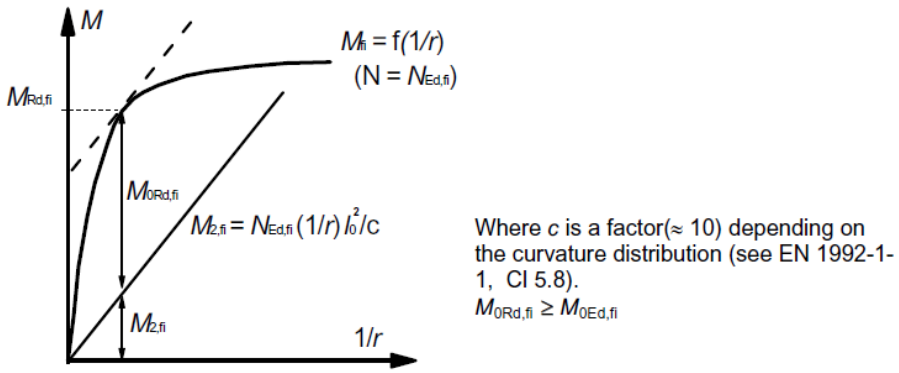


*Figure 22: Determination of ultimate moment capacity, second order moment and ultimate first order moment capacity [3].*

At list, using conventional calculation methods the ultimate moment capacity, for certain normal force and the nominal second order moment, for the corresponding curvature could be determined, Figure 22.

The **Advanced Calculation Methods** are the models most closely adhere to the physics of the phenomenon and are applicable to all possible cases. The advanced calculation method can be applied to evaluate the structural behaviour of individual members, substructures, and the entire structure subjected to the fire scenario. The Eurocode allows national normative annexes to determine the applicability limits of advanced calculation models. Advanced calculation methods can be used with any type of cross-section and for any heating curve, as they involve performing finite element analyses both for calculating temperature variations and for mechanical analysis.

Advanced calculation methods for mechanical response are based on the recognized principles and assumptions of structural mechanics theory, considering the changes in mechanical properties with temperature. These methods evaluate the effects of deformations and stresses induced by thermal variations and also include the geometric non-linear effects in the mechanical response of the advanced model. The total strain in these cases

will be:

$$\varepsilon = \varepsilon_{th} + \varepsilon_{\sigma} + \varepsilon_{creep} + \varepsilon_{tr} \quad (53)$$

Where:

- $\varepsilon_{th}$ is the thermal strain;
- $\varepsilon_{\sigma}$ is the instantaneous stress-dependent strain;
- $\varepsilon_{creep}$ is the creep strain;
- $\varepsilon_{tr}$ is the transient state strain;

Another important aspect is the spalling of the concrete cover in the compressed zone of the section, especially if it is directly exposed to fire. It is necessary to consider the spalling phenomenon and its potential effects on the reinforced concrete sections and their strength. To use these models, it is important to verify the accuracy of the calculation models based on the results of relevant tests. The verification should address temperatures, deformations, and fire resistance times. To apply this methodology, it is possible to use various software programs available on the market that have been validated and are also used in research. Among the most common and widely used are:

- ABAQUS that is a general-purpose finite elements code developed in USA;
- ALGOR that is a general-purpose finite elements code developed in USA;
- ANSYS that is a general-purpose finite elements code developed in USA;
- COMSOL that is a general-purpose finite elements code developed in USA;
- LUSAS that is a general-engineering analysis software developed in UK;
- NASTRAN that is a general-purpose finite elements code developed in USA;
- SAFIR that is the software developed in Belgium to analyse thermomechanically the structures exposed to fire.

In the present work the software used is SAFIR.

Regarding underground structures and particularly tunnels, many studies in the

literature have demonstrated the importance of using advanced thermo-mechanical analyses for evaluating fire resistance. These structures are characterized by a significant degree of restrain, so accurate modelling allows for capturing all the consequences of heating on the structures. In the paper [5] the authors have explored diverse modelling approaches to replicate the behaviour of (RC) tunnel slabs under the influence of fire-induced heating and subsequent cooling. Three modelling strategies were scrutinized, employing beam, shell, and solid elements, accompanied by different techniques to account for axial restraint effects on the slabs.

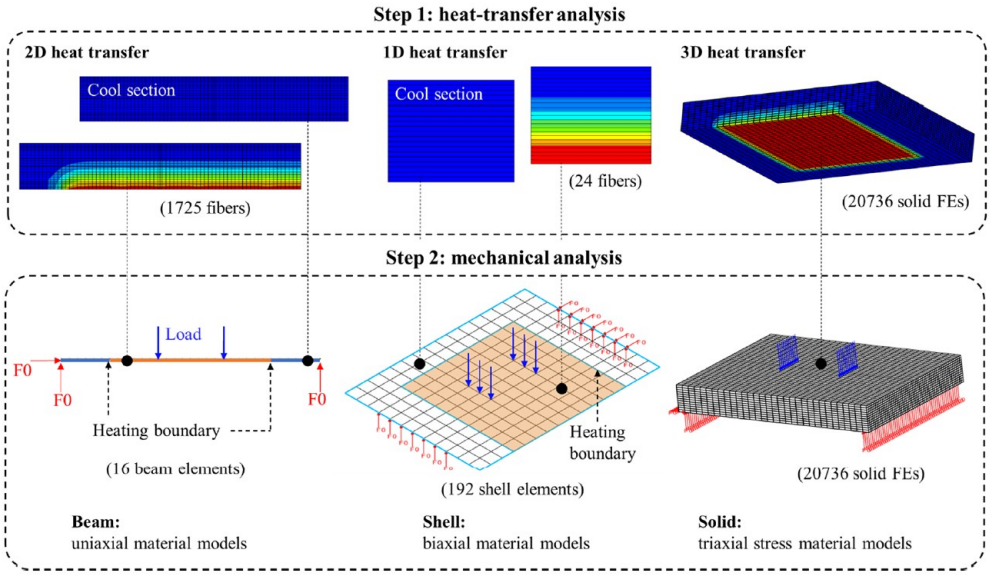


*Figure 23:Three models with different element types to simulate the fire behaviour of RC slabs [5].*

Comparative analyses were conducted between the outcomes of these modelling strategies and fire tests conducted on large-scale RC tunnel slabs, which underwent loading and restraint under various concrete strengths, levels of restraint, and fire scenarios. The evolution of temperature and displacement during heating and cooling, as predicted by the numerical models, was juxtaposed with experimental test data. Evaluating model ac-

curacy and efficiency as primary benchmarks, the utilization of shell elements for evaluating the fire resistance of reinforced concrete tunnel segments demonstrated the most favourable balance between the two considerations. Shell elements are preferred for assessing the fire performance of RC tunnel slabs or segments due to their conservative thermal predictions, accurate displacement forecasts, and reasonable computational expense.

In recent decades, efforts have been made to increase the strength of concrete, making structures more economical, lighter, and more durable. However, this increase in strength has led to greater compactness in concrete, with a reduced percentage of voids, making it more brittle and susceptible to explosive failure in the event of a fire, especially in high-strength concretes. To address this phenomenon, fiber-reinforced concretes with enhanced fire resistance have been developed and tested in the literature, suitable for structural applications in underground environments, such as precast tunnel segments. However, the study of such types of structures is not the subject of this thesis work, and their discussion within the developed methodology is deferred to potential future developments.

Chapter 3

# Performance levels of concrete linings of tunnels subjected to fire

In the present part of the work done, we provide some indications about structural safety checks of PC and RC linings in fire conditions. In many national standards, as well as in Eurocodes, there is no trace of these safety checks and, in general, there are only few guidelines concerning the fire design of underground structures. To estimate by probabilistic framework the structural fire safety of tunnels and underground structures, only a few works are present in scientific literature and in technical references. Some of these, such as the work [31] developed at Ghent University in Belgium, sink the problem with a more general approach, including the appearance of the exodus and the safety measures in the tunnel. The generality of these approaches leads to the use of simplified criteria related to structural fire safety, often based only on the analysis of temperature fields. With this in mind, in order to deepen the structural aspect of the problem, in this work we analyse the actual structural damage caused by fires in tunnels, criteria for estimating such damage shall be provided and linked to performance levels. The procedure starts from the shorter review of the technical reports about some fire accidents occurred in the underground space, to arrive at defining damage states. The process of defining the damage states of underground structure lining subjected to fire is described. The configurations of damage leading to the consideration of a predefined damage state have been defined, and it has been possible to quantify them through analytical equations. These

relationships enable the monitoring of the damage state of underground structures' reinforced concrete linings in the event of fires. Finally, in line with the approach adopted by international and national fire safety standards, performance levels have been defined to be used in the design phase of structures to ensure fire structural safety based on the intended use of the underground structure.

## 3.1 Definitions of damage states for underground structures subjected to fire

Analyzing the consequences of exceptional events such as fire, which occur within specific structures like underground ones, is a highly relevant aspect to gain a clear overview of potential damages. Studying the effects caused by a particular event allows an understanding of the phenomena that occur during it and that can stress the structure. This can lead to a clearer understanding of the actions that structural elements may undergo throughout their service life. These aspects have inspired the authors of the article [32] in which, based on the analysis of the consequences of several fires really occurred in the tunnels, the definition of the damage states for concrete tunnel linings has been made. The occurred tunnel fires analyzed regarding the tunnels around the word, starting from the until reaching Asian countries and the Americas. The authors, by analyzing post-event reports, managed to categorize the types of damage and group them based on their severity, obtaining five different damage states:

- *ds0* (None): No structural damage;
- *ds1* (Minor): Localized and shallow cracks;
- *ds2* (Moderate): Several cracks and localized spalling;
- *ds3* (Serious): Wide and deep cracks, extensive spalling and local collapse;
- *ds4* (Collapse): Lining collapse.

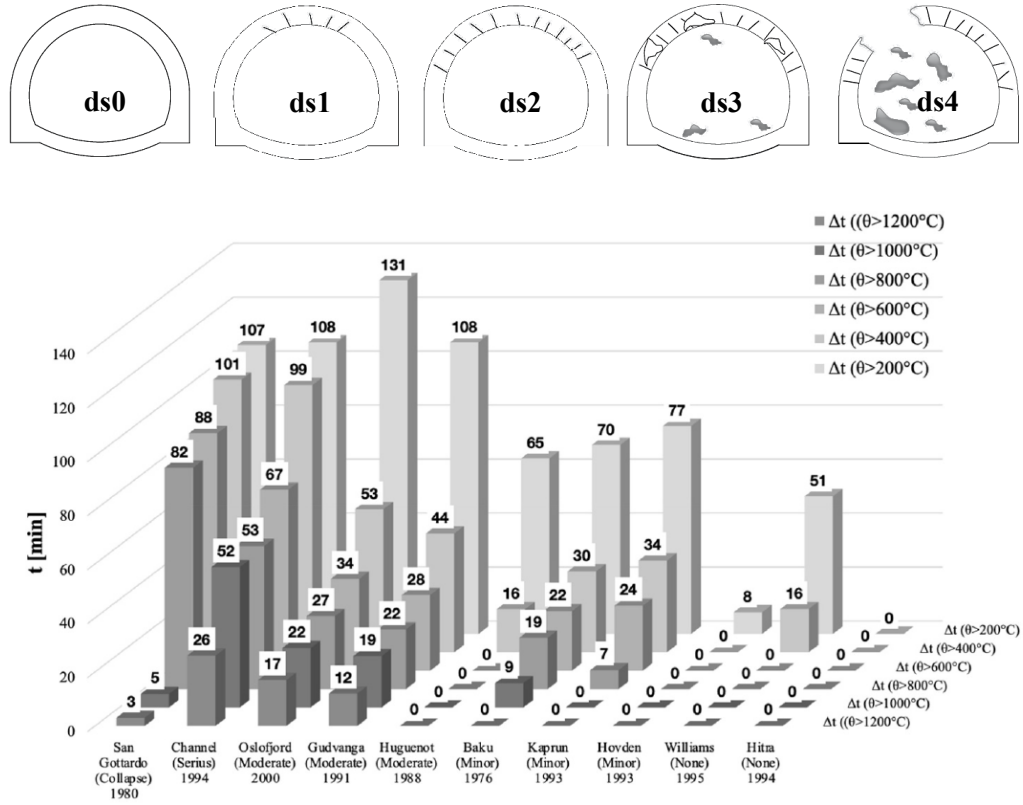


*Figure 24: Qualitative representation of damage states and the corresponding maximum temperature [33].*

After the definitions of the damage states, the authors attempted to correlate a limit state function to each damage state $g_i(x)$. It is used to mathematically define the achievement/exceedance of a limit state.

Limit states are defined as situations in which a structure, or one of its components, ceases to fulfill the function for which it was intended and for which it was designed and constructed. Safety is, therefore, associated with the potential occurrence of one or more of these states, and the probability of collapse is precisely the probability of the occurrence of the limit condition of interest for the system under consideration. The limit function is dependent on random variables related to the structure $(x_1, x_2, \dots, x_n)$.

Conventionally, the limit function is arranged to be positive when the structure is in a safe condition and takes non-positive values in the case of reaching or exceeding the limit condition, while the condition $G = 0$ in the n-dimensional space of variables defines a surface known as the collapse surface.

The actions applying on structures vary over time, as do the properties of materials and their respective strengths. In general, therefore, reliability should be expressed as the probability that the limit function is positive over the entire time interval of interest expressed in the equation.

The type of limit functions that need to be considered in the design of structures subject to fire generally will have to be the equation ( 54 ).

$$g_i(X) = (\varepsilon_t(T), t_{exp}, T_{texp}, R_{d,t,fi}, E_{d,t,fi}) \quad (54)$$

Where $\varepsilon_t(T)$ is the structural elements thermal deformation, $t_{exp}$ is the time of fire exposure, $T_{texp}$ the temperature of the structural elements, $R_{d,t,fi}$ the resistance of the structural materials and $E_{d,t,fi}$ the stresses on the structure in relation to thermal action.

Subsequently, to implement a performance-based approach, in [33] the authors present a fire design and verification approach for reinforced concrete tunnel linings. Starting from a literature review and analysing tunnel fires, the authors used the collected data to model fire scenarios. Retrospective and fluid-dynamic analyses (zone models and CFD) were conducted to determine the parameters and temperatures characterizing the previously described damage states. The damage level is identified through the gas temperatures reached during various real fire scenarios. The methodology is innovative and, as such, presents potential future developments, as stated by the authors. To fully apply the performance-based approach for the fire resistance evaluation of tunnels, quantifying the damage levels related to the mechanical parameters of the structural material, in addition

to temperatures, is necessary. Furthermore, additional effort is needed to understand and model the spalling phenomenon, given its significant influence on the structural performance of tunnels in the event of a fire.

For these reasons, in the present chapter the next step after defining the damage states is related to the quantification of performance levels that delineate each damage state, considering also the spalling. The following paragraph will present the mentioned quantification.

## 3.2 Quantifications of damage states for underground structures subjected to fire

The characterization of the damage state represents the ability to group different damage configurations into a set that unites them as seen in the previous. To group the configurations, it is necessary to define and quantify performance levels that represent the thresholds of transition between different damage states. To define and evaluate the level of performance of underground structures subjected to fire, below are the conditions that determine the assignment of a predefined damage states.

### 3.2.1 Damage state zero (*ds0)*

As seen below the **Damage State zero *"ds0"*** define the damage configuration in which there is the total absence of damage in the underground RC structures after the fire. There is the complete absence of damage resulting from the thermal action of the fire, such as cracking, spalling, or partial collapse of the tunnel lining. The verification conditions for this damage state, for the linings of underground structures in RC or PC, can be as follows.

- No spalling:

To consider the absence of structural damage, the most superficial part of the reinforced concrete elements must also be intact to ensure the designed durability level of the structure. Therefore, the depth of spalling induced by the fire must be zero, equation ( 55 ).

$$d_s = 0\ mm \qquad (55)$$

Where $d_s$ is the spalling depth induced by fire.

The absence of spalling can be preliminarily determined through the analysis of the fire curve, which describes the heating of the exposed surface when no protective elements are applied to the structural element. Alternatively, when protective elements (fireproof boards, protective coatings, etc.) are present, it can be determined through the thermal analysis of the section. This can be done thanks to various studies in the literature and based on the tests studied and analyzed in this work. In particular, in [34], it is shown, based on experimental results, that for particularly severe fire curves in terms of temperature the spalling occurs only after exceeding certain values of couple exposed surface temperature $T_s$ [°C] and heating rate $\dot{T}_s$ [°C/min], respectively of (120°C; 25°C/min).Similarly, in this thesis, a series of scientific reports related to experimental campaign results have been analyzed (which will be discussed in the chapter on spalling), finding in the plane exposed surface temperature $T_s$ [°C] and heating rate $\dot{T}_s$ [°C/min] the region in which spalling was recorded. In the study, two different regions were identified based on the heating curve to which the specimens were subjected. We are referring to the HC curve (Figure 25) and the ISO 834 curve (Figure 26). For the specimens subjected to HC fire curve the relations that describe the region in which the spalling was recorded are in ( 56 )( 57 )( 58 ).

$$no\ spalling\ recorded \qquad for \quad 0 < \dot{T}_s < 12 \qquad (56)$$

$$T > -4.9599 \cdot \dot{T}_s + 1069.9 \qquad for\ 12 < \dot{T}_s < 56 \quad (57)$$

$$T > 544 \qquad for \qquad \dot{T}_s > 56 \quad (58)$$

For the specimens subjected to ISO fire curve the relations that describe the region in which the spalling was recorded are in ( 59 )( 60 )( 61 ).

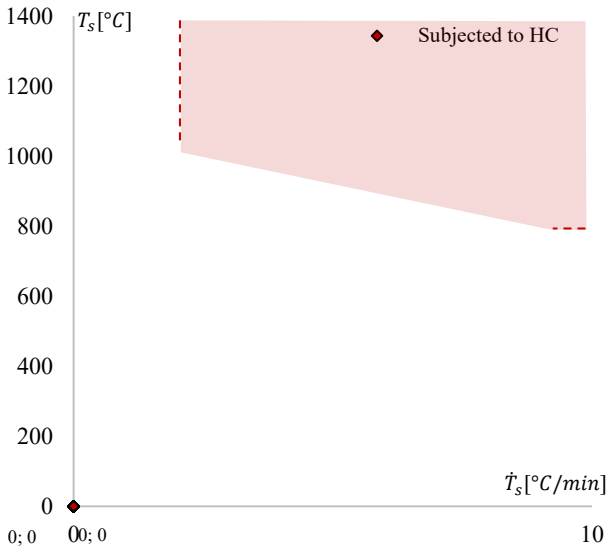


*Figure 25: The interpolating function of the temperature-heating rate pairs at which spalling was recorded during exposure to the HC curve.*

$$no\ spalling\ recorded \qquad for\ \ 0 < \dot{T}_s < 6 \quad (59)$$

$$T > -9.4827 \cdot \dot{T}_s + 833.34 \qquad for\ 6 \leq \dot{T}_s \leq 36 \quad (60)$$

$$T > 544 \qquad for \qquad \dot{T}_s > 36 \quad (61)$$

In addition, several authors have instead studied the behaviour of concrete specimens exposed to other fire curves, recording the temperature of the exposed surface and the heating rate when the spalling occurs. The fire curve used is less severe (shown in Figure 28) than ISO 834 and HC, for which the regions have

been defined in the previous figures.

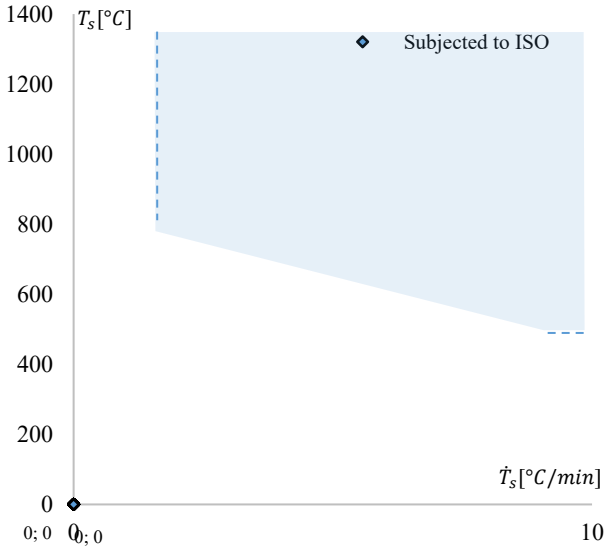


*Figure 26: The interpolating function of the temperature-heating rate pairs at which spalling was recorded during exposure to the ISO curve.*

The temperature-heating rate pairs for which spalling was recorded, even for a fire curve less severe than ISO and HC, are reported below to show the corresponding region. The equations that describe the region in which the spalling could occur are reported in the ( 68 ), ( 69 ) and ( 70 ).

$$no\ spalling\ recorded \qquad for \quad 0 < \dot{T}_s < 20 \qquad (62)$$

$$T > -3.6641 \cdot \dot{T}_s + 334.97 \qquad for\ 20 \leq \dot{T}_s \leq 85 \qquad (63)$$

$$T > 50 \qquad for \qquad \dot{T}_s > 85 \qquad (64)$$

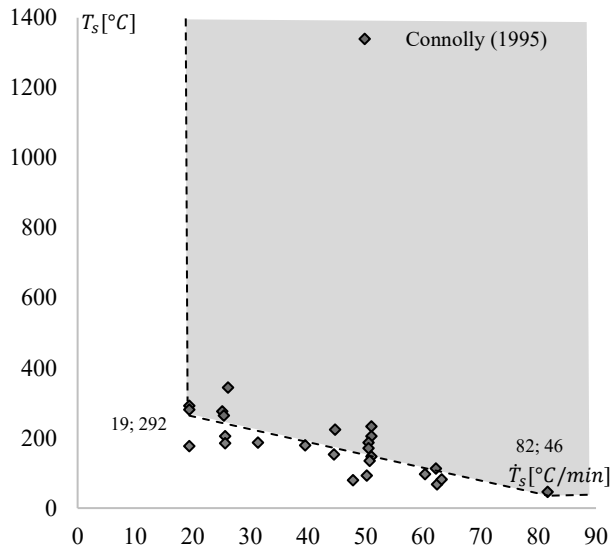


*Figure 27:The interpolating function of the temperature-heating rate pairs at which spalling was recorded during exposure to fire curve in Figure 28.*

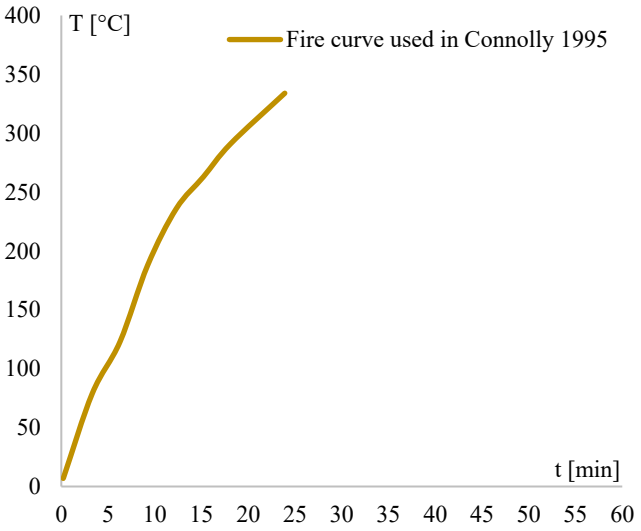


*Figure 28: Fire curve used for spalling tests in Connolly 1995.*

The graphs shown in Figure 27 allow for identifying regions where all temperature-heating rate pairs that could lead to spalling lie. The boundaries of these

regions are determined by pairs of values recorded experimentally. Additionally, by observing the differences between the aforementioned figures, the influence of the fire curve on the extent of this region is also clear. Therefore, in a simplified approach, one could initially assess the possibility of spalling occurrence by overlaying the characteristic temperature-heating rate function of the fire curve of the case study with the regions represented in Figure 25, Figure 26 and Figure 27. If the curve does not intersect these regions, the possibility of spalling can be excluded. Conversely, if the curve does intersect these regions, the occurrence can first be perceived, and then the time range in which the phenomenon may occur can be initially identified. In the case of intersection, it is necessary to apply a suitable procedure to evaluate the spalling time and the depth of the affected section.

- The bending moment induced by fire and affected by membrane forces at least equal to first cracking moment:

  The damages in terms of shallow cracks are caused by the presence of internal stresses in the structural elements that exceed the first cracking moment capacity. Therefore, to prevent this state of damage, it can be ensured that the fire-induced bending moment, as a function of membrane forces, is lower than the first-cracking moment of the section ( 65 ).

$$M_{Ed,fi} \leq M_{cr,fi}\left(N_{Ed,fi}\right) = \frac{f_{c,tk,fi} \cdot I_{1,y}}{x} \pm \left(\frac{N_{Ed,fi}}{A}\right)\frac{I_{1,y}}{x} \qquad (65)$$

  Where $M_{cr,fi}\left(N_{Ed,fi}\right)$ is the cracking moment affected by normal force and fire, $I_{1,y}$ is the moment of inertia of concrete cross section in the first stage.

### 3.2.2 Damage state one *(ds1)*

The **Damage State one "*ds1*"** describe the configuration in which there are shallow damages represented by localized cracks without any types of concrete fall by the exposed surface. The verification conditions for this damage state, for the linings of underground structures in RC or PC, could be checked as reported below.

- Spalling not triggered:

  To consider the presence of spalling lower than maximum aggregate diameter $\phi_{\mathrm{agr,max}}$ that do not compromise the safety of rescue teams, the limit at ( 66 ) could be checked.

$$d_s \leq \phi_{\mathrm{agr,max}} \qquad (66)$$

- The bending moment induced by fire and affected by membrane forces at least equal to the yielding bending moment:

  The exceeding of the first cracking moment leads to the presence of fire-induced microcracks, but with stress levels contained within the sections. This can be checked by verifying relation ( 67 ).

$$M_{cr,fi}\left(N_{Ed,fi}\right) < M_{Ed,fi} \leq M_{y,fi}\left(N_{Ed,fi}\right) \qquad (67)$$

  Where $M_{y,fi}\left(N_{Ed,fi}\right)$ is the yielding bending moment capacity affected by normal force and fire.

### 3.2.3 Damage state two *(ds2)*

The **Damage State two "*ds2*"** describe the configuration in which there are damages in terms of limited spalling and cracks. The limited spalling consists in a localized

falling-off of concrete pieces that are characterized by limited depth in order to consider the fire rescue team safety. This damage state could be checked as shown below.

- Limited spalling:

  In scientific literature and in the aforementioned fire incident reports, it has been observed that the maximum spalling tends to extend to the depth of the rebars cover, for which the limited spalling corresponds to the spalling depth within the limits shown in ( 68 ).

$$\phi_{\text{agr,max}} \leq d_s \leq c \qquad (68)$$

  Where $c$ is the concrete cover.

- The bending moment induced by fire and affected by membrane forces at list equal to the ultimate bending moment:

  In order to check this condition, the relation in the ( 69 ) could be used.

$$M_{Ed,fi} \leq M_{Rd,fi,red}\left(N_{Ed,fi}\right) \qquad (69)$$

  Where $M_{Rd,fi,red}\left(N_{Ed,fi}\right)$ is the ultimate bending moment resistance affected by normal forces, reduced by fire calculating on a spalling reduced section.

### 3.2.4 Damage states three *(ds3)*

The **Damage State three *"ds3"*** describe the configuration in which there are wide and deep cracks, extensive spalling and local collapses. In order to verify that this state of damage is reached, it is possible to check the following relations.

- Extended spalling:

  Conventionally the spalling depth could be considering extended when it exceeds

the concrete cover $c$ ( 70 ), exposing the reinforcement steel directly to the flames, which quickly reduces its capacity.

$$d_s \geq c \quad (70)$$

- The bending moment induced by fire and affected by membrane forces exceed the ultimate bending moment in no more than 3 sections to avoid that the structure becomes hypostatic:

  This state of damage could also be controlled through an advanced three-dimensional thermomechanical analysis, in which the potential collapse of the structure can be captured. Alternatively, by analysing the structure from a two-dimensional perspective, specifically focusing on a cross-section of the tunnel, it is possible to verify that the relationship ( 71 ) is satisfied.

$$M_{Ed,fi} > M_{Rd,fi,red}\left(N_{Ed,fi}\right) \ in\ no\ more\ than\ 3\ sections \quad (71)$$

### 3.2.5 Damage state four *(ds4)*

The **Damage State four "*ds4*"** describe the configuration in which there are the collapses of underground structures lining. To verify that this state of damage occurs, can be checked that the bending moment induced by fire and affected by membrane forces exceed the ultimate bending moment in more than 3 sections so that the structure becomes hypostatic ( 72 ). This state of damage could also be controlled through an advanced three-dimensional thermomechanical analysis, in which the potential collapse of the structure can be captured.

$$M_{Ed,fi} > M_{Rd,fi,red}\left(N_{Ed,fi}\right) \ in\ more\ than\ 3\ sections \quad (72)$$

Thanks to the quantification of damage states, the next paragraph illustrates how

to define performance levels for underground structures under fire conditions.

## 3.3 Performance levels and assignment criteria

The performance of structures is a broad topic that can encompass various types of structures, including buildings, bridges, dams, and more. The performance of a structure is typically assessed based on several key factors:

- **Structural Integrity:** this refers to the ability of a structure to withstand its intended loads without experiencing failure, deformation, or collapse. Engineers assess the integrity of materials used in construction and the overall design to ensure the structure can support its intended loads.
- **Safety:** safety is a critical aspect of structural performance. Structures must be designed to prevent accidents and injuries. This involves considering factors such as load capacity, redundancy, and the ability to withstand extreme events like earthquakes, floods, or high winds.
- **Durability:** a structure's ability to withstand environmental factors, corrosion, and deterioration over time contributes to its durability. Proper material selection and maintenance play key roles in ensuring the long-term performance of structures.
- **Functionality: t**he functionality of a structure is tied to its intended purpose. For example, a bridge should facilitate the safe passage of vehicles and pedestrians, while a building should provide suitable spaces for its occupants. Performance is evaluated based on how well the structure meets its functional requirements.
- **Economic Considerations:** the cost-effectiveness of a structure is crucial. This involves not only the initial construction costs but also maintenance expenses over its lifespan. Balancing performance with economic considerations is a key

aspect of structural engineering.

- **Environmental Impact:** modern structures are often evaluated based on their environmental impact. Sustainable and eco-friendly construction practices are increasingly important. This includes considering the materials used, energy efficiency, and the overall carbon footprint of a structure.
- **Adaptability and Resilience:** structures that can adapt to changing conditions and remain resilient in the face of unexpected events (such as natural disasters or changes in use) are considered to have good performance. Adaptability and resilience may involve features like flexible designs or retrofitting options.
- **Compliance with Codes and Standards: s**tructures must adhere to relevant building codes and standards to ensure they meet minimum safety and performance requirements. Compliance with these regulations is a key aspect of evaluating the performance of a structure.

*Table 1: Performance levels for construction works by fire safety strategy S.2 in [11].*

| Performance level (PL) | Description |
|---|---|
| I | Absence of external consequences due to structural collapse |
| II | Maintenance of the fire resistance requirements for a period sufficient for the evacuation of occupants to a safe area outside of the building. |
| III | Maintenance of the fire resistance requirements for a period of time equal (congruent) to the duration of the fire. |
| IV | Fire resistance requirements such that they ensure, at the end of the fire, there is limited damage to the structures themselves. |
| V | Fire resistance requirements such that they ensure, at the end of the fire, maintenance of the full operational functionality of the structure. |

The assessment of structural performance involves a combination of engineering analysis, material science, and consideration of various external factors. Engineers use tools such as structural analysis software, mathematical modelling, and physical testing to evaluate and improve the performance of structures.

In this paragraph, we address the definition of performance levels for fire resistance of underground structures and the corresponding criteria for assignment. As it has been done for building structures and regulated, for example at the fire safety strategy S.2 (fire resistance) in the Italian fire prevention code [11] and below reported.

These performance levels were not designed for underground structures and infrastructures but for structures intended for buildings, even with diversified intended uses. For example, the PL I consider preserving, even while allowing the collapse of the structure affected by the fire, the absence of consequences on adjacent constructions.

The potential collapse of a tunnel lining cannot cause damage to other structures. Conversely, however, the other performance levels could be adapted. In fact, when we talk about the evacuation of occupants, it is a characteristic applicable even to U-shaped tunnels, for any use.

At this point, the performance levels that could be monitored for the linings of underground structures and infrastructures could be that in the following Table 2. When it comes to the design and/or assessment of an underground structure concerning the action of fire, it is necessary to define the performance level that one wants to ensure for it. To this end, it is also necessary to establish criteria that allow for the attribution, based on the intended use of the infrastructure and the risk associated with a potential exceptional event such as a fire, of the performance level. These criteria, as already coined by [11], are defined as attribution criteria, and they have already been standardized for constructions.

*Table 2: Performance levels for underground structures.*

| Performance level (PL) | Description | Corresponding damage state |
|---|---|---|
| I | Restoration times and costs post-fire should be lower than the economic losses associated with the interruption of services. | Ds4 |
| II | Maintenance of the fire resistance requirements for a period sufficient for the evacuation of occupants to a safe area outside of the underground space affected by fire. | Ds3 |
| III | Maintenance of the fire resistance requirements for a period of time equal to the duration of the fire also recording several damages and local collapses. | Ds2 |
| IV | Fire resistance requirements such that they ensure, at the end of the fire, there is limited damage to the lining of underground space themselves with absence of spalling. | Ds1 |
| V | Fire resistance requirements such that they ensure, at the end of the fire, maintenance of the full operational functionality of the underground space without any type of damages. | Ds0 |

The Performance Levels can be monitored through the relationships discussed in the section on quantifying damage states. In the aforementioned chapter, it was highlighted how crucial it is to estimate the potential portion of concrete that tends to detach due to spalling induced by the fire. Exactly for this reason, in the next paragraph, the phenomenon of spalling is addressed in a detailed manner. It begins with a general overview of the current understanding of the phenomenon, examining the main physical mechanisms that determine it, and the most innovative models that allow for its prediction. The discussion then proceeds by tackling the problem with an approach based on experimental evidence, which enables the estimation of the time and depth of spalling.

Chapter 4

# Spalling phenomenon and its modelling

The use of concrete as a building material for underground structures and infrastructures is an excellent compromise between simplicity and durability, especially with the development of modular construction techniques and prefabrication of structural elements made of PC or RC. Another merit of concrete for structural applications is the good behaviour to the exceptional actions, like the fire, make the concrete an excellent structural material to be employed for the construction of extremely confined environments and with a not negligible fire risk, such as underground structures for road and rail transport. However, the concrete is a heterogeneous materials composed by aggregates, cement and water and whose mechanical features strongly depend on these and their relative weight ratio. This dependence is maintained even in fire conditions, during which the likely hygro-thermo-mechanical phenomena could develop that can degrade the material causing the detachment of pieces near the exposed surface, called spalling.

## 4.1 Description of phenomenon

The spalling consists in the estrangement of portions of concrete close to the heated surface. This detachment can occur in an explosive way, dissipating a considerable amount of energy or in a gradual way. The phenomenon of spalling is entirely natural and often man, although not fully aware of it, has used it to facilitate rock extraction processes. Indeed, in the early 17th century, in order to extract rock chips for use as construction material, the surfaces of large blocks of rock were heated. As regarding the fire

induced spalling of concrete, the first description was made in the 1854 [35]. Some authors believed that if flint was used as aggregate in concrete it could make it unstable in fire conditions.

As reported in numerous experimental results and reports of fires occurred in real tunnels, the pieces of concrete that are detached are ranging in size from a few millimetres to a dozen centimetres [36], [37]. In the RC structural elements generally the depth of spalling is limited to the concrete cover [38], [39],.

Analysing the literature, several factors were studied to understand the influence on the spalling phenomenon in concrete structures exposed to the fire. Several factors contribute to spalling occurrence and the fact that they are interrelated increases the complexity in the definition of the parameters to predict its occurrence. The main factors are related to concrete composition, structural element characteristics and exposure mode. Thus, concrete age and compressive strength, size and type of aggregates, moisture content and permeability, maximum temperature and heating rate, shape and size of cross section, reinforcement configuration, presence and shape of fibres and load magnitude can influence in its occurrence and magnitude [40], [41], [42]. The spalling phenomenon is related to the high thermal gradient between heated exposed side and its cooled core. Two types of mechanisms are generated due to the development of thermomechanical stresses and hydrothermal ones [43]. The stress increase is due to the expansion and distortions of the portion of heated structural elements and restrained by the cold one.

The main consequences of spalling are the reduction of the concrete cover to the internal reinforcement and the reduction of the load bearing cross section of the concrete elements, which can lead to the loss of its structural capacity and stability. Indeed, when spalling occurs in RC structures the reduction of load bearing capacity of section could occur, but there is also the risk of loss of the concrete cover leading to direct fire exposure of steel bars. This means that, due to the high thermal conductivity of the steel (55 W/mK

at 20°C and 27,30 W/mK over the 800 °C), it could have a rapid heating of the reinforcements with a consequent reduction of the resistance of the material ( see the mechanical properties of steel as a function of temperature in the Figure 29 ).

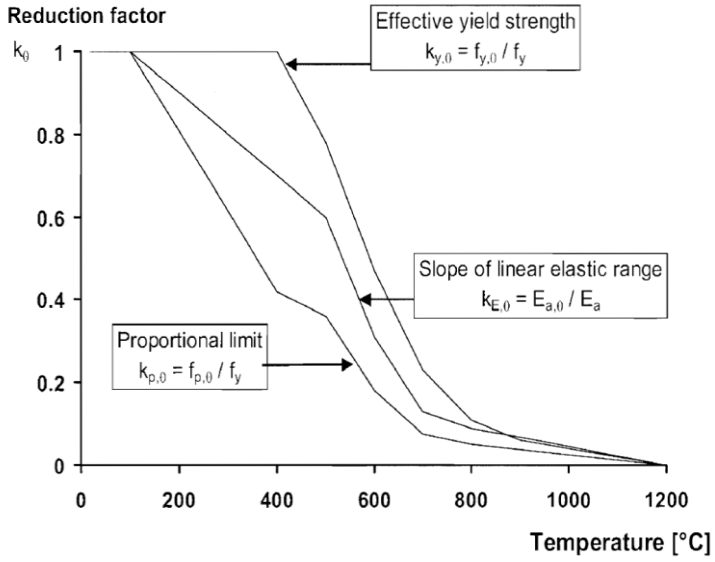


*Figure 29: Reduction factors for the stress-strain relationship of carbon steel at elevated temperatures [27].*

As seen in many experimental studies, the presence of a high moisture content and high compressive stresses in cold conditions (for example in the prestressed elements) lead to an increased risk of spalling [44].

In order to better understand the evolution of the phenomenon concerning the fires that cause it and to improve the ability to predict it, it is necessary to study the most relevant experimental findings present in the literature, as we will see in the following paragraph.

## 4.2 Experimental tests from literature

In the last decades numerous experimental studies were conducted to understand the phenomenon of spalling, being a mechanism governed by many complex factors. The Scientific and Technical Centre for Building (CSTB) based in the Marne-la Vallèe has made many tests on different size specimen, both for research and commercial project. Since tested concrete and test configurations vary from one test to the other, many useful information and teachings could be drawn out this extended experimental feedback. A data base has been built on these tests to gather, not only test results, but also concrete properties and test configurations and then provide valuable experimental information to the community [45]. In this work all the tests consisted in exposing 6 middle-size (1425 mm x 1250 mm) slabs on the top of a horizontal furnace. The size of the slabs is chosen so as to prevent a too large impact of edge effect on the measures. The thermal program follows the Increased Hydrocarbon Curve (IHC). Slabs are hanging on support beams, so as it can be considered that they are not mechanically loaded. Tests generally run for 2 hours, temperatures inside the slabs are measured 150 mm × 150 mm. Tests have been carried out on normal and high strength, non-fibred concrete. Some slabs are cut specimens from existing tunnels, and consequently some information on the concrete is missing. For every test have been provided several features as type of cement and nature of aggregates, water/cement ratio of the mix, size of the slab (thickness), mean concrete compressive and tensile strength at the age of the test, mean water content of the slab at the age of the test. The results show that spalling differs in the centre of the slab and in the edges. It seems that, when damaged concrete layer is thick, spalling is smaller near the edges of the slab. In the contrary, when concrete is lightly damaged (for instance with PP-fibered concrete), edges could be adversely impacted. Number of values is too small to conclude on a possible effect of the cement type. A clear correlation between moisture content and spalling depth can be found. As the water content increases, the spalling thickness increases.

An Australian research group performed several experimental investigations to study the occurrence of fire-induced concrete spalling and the integrity of macro-PP-fibres after cooling using an H-TRIS test method set to condition concrete test samples to have an in-depth temperature gradient equivalent to that modelled for identical concrete under the HC curve in a standard furnace [46]. The dimensions of the concrete samples casted for spalling tests were 600 × 500 $mm^2$, with a depth of 300 mm; typical depth of a concrete tunnel lining and they are not mechanically loaded. Two samples were casted for each concrete mix. All samples suffered from progressive spalling, which started between 1 and 2 minutes from the start of heating and lasted for as long as 18 min after which no spalling occurred for the remainder of the test. Test results show that the time-to-spalling was directly influenced by the presence of macro and micro PP fibres. The random nature of the damage induced by single spalling events during heating might explain the reason for which it is not possible to conclude much information from the depth of spalling data.

At the SP Technical Research Institute of Sweden an extensive experimental study on the behaviour of self-compacting concrete when exposed to fire has been carried out [47]. More than 200 fire tests have been made on about 50 types of self-compacting concrete. Different factors such as influence of compressive load, fire curve (HC and ISO834) and concrete admixture have been examined. The study of the results of the different tests showed that the orthogonal load level does not particularly influence spalling, whereas the membrane pressure does. The tested small slabs had the dimensions 600 x 500 x 200 $mm^3$ (Figure 30). There was no reinforcement in the small slabs, except the post-stress bars used for applying the external compressive load. The tests were performed on a small furnace. The clear opening of the furnace, the dimensions of the fire exposed surface of the specimens, had the dimensions 500 x 400 $mm^2$. The specimens were always placed horizontally on the furnace and the fire exposure was always one-sided. Most tests were performed on loaded specimens by post- stressing Dywidag bars with a diameter of 36

mm. Three bars were used in each specimen (Figure 31).

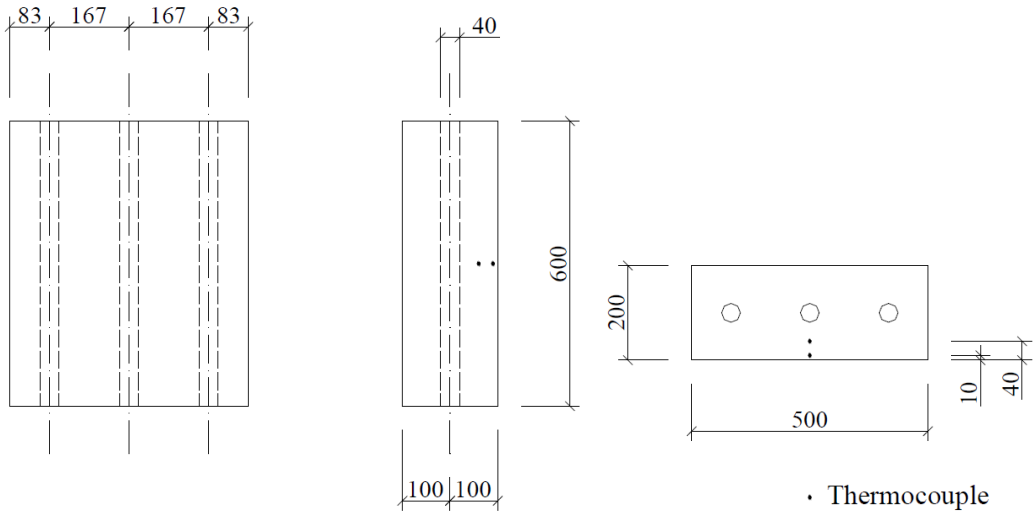


*Figure 30:Dimensions of small slab specimens tested in [45].*

Between the nut and the specimen, a steel plate with thickness 50 mm was mounted in order to transfer the load to the surface of the specimen. A load cell was mounted on each bar. Hence the load was monitored and recorded during the fire test. The spalling depth was measured in a grid with a mesh-size of 100 x 100 $mm^2$. Accordingly, a total of 7 x 6 measurements were made on each specimen. It was thus possible to produce a map on the spalling depth over the fire exposed surface of the specimens. Due to boundary effects the amount of spalling is always less at the boundaries. Therefore, measurements on spalling depth close to the boundary are uncertain and should not be considered in an analysis of the results. When presenting the results on spalling depth it is the value obtained when the boundary measurements are omitted. In addition to the spalling depth also the weight loss has been determined. It shall, however, be noted that the weight loss is not a good measure on spalling since other effects such as loss of water due to evaporation is included in the measure. Based on the experimental results of the aforementioned work, simulations with a specific spalling model will first be carried out in the following chapter, followed by a benchmark between the calculated values.

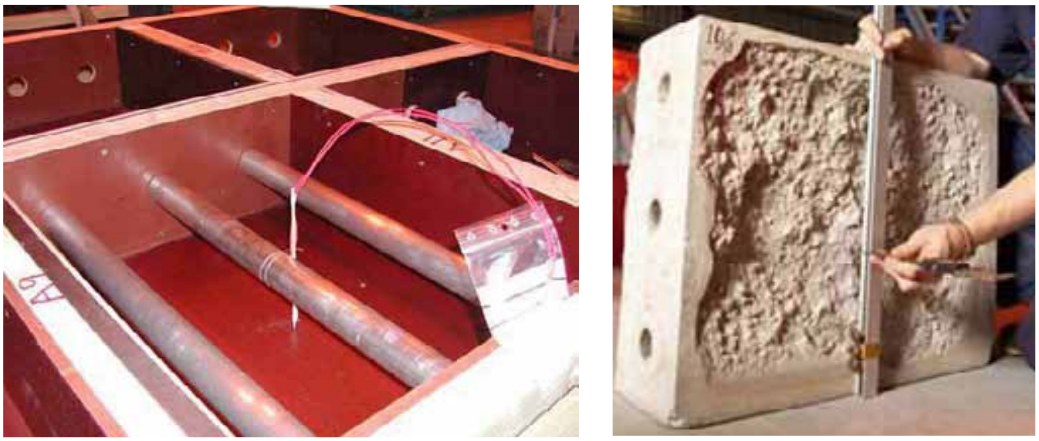

*Figure 31: Image of sampling casings with sheaths for post-tension cables and thermocouples; b) Image of the specimen after the test (by [45]).*

## 4.3 Spalling models in scientific literature

In the scientific literature there are several studies done and presented with the aim of providing models that would allow the possible spalling associated with a given fire to be assessed at the design stage. Below are the most important works done on spalling modelling (from my humble point of view):

1. The model presented by the ETH of Zurich [48] considering the combined effects from pore pressure and thermal stress. However, the explosive spalling of concrete cannot yet be quantitatively predicted due to the lack of a framework considering all the relevant factors found in research. Using both pore pressure and thermal stresses, the influences from permeability, heating rate, moisture content, tensile strength, external loads etc. can be taken into account. The authors observed that the permeability of concrete increases generally with temperature and pore pressure, Based on these observations and test results changing the moisture contents, a permeability model has been proposed. The verification of the spall-

ing model has been performed by predicting spalling time and depth of test results from literature. The accuracy of the prediction can be further improved by calibration to test results and by measuring the properties of concrete. An evaluating strategy has been introduced for the evaluation of spalling risk, the measurements of concrete properties are listed according to the actual experimental conditions. The authors also investigated the effect of the presence of PP-fibres prevent explosive spalling by increasing the permeability above the melting point. The effects have been proved by permeability measurement. The modified permeability model considers the permeability increase by introducing the increasing factors, which were determined by test results. The pore pressure was predicted for specimens with various amounts PP-fibres. The results are in favour of the PP-fibers amount of 2 kg/m$^3$, recommended by Eurocode 2 [3].

2. Other authors have proposed a numerical approach for predicting spalling in concrete structural members under fire conditions [49]. The proposed approach evaluates spalling by taking into account the effects of pore pressure, thermal gradients, and structural loading under fire conditions. This approach is incorporated as a spalling sub-model into a macroscopic finite element-based model that is capable of tracing the thermo-mechanical response of RC beams from pre-cracking stage to collapse under fire conditions. Temperature-induced pore pressure in each element is evaluated by applying mass balance equations, wherein the principles of thermodynamics, including the conservation of mass of liquid water and water vapor, is applied to calculate the pore pressure The spalling criterion is incorporated as a ‘spalling sub-model’ and then combined into a macroscopic finite element (FE) based model for evaluating fire resistance of RC beams. At each time step, calculations are carried out to evaluate various stresses as discussed above. The occurrence of spalling in an element is evaluated by applying the spalling criterion. If spalling occurs, the spalled concrete element is removed

from the cross-section at each segment. The proposed numerical procedure takes into account stresses resulting from structural loading and thermal gradients, in addition to stresses arising pore pressure in evaluating spalling. The updated reduced concrete section and the new boundary conditions are considered in the following time steps of analysis. However, the application of this model requires advanced knowledge of the characteristics of the material and the application of an articulated methodology for the prediction of spalling. It may not be a useful tool for designers to evaluate spalling at the design stage. Moreover, it was developed for beam elements, which from the point of view of numerical calculation do not have a high computational burden. Extending the application also to shell elements representing the structure of a small tunnel, could lead to a high computational burden not always sustainable.

3. The simplified spalling model, considering an initiation time, rate of spalling, and finishing time, has been developed by the Hua et al. [50]. This model is incorporated within the analysis to provide a more realistic measure of the damage. The results show that incorporation of spalling makes a significant difference in the damage assessment. This study assumes that, for a given location of tunnel lining exposed to a certain temperature demand, the heat-induced concrete spalling is a gradual and uniform process with a constant spalling rate (i.e., spalling depth changes linearly with time, specified with a unit of mm/min). Thus, the spalling process is characterized using three factors: spalling start time ($t_{start}$), spalling rate ($R_s$), and the spalling end time ($t_{end}$). The mentioned factors have been defined starting from the collected data. Most data sets are from a compilation reported by the International Workshops on Concrete Spalling due to Fire Exposure, which is a workshop held bi-annually, and publishes recent results in experimental research to advance the understanding of spalling under various

conditions [51], [52]. This paper characterizes the spalling starting time as a function of gas temperature. That is, when the gas temperature in proximity of the tunnel lining reaches the spalling starting temperature, the concrete lining will begin to spall. Compiling the data, the spalling starting temperature is set to 740 ◦C and the spalling rate is set to 2.6 mm/min, with both values taken as the mean of the experimental value. Data that could be used to determine the endpoint of the spalling process is quite limited, as many experiments were terminated shortly after the first indication of spalling. To incorporate the described fire spalling model within the thermo-mechanical finite element analysis, a fine mesh has been created in SAFIR [29], for which the concrete cover of the reinforced concrete section is composed of relatively fine layers of concrete fibers to enable proper removal of concrete when spalling occurs. An interactive MATLAB/SAFIR script has been coded to control and repeat the heat transfer process when applied to different fire scenarios. The MATLAB code writes and updates the input file for SAFIR over the duration of fire as spalling occurs. The code automatically generates input files for the SAFIR thermal analysis, indicates whether spalling occurs, removes concrete layers based on the spalling rate, updates the input file and the thermal boundary given the removed concrete layers, restarts SAFIR to continue the thermal analysis, and finally reads output files from SAFIR for damage quantification. This model of spalling does not directly considerate the modelling of the main physical phenomena that occur, but on an experimental data base uses a criterion for the definition of the start time, the speed and the end of spalling. This makes it very easy to use but not very sensitive to changes in the characteristics of the structural elements that affect spalling.

4. Some authors developed an analytical model for spalling based on the occurrence

of a coupled buckling instability and crack failure [53]. This model is called *Coupled buckling instability and crack failure spalling analytical model.* It allows to include the effect of the imposed thermal deformations, but it does not take into account the effect of the pore pressure. The authors provide the guide to use the model witch is given below:

- Initially, the thermal analysis of the section have to be performed;
- The assumption of the potential spalling thickness (equal to the aggregate size) must be made;
- Starting from the thickness assumption, the occurrence (or not) of the buckling may be assessed obtaining the mean temperature at which the buckling may occur;
- Knowing the mean temperature in the assumed thickness, the time at witch the buckling may occur can be assessed;
- The time instant allows estimation of internal stresses and assessment of the optimal thickness at which buckling can occur;
- If the optimal thickness is less or equal than the assumption the thickness and time of buckling are defined, otherwise the process is reiterated and the only thing missing is the occurrence of the crack;
- Defining the thickness and the time at which the buckling occur the crack occurrence must be evaluated;
- If the buckling and the crack occurred there is spalling otherwise not.

The authors appreciated the model effectiveness using a few experimental results data in terms of time and depth of spalling observing that the model shows good general agreement with these. Therefore, more data sets from tests are required to establish verification to this promising theory.

5. Through various experimental studies found in the literature, it has been demonstrated how the phenomenon of spalling is related to critical values of temperature and heating rate on the exposed concrete surface during a fire. In this regard, in [54], it was observed that for normal-weight concrete, the critical spalling temperature falls within the range of 375-435 °C, while the critical heating rate is in the range of 20-32 °C/min. For conventional fire curves, we are referring to temperature and heating rates that occur in the early minutes of exposure to fire. However, in the [55], in the case of fire curves that are not particularly severe, such as the case of the constant temperature curve of 450 °C (used for railway tunnels with a length of less than 1 km), heating rates above 2 °C/min are considered critical, and the temperature range of 200-300 °C is identified as the interval where spalling phenomena begin to manifest.

The models studied gave insight that it is difficult to create an analytical tool for practical use by designers to assess the occurrence of spalling and estimate its magnitude. There are the models that consider many of the physical phenomena that affect the spalling (such as 1 and 2), that are based on numerical solutions of high complexity systems. However, simpler tools based on experimental observations fail to capture the variability of the main mechanical, physical and thermal characteristics of structural elements (such as 3). This model takes into account the stresses in the elements at the beginning of the fire, the moisture content (only the influence on heat propagation), the strength of materials, the inert diameter and temperature, only the pore pressure is not considered. For this reason, in the following paragraphs benchmarks between model results and experimental test results are reported to evaluate the effectiveness of the studied model.

## 4.4 Benchmark between spalling model and experimental results

In the previous paragraph, a series of spalling models, currently present in the

scientific literature and considered among the most applicable in a fire resistance assessment of structures, were mentioned. Among the studied models, only one has drawn particular attention in the present work, as it is based on thermomechanical principles that take into account many of the known factors influencing the spalling phenomenon. Let's talk about the model called *Coupled buckling instability and crack failure spalling analytical model* [53]. In this paragraph, the mentioned model is studied, implemented in a Python code, and applied to a series of specimens of RC tunnel linings, for which there are recordings of the spalling phenomenon as results of experimental campaigns. Downstream of the applications, a comparison is reported between the experimental results and those derived from the application of the model in terms of time and thickness characterizing the spalling phenomenon.

### 4.4.1 Experimental data base used

In order to assess the effectiveness of the model IV seen at the paragraph Spalling models in scientific literature, during the work done several experimental results data have been analysed from the report [47] and grouped according to the exposure curve to which they have been subjected. Only test information used for benchmark between the test and model results is reported in Table 3 below.


*Figure 32:The picture of specimen on the furnace test [47].*

The tests above have been conducted on the small slab specimens characterized

by dimensions $600\ x\ 500\ x\ 200\ mm^3$. There was no reinforcement in the small slabs, except the post-stress bars used for applying the external compressive load. As showed in the Figure 32, every single specimen it was used as if it were the furnace cover.

*Table 3: derived test results and their main features [47].*

| Specimen | Fire curve | Spalling depth | Initial Spalling time | Final Spalling time | Duration | Applied stress | Moisture content | Compres-sive strength |
|---|---|---|---|---|---|---|---|---|
| [-] | [-] | $d_s$ [mm] | $t_{s,i}$ [min] | $t_{s,f}$ [min] | Δt [min] | $\sigma_{ext}$ [MPa] | MC % | $R_{ck}$ [MPa] |
| 46-12 | HC | **25** | **3** | **15** | **12** | 5.7 | 5.2 | 58 |
| 30-2 | HC | **31** | **5.13** | **16** | **10.87** | 10.2 | 4.1 | 105 |
| 31-4 | HC | **11** | **4.2** | **17.57** | **13.37** | 7.5 | 4.1 | 75 |
| 31-5 | HC | **14** | **4.1** | **24.17** | **20.07** | 7.6 | 4.1 | 75 |
| 31-8 | HC | **8** | **6.42** | **15** | **8.58** | 0 | 4.1 | 75 |
| 31-9 | HC | **4** | **5.52** | **13.62** | **8.1** | 0 | 4.1 | 75 |
| 34-1 | HC | **26** | **4** | **14** | **10** | 7.6 | 0 | 77 |
| 34-2 | HC | **25** | **3.33** | **17** | **13.67** | 7.5 | 0 | 77 |
| 39-13 | HC | **21** | **2.83** | **14.5** | **11.67** | 10.2 | 4.8 | 74 |
| 39-14 | HC | **16** | **3.75** | **15** | **11.25** | 7.3 | 5.5 | 74 |
| 39-15 | HC | **14** | **3.67** | **13** | **9.33** | 7.3 | 5.5 | 103 |
| 39-17 | HC | **22** | **2.58** | **16** | **13.42** | 10 | 4.8 | 74 |
| 39-18 | HC | **24** | **2.8** | **16.33** | **13.53** | 3.6 | 5.5 | 103 |
| 39-19 | HC | **29** | **3.25** | **20** | **16.75** | 5.1 | 4.8 | 74 |
| 39-20 | HC | **28** | **3** | **20** | **17** | 3.6 | 5.5 | 103 |
| 39-23 | HC | **26** | **3.17** | **20** | **16.83** | 5 | 4.8 | 92 |
| 39-25 | HC | **10** | **3.8** | **9** | **5.2** | 0 | 4.9 | 92 |
| 39-27 | HC | **28** | **2** | **15** | **13** | 4.6 | 4.9 | 92 |
| 39-28 | HC | **25** | **3** | **15** | **12** | 9.5 | 4.9 | 92 |
| 39-29 | HC | **29** | **3** | **17** | **14** | 9.3 | 4.9 | 92 |
| 39-30 | HC | **12** | **2.7** | **8.5** | **5.8** | 0 | 4.9 | 92 |
| 44-4 | HC | **6** | **9.33** | **20** | **10.67** | 8.4 | 0 | 84 |
| 45-1 | HC | **2** | **3.92** | **10** | **6.08** | 0 | 4.8 | 82 |
| 45-11 | HC | **2** | **4.25** | **15** | **10.75** | 4 | 4.6 | 78 |
| 45-15 | HC | **4** | **4.6** | **20** | **15.4** | 8.6 | 4.3 | 88 |
| 45-16 | HC | **5** | **3** | **7** | **4** | 4.8 | 4.3 | 88 |
| 45-17 | HC | **2** | **3.37** | **6.38** | **3.01** | 8.9 | 4.3 | 88 |
| 45-18 | HC | **5** | **3.47** | **6.13** | **2.66** | 4.4 | 4.3 | 88 |
| 45-2 | HC | **2** | **3.33** | **8** | **4.67** | 0 | 4.8 | 82 |
| 45-21 | HC | **7** | **2** | **7** | **5** | 9.2 | 4.3 | 85 |
| 45-22 | HC | **3** | **3** | **7** | **4** | 4.4 | 4.3 | 85 |
| 45-23 | HC | **8** | **1.67** | **6.5** | **4.83** | 8.6 | 4.3 | 85 |

| | | | | | | | | |
|---|---|---|---|---|---|---|---|---|
| 45-24 | HC | **5** | **2.17** | **7** | **4.83** | 2.8 | 4.3 | 85 |
| 45-4 | HC | **4** | **3.7** | **5.17** | **1.47** | 8.2 | 4.8 | 82 |
| 45-6 | HC | **6** | **3** | **5.17** | **2.17** | 8.6 | 4.8 | 82 |
| 45-7 | HC | **8** | **3.67** | **7.67** | **4** | 7.9 | 4.6 | 78 |
| 45-8 | HC | **5** | **5.33** | **11.17** | **5.84** | 3.9 | 4.6 | 78 |
| 39-33 | ISO 834 | **28** | **13** | **29.5** | **16.5** | 4.4 | 4.9 | 92 |
| 39-35 | ISO 834 | **22** | **10** | **30** | **20** | 9.2 | 4.9 | 92 |
| 1-1 | ISO834 | **20** | **6.25** | **9.25** | **3** | 6.2 | 4.5 | 63 |
| 2-1 | ISO834 | **32** | **4** | **17** | **13** | 6.2 | 4.1 | 61 |
| 2-4 | ISO834 | **19** | **12.83** | **20.17** | **7.34** | 6.2 | 4.1 | 61 |
| 3-3 | ISO834 | **33** | **19.4** | **31.72** | **12.32** | 6.2 | 5.1 | 60 |
| 3-5 | ISO834 | **33** | **14** | **27.87** | **13.87** | 6.1 | 5.1 | 60 |
| 6-4 | ISO834 | **20** | **14.57** | **25.5** | **10.93** | 4.6 | 4.6 | 46 |
| 9-3 | ISO834 | **26** | **13.83** | **27.67** | **13.84** | 4.1 | 5 | 42 |
| 9-6 | ISO834 | **27** | **17** | **27** | **10** | 4.3 | 5 | 42 |
| 10-1 | ISO834 | **26** | **21.62** | **48.3** | **26.68** | 3.9 | 4.6 | 47 |
| 10-2 | ISO834 | **24** | **17.17** | **28.67** | **11.5** | 3.9 | 4.6 | 47 |
| 10-3 | ISO834 | **18** | **19.87** | **24.97** | **5.1** | 1.9 | 4.6 | 47 |
| 10-4 | ISO834 | **17** | **18.33** | **23.83** | **5.5** | 2.3 | 4.6 | 47 |
| 10-5 | ISO834 | **19** | **22.03** | **26.52** | **4.49** | 1.9 | 4.2 | 48 |
| 10-12 | ISO834 | **15** | **15.45** | **36.3** | **20.85** | 2 | 5.3 | 39 |
| 10-16 | ISO834 | **11** | **23.1** | **23.1** | **0** | 4 | 4.6 | 47 |
| 10-17 | ISO834 | **25** | **15.68** | **30.72** | **15.04** | 2 | 5.3 | 39 |
| 10-18 | ISO834 | **21** | **14.77** | **26.07** | **11.3** | 3.7 | 4.6 | 39 |
| 10-21 | ISO834 | **19** | **17.67** | **26.08** | **8.41** | 3.9 | 5 | 46 |
| 10-26 | ISO834 | **19** | **13.37** | **32.38** | **19.01** | 4 | 5 | 46 |
| 12-1 | ISO834 | **20** | **10** | **24.62** | **14.62** | 4.2 | 5.7 | 41 |
| 12-2 | ISO834 | **29** | **13.4** | **28.97** | **15.57** | 4.1 | 5.7 | 41 |
| 12-3 | ISO834 | **14** | **16.78** | **24.47** | **7.69** | 0 | 5.7 | 41 |
| 12-8 | ISO834 | **13** | **15.47** | **19.77** | **4.3** | 0 | 5.7 | 41 |
| 13-6 | ISO834 | **22** | **17.77** | **27.4** | **9.63** | 4.4 | 5.7 | 45 |
| 13-7 | ISO834 | **21** | **21.27** | **34.08** | **12.81** | 4.6 | 5.7 | 45 |
| 15-5 | ISO834 | **26** | **10.22** | **26.43** | **16.21** | 7 | 6 | 70 |
| 15-6 | ISO834 | **26** | **9.98** | **27.37** | **17.39** | 7 | 6 | 70 |
| 16-10 | ISO834 | **8** | **17.83** | **20.95** | **3.12** | 0 | 6.6 | 56 |
| 16-4 | ISO834 | **22** | **12.72** | **23.72** | **11** | 5.5 | 6.6 | 56 |
| 16-6 | ISO834 | **25** | **12.97** | **24.7** | **11.73** | 5.5 | 6.6 | 56 |
| 16-9 | ISO834 | **8** | **18.33** | **22.02** | **3.69** | 0 | 6.6 | 56 |
| 46-10 | ISO834 | **42** | **9.5** | **25.25** | **15.75** | 5.8 | 5.2 | 58 |
| 46-14B | ISO834 | **20** | **14.92** | **28** | **13.08** | 0 | 5.2 | 58 |
| 46-17 | ISO834 | **38** | **10.07** | **37** | **26.93** | 6.1 | 5.2 | 62 |
| 46-18 | ISO834 | **25** | **12.25** | **32.25** | **20** | 6.1 | 4.7 | 62 |
| 46-19 | ISO834 | **21** | **11.33** | **30** | **18.67** | 2.8 | 5.2 | 58 |

| | | | | | | | | |
|---|---|---|---|---|---|---|---|---|
| 46-20A | ISO834 | **35** | **11.72** | **39.08** | **27.36** | 3.1 | 4.7 | 62 |
| 46-20B | ISO834 | **42** | **9.92** | **35** | **25.08** | 2.9 | 5.2 | 58 |
| 46-21 | ISO834 | **25** | **14.92** | **30** | **15.08** | 3.1 | 4.7 | 62 |
| 46-22 | ISO834 | **27** | **13.03** | **29** | **15.97** | 3 | 5.2 | 62 |
| 46-23 | ISO834 | **36** | **14.05** | **38** | **23.95** | 6.4 | 4.7 | 62 |
| 46-24 | ISO834 | **41** | **13.08** | **36** | **22.92** | 3 | 5.2 | 62 |
| 46-25 | ISO834 | **45** | **10.75** | **40** | **29.25** | 2.8 | 5.2 | 56 |
| 46-27 | ISO834 | **39** | **11.17** | **37** | **25.83** | 5.6 | 5.2 | 56 |
| 46-28 | ISO834 | **53** | **10.25** | **41** | **30.75** | 5.8 | 5.2 | 56 |
| 39-40 | ISO834 | **41** | **11** | **33** | **22** | 9.2 | 4.9 | 92 |

Knowing the geometry, the construction materials, the stress field, the fire curve, the moisture content and the exposed side for every specimen it has been possible to perform on them the thermal analyses obtaining that shown in the next paragraph.

### 4.4.2 Thermal analyses

The thermal analyses were performed using SAFIR software [29] that allows to calculate the temperature filed inside the structural elements, due to the fire explosion.

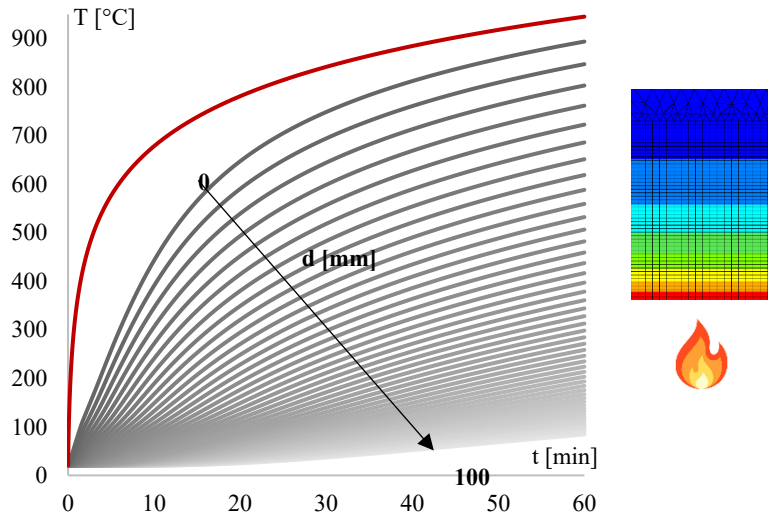


*Figure 33: Temperature distribution from exposed surface to 100 mm of depth in RC section under ISO834.*

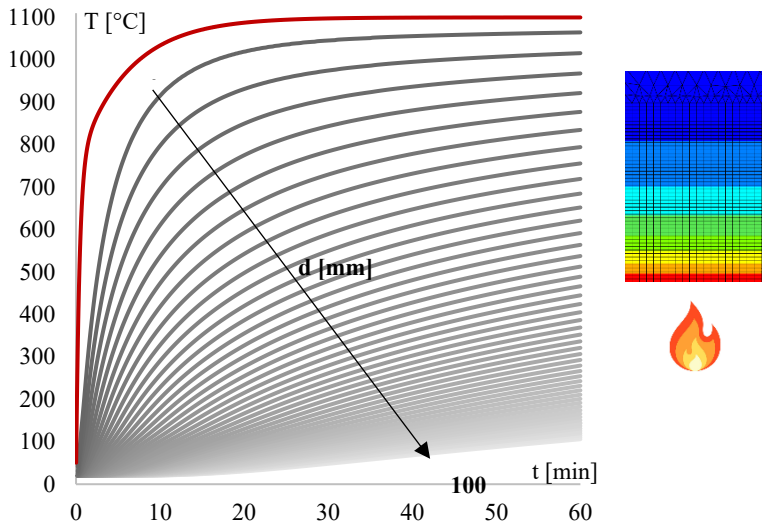


*Figure 34: Temperature distribution from exposed surface to 100 mm of depth in RC section under HC.*

The temperature field is given solving numerically the Fourier equation trough the Finite Element (F.E.) technique. The temperature distributions below for both exposures at ISO834 and HC curves (Figure 33 and Figure 34). To perform the thermal analyses on the concrete elements several parameters have to be fixed as specific mass, moisture content, convention coefficients (hot and cold), relative emissivity and the parameter of thermal conductivity. In the model the material called CALCON_EN was used in according to the Eurocode 2 [3] and the manual of SAFIR [56]. For this material the parameters range values shown in the Table 4 below were used.

*Table 4: Used parameters for thermal analysis.*

| Specific Mass | Water content | Hot convention coefficient | Cold convention coefficient | Relative emissivity | Thermal conductivity parameter |
|---|---|---|---|---|---|
| [Kg/m$^3$] | [Kg/m$^3$] | [W/m$^2$K] | [W/m$^2$K] | [-] | MC % |
| 20 ÷ 25 | 41 ÷ 66 | 35 | 4 | 0.7 | 0.85 |

It's important to understand that for the RC structural elements the fire is not more relevant in terms of material strength reduction because the material features guaranty the low thermal conductivity and high thermal inertia. While, observing the Figure 33 and Figure 34 it's possible to understand that, after one hour of ISO834 fire curve exposure, the temperature in the mean concrete cover is less than 400 °C (the temperature at which the strength of steel start to decrease according to [3]). This would mean that the structures in RC would have an excellent fire behaviour, however the phenomenon of spalling belies this.

### 4.4.3 Coupled buckling instability and crack failure spalling analytical model application

The *Coupled buckling instability and crack failure spalling analytical model,* as seen in the previous paragraph, is characterized by the iterative process that lead to check the occurrence of two different phenomena in the reverse way, the formation of a crack parallel to the fire-exposed surface and the buckling of the concrete portion enclosed by it.

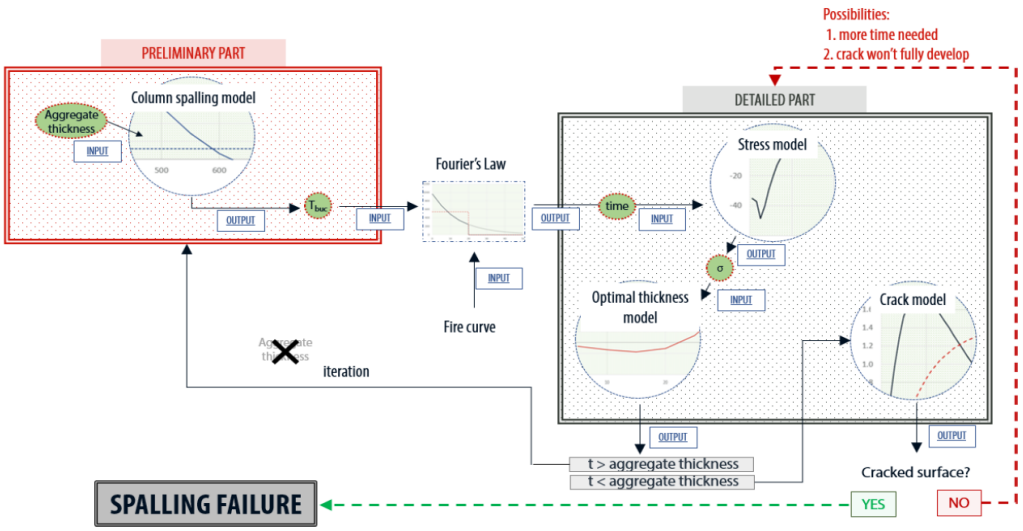


*Figure 35: Logical flow of the application procedure for the spalling model presented in [53].*

The occurrence of buckling assessment starts assuming an initial depth $d_{i,1}$ of the concrete portion that can buckle and from the results of previous performed thermal analyses. The value of $d_{i,1}$ is generally assumed equal to maximum diameter of concrete aggregate and allow to define the average temperature $T_{avg}$ at which the buckling of the ideal column might occurs.

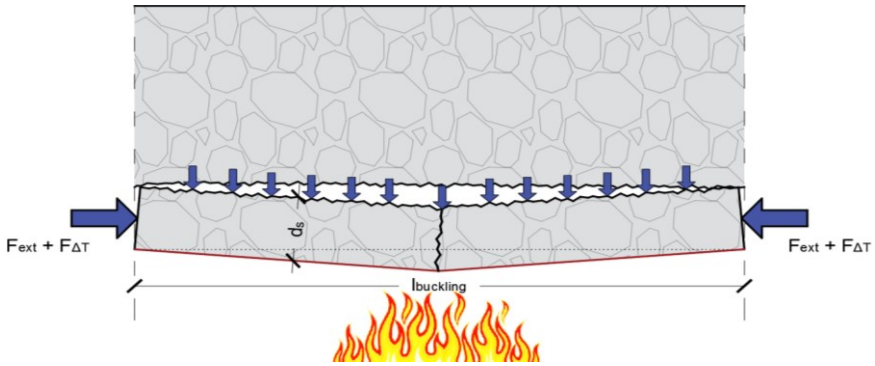


*Figure 36: Spalling due to the buckling failure of heated peace of concrete.*

The $T_{avg}$ might be calculated from the inequality relation between the acting force (including the restricted thermal expansion forces) and the buckling resistance of the ideal column as declared by the authors showed in [53] and reported below ( 73 ),( 74 ) and ( 75 ).

$$F_{Ed} \geq F_{Rd} \quad \rightarrow \quad F_{ext} + F_{\Delta t} \geq F_b \tag{73}$$

$$\sigma A \; + \; E_c(T)\, \epsilon_c(T)\, A \geq \frac{\pi^2 E_c(T) I}{l_b^2} \tag{74}$$

$$\sigma b d_{i,1} + E_c(T) \epsilon_c(T) b d_{i,1} \geq \frac{\pi^2 E_c(T) b {d_{i,1}}^3}{l_b^2 12} \tag{75}$$

The buckling length $l_b$ is directly correlated to the depth of concrete buckled $d_{i,1}$ trough the fixed angle which is function of the experimental evidence.

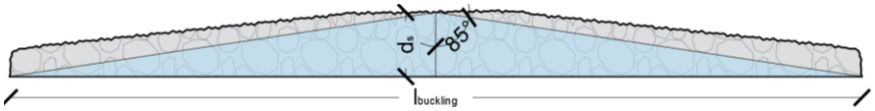


*Figure 37: Scheme of $l_{buckling}$ and $d_s$ geometrical relation, based on experimental data.*

After the evaluation of the $T_{avg}$, knowing the initial depth, the time at which the buckling occurs $t_b$ could be calculated trough the temperature distributions in the section as showed in Figure 38. In this graph, among the curves the one that exhibits, at the depth of $d_{i,1}$, the calculated temperature $T_{avg}$ can be selected, obtaining the instant of time at which the buckling occurs $t_{buck}$.

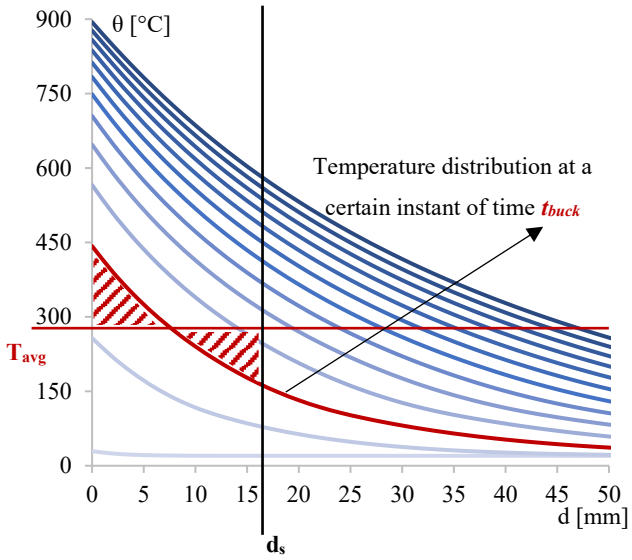


*Figure 38: Example of buckling time definition scheme.*

At this point, knowing the primary depth of concrete piece $d_{i,1}$ and the time at which the buckling could occurs $t_b$, it's possible to measure the temperature distribution in the section and calculate the correlated thermal deformations $\epsilon_c(T)$ , obtaining the thermal stresses in function of the depth as reported in the Figure 39.

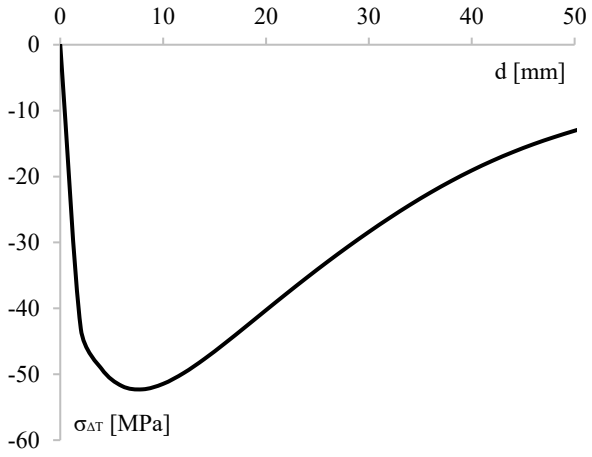


*Figure 39: The example of thermal stress distribution in the concrete section a certain instant of time $t_b$.*

The stress distributions have been calculated according to the *stress model* by Lottman in [57], and, in addition, knowing the temperature distribution in the section, also the reduction factor $K(T)$, according to the [3], could be evaluated to calculate the fire resistance of concrete at the different depth. If the benchmark between the acting load $F_{Ed}$ and Buckling resistance $F_{b,Rd}$ is plotted for every possible depth, the overcome of the acting load respect to resistance could be observed for several values of depth.

$$\Delta F = F_{b,Rd} - F_{Ed} \qquad (76)$$

The authors in [53] associate the optimal depth of buckling $d_{opt}$ to the thickness for which the maximum difference between action load and resistance occur, in other words, the minimum of the function ( 76 ) as showed in the Figure 40.

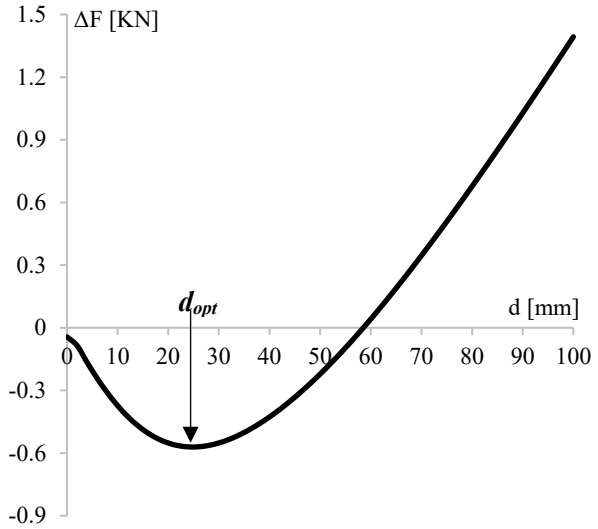


*Figure 40:Example of the difference between resistance and acting force $\Delta F = F_{b,Rd} - F_{Ed}$ distribution in function of the depth.*

Estimated the $d_{opt}$ of concrete that could lead to buckling:

- if $d_{opt} \leq d_i$ the buckling occurs, and the depth of concrete peace is equal to $d_i$ (representing the minimum value of spalling depth due to the aggregate size). The presence of spalling could be checked by moving to the next step (*the crack occurence*);

- if $d_{opt} > d_i$ the buckling does not occur for the initial depth and it's necessary to iterate the process starting from the new initial depth $d_{i,2} = d_{opt}$.

It is evident, therefore, that both the spalling time $t_s (= t_{buck})$ and the spalling depth $d_s$ are determined in the first part of the model.

The second part of the model, as mentioned earlier, allows verifying the underlying hypothesis that enables the buckling of the concrete portion near the fire-exposed

surface, the *crack occurrence*. This occurrence is evaluated a purely mechanical approach, based on a strut and tie system, as shown in the Figure 41.

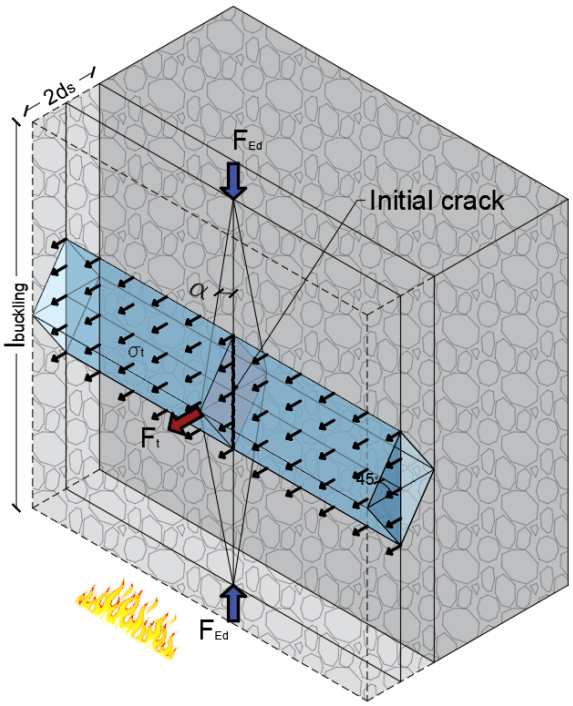


*Figure 41: Scheme of crack due to the strut and tie mechanism induced by fire.*

In particular, the external force $F_{Ed}$ lead to an orthogonal tensile force $F_t$ ( 77 ) which could lead to exceeding the tensile strength of concrete and, consequently, to cracking.

$$F_t = F_{Ed} \cdot \tan \alpha \qquad (77)$$

$$\sigma_t = \frac{F_t}{2d_s \cdot \tan 45} > f_{ctk,T} \rightarrow the\ crack\ occurs \qquad (78)$$

If the tensile stress in the concrete exceeds its tensile strength, cracking occurs, and the exposed concrete portion can become unstable, leading to spalling. If cracking does not occur, then destabilization of the exposed concrete portion cannot take place,

and consequently, there is no spalling. The peculiarity of the model is that, for spalling to occur, both the cracking of the concrete leading to the definition of a detached portion and the destabilization of this portion due to increases in forces and decreases in resistances, both caused by the heating of the structural element, must occur. The authors of the model have assessed its accuracy by applying it to only a few case studies. In fact, they state that, to consider it reliable, further applications and comparisons with experimental results are necessary. For this reason, the model was implemented in Python code and applied to all samples already tested experimentally, resulting in a database to support the validation process, which is currently incomplete. Below are the results of the applications made, accompanied by observations on the direct comparisons between these results and the experimental findings.

The results of the applications are showed numerically below in the Table 5. In order to compare the data and evaluate the model's goodness, the representation of coordinate points ($d_{s,test}$, $d_{s,model}$) and ($t_{s,test}$, $t_{s,model}$) overlaid on the equivalence lines has been included in Figure 42, Figure 44 and Figure 45.

*Table 5: The spalling model application results compared to experimental data.*

| Experimental data | | | | Model application data | |
|---|---|---|---|---|---|
| **Specimen** [-] | **Fire curve** [-] | **Spalling depth** $d_{s,test}$ [mm] | **Spalling time** $t_{s,test}$ [min] | **Spalling depth** $d_{s,model}$ [mm] | **Spalling time** $t_{s,model}$ [min] |
| 46-9 | HC | **29** | **4** | **20** | **6** |
| 46-12 | HC | **25** | **3** | **20** | **6** |
| 46-14A | HC | **36** | **3,4** | **20** | **6** |
| 30-2 | HC | **31** | **5,1** | **10** | **3,4** |
| 31-4 | HC | **11** | **4,2** | **20** | **5,6** |
| 31-5 | HC | **14** | **4,1** | **20** | **5,6** |
| 31-8 | HC | **8** | **6,4** | **NS** | **NS** |
| 31-9 | HC | **4** | **5,5** | **NS** | **NS** |
| 34-1 | HC | **26** | **4** | **NS** | **NS** |
| 34-2 | HC | **25** | **3,3** | **NS** | **NS** |
| 39-13 | HC | **21** | **2,8** | **20** | **5,2** |
| 39-14 | HC | **16** | **3,8** | **18** | **5,2** |

| | | | | | |
|---|---|---|---|---|---|
| 39-15 | HC | **14** | **3,7** | **NS** | **NS** |
| 39-17 | HC | **22** | **2,6** | **NS** | **NS** |
| 39-18 | HC | **24** | **2,8** | **NS** | **NS** |
| 39-19 | HC | **29** | **3,3** | **NS** | **NS** |
| 39-20 | HC | **28** | **3** | **NS** | **NS** |
| 39-23 | HC | **26** | **3,2** | **NS** | **NS** |
| 39-25 | HC | **10** | **3,8** | **NS** | **NS** |
| 39-27 | HC | **28** | **2** | **NS** | **NS** |
| 39-28 | HC | **25** | **3** | **NS** | **NS** |
| 39-29 | HC | **29** | **3** | **NS** | **NS** |
| 39-30 | HC | **12** | **2,7** | **NS** | **NS** |
| 39-31 | HC | **33** | **3** | **NS** | **NS** |
| 44-3 | HC | **3** | **3,8** | **NS** | **NS** |
| 44-4 | HC | **6** | **9,3** | **NS** | **NS** |
| 45-1 | HC | **2** | **3,9** | **8** | **3** |
| 45-11 | HC | **2** | **4,2** | **NS** | **NS** |
| 45-12 | HC | **9** | **4,2** | **18** | **5** |
| 45-15 | HC | **4** | **4,6** | **NS** | **NS** |
| 45-16 | HC | **5** | **3** | **NS** | **NS** |
| 45-17 | HC | **2** | **3,4** | **NS** | **NS** |
| 45-18 | HC | **5** | **3,5** | **NS** | **NS** |
| 45-2 | HC | **2** | **3,3** | **8** | **3** |
| 45-21 | HC | **7** | **2** | **NS** | **NS** |
| 45-22 | HC | **3** | **3** | **NS** | **NS** |
| 45-23 | HC | **8** | **1,7** | **NS** | **NS** |
| 45-24 | HC | **5** | **2,1** | **NS** | **NS** |
| 45-4 | HC | **4** | **3,7** | **NS** | **NS** |
| 45-6 | HC | **6** | **3** | **NS** | **NS** |
| 45-7 | HC | **8** | **3,7** | **18** | **5** |
| 45-8 | HC | **5** | **5,3** | **NS** | **NS** |
| 39-33 | ISO 834 | **28** | **13** | **NS** | **NS** |
| 39-35 | ISO 834 | **22** | **10** | **NS** | **NS** |
| 1-1 | ISO834 | **20** | **14,8** | **48** | **31,2** |
| 1-4 | ISO834 | **21** | **14,8** | **48** | **31,2** |
| 1-5 | ISO834 | **17** | **12,7** | **48** | **31** |
| 2-1 | ISO834 | **32** | **9** | **50** | **32,2** |
| 2-4 | ISO834 | **19** | **12,8** | **50** | **32,2** |
| 3-3 | ISO834 | **33** | **19,4** | **48** | **31,6** |
| 3-5 | ISO834 | **33** | **14** | **48** | **31,6** |
| 6-2 | ISO834 | **28** | **15,4** | **50** | **34** |
| 6-4 | ISO834 | **20** | **14,6** | **50** | **34** |
| 9-3 | ISO834 | **26** | **13,8** | **50** | **34,8** |
| 9-6 | ISO834 | **27** | **17** | **50** | **34,6** |

| | | | | | |
|---|---|---|---|---|---|
| 10-1 | ISO834 | **26** | **21,6** | **50** | **34,8** |
| 10-2 | ISO834 | **24** | **17,2** | **50** | **34,8** |
| 10-3 | ISO834 | **18** | **19,9** | **52** | **38,6** |
| 10-4 | ISO834 | **17** | **18,3** | **52** | **38,2** |
| 10-5 | ISO834 | **19** | **22** | **50** | **36,4** |
| 10-12 | ISO834 | **15** | **15,4** | **52** | **38** |
| 10-16 | ISO834 | **11** | **23,1** | **50** | **34,8** |
| 10-17 | ISO834 | **25** | **15,7** | **50** | **35,2** |
| 10-18 | ISO834 | **21** | **14,9** | **50** | **35** |
| 10-21 | ISO834 | **19** | **17,7** | **50** | **35** |
| 10-22 | ISO834 | **3** | **15,4** | **54** | **42,8** |
| 10-26 | ISO834 | **19** | **13,4** | **50** | **35** |
| 12-1 | ISO834 | **20** | **10** | **50** | **35,2** |
| 12-2 | ISO834 | **29** | **13,4** | **48** | **34** |
| 12-3 | ISO834 | **14** | **16,8** | **52** | **41,8** |
| 12-8 | ISO834 | **13** | **15,5** | **52** | **41,8** |
| 13-6 | ISO834 | **22** | **17,8** | **50** | **35** |
| 13-7 | ISO834 | **21** | **20,4** | **50** | **34,8** |
| 15-5 | ISO834 | **26** | **10,2** | **46** | **30** |
| 15-6 | ISO834 | **26** | **10** | **46** | **30** |
| 16-10 | ISO834 | **8** | **17,8** | **52** | **42,4** |
| 16-4 | ISO834 | **22** | **12,7** | **48** | **33** |
| 16-6 | ISO834 | **25** | **13** | **48** | **33** |
| 16-9 | ISO834 | **8** | **18,3** | **52** | **42,4** |
| 46-10 | ISO834 | **42** | **9,5** | **48** | **32** |
| 46-11 | ISO834 | **26** | **11,3** | **48** | **32** |
| 46-13B | ISO834 | **11** | **10,2** | **52** | **41,4** |
| 46-14B | ISO834 | **20** | **14,9** | **52** | **41,4** |
| 46-16B | ISO834 | **31** | **10,3** | **48** | **31,6** |
| 46-17 | ISO834 | **38** | **10,1** | **48** | **31,6** |
| 46-18 | ISO834 | **25** | **12,2** | **48** | **31,4** |
| 46-19 | ISO834 | **21** | **11,3** | **50** | **36,6** |
| 46-20A | ISO834 | **35** | **11,7** | **52** | **37,4** |
| 46-20B | ISO834 | **42** | **9,9** | **50** | **36,6** |
| 46-21 | ISO834 | **25** | **14,9** | **52** | **37,4** |
| 46-22 | ISO834 | **27** | **13** | **50** | **36,2** |
| 46-23 | ISO834 | **36** | **14** | **48** | **31,2** |
| 46-24 | ISO834 | **41** | **13,1** | **50** | **36,2** |
| 46-25 | ISO834 | **45** | **10,8** | **50** | **36,6** |
| 46-26 | ISO834 | **44** | **11** | **50** | **36,2** |
| 46-27 | ISO834 | **39** | **11,2** | **48** | **32,2** |
| 46-28 | ISO834 | **53** | **10,2** | **48** | **32** |
| 39-40 | ISO834 | **41** | **11** | **46** | **27,4** |

NS = No Spalling.

Referring to the samples subjected to the ISO 834 fire curve, the comparison made on the spalling depths demonstrates that the model provides more conservative predictions. This because the spalling is not observed in only 2 of the samples and in the other ones the result of the model is greater than the experimental one. This is evident by analysing how the data points cluster mostly above the equivalence line in the Figure 42.

From the analysis of the results in terms of spalling depth, relating to the samples subject to the fire curve HC, it is observed that there is a greater imprecision of the model, which in many cases does not grasp spalling, even when the spalling depth resulting from the experimental results is of the order of 30-40 mm as shown in Figure 43. Therefore, compared to what has been seen for applications on samples subject to the ISO834 curve, the model returns results that are not precautionary.

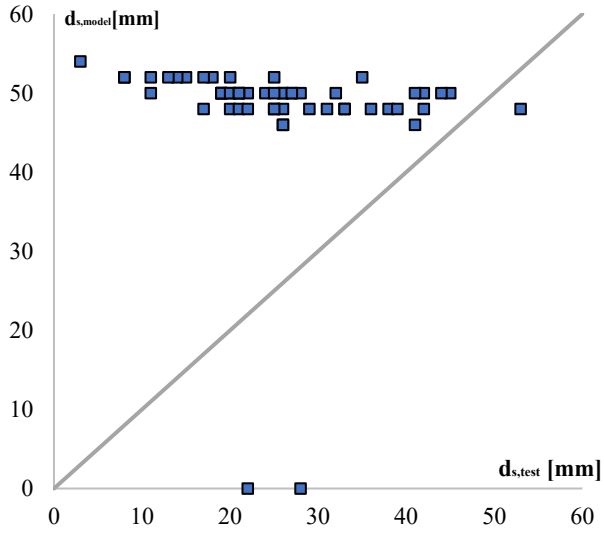


*Figure 42: Comparison between the spalling depth from experimental evidence and that from the model for ISO834 fire curve.*

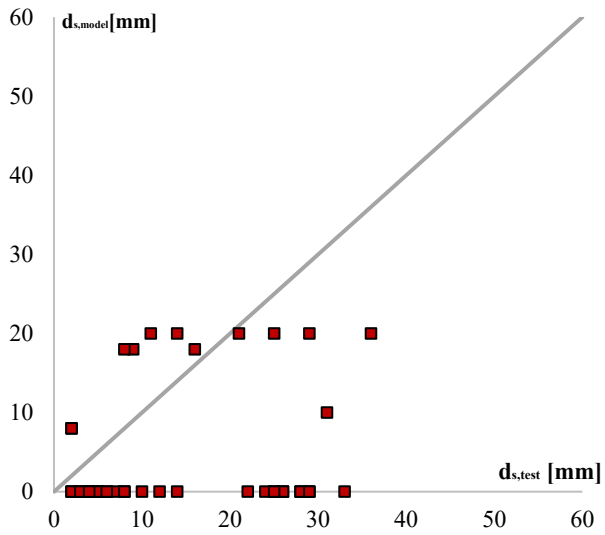


*Figure 43: Comparison between the spalling depth from experimental evidence and that from the model for HC fire curve.*

This could be considered non precautionary because, by dilating the spalling time, the exposure to fire of the reinforcement steel bars and, consequently, the reduction of load bearing capacity of RC concrete section are delayed.

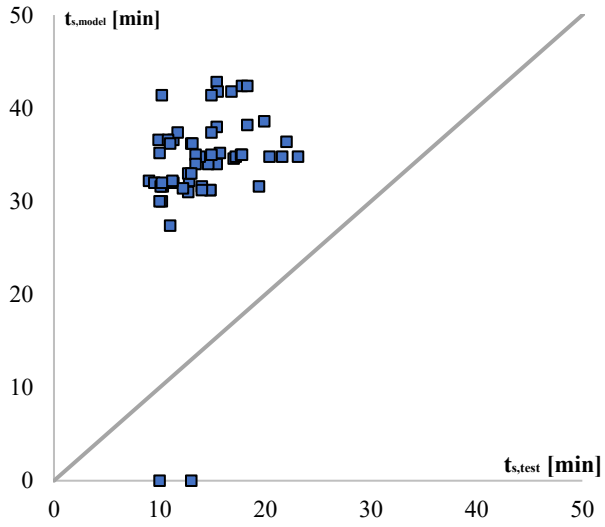


*Figure 44:Comparison between the spalling time from experimental evidence and that from the model for ISO834 fire curves.*

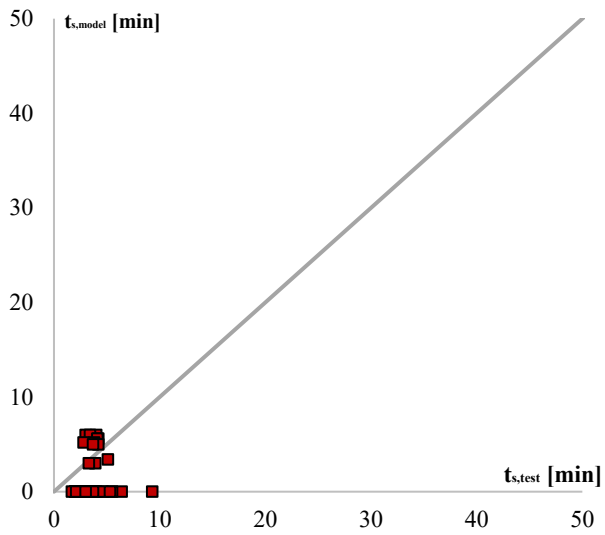


*Figure 45:Comparison between the spalling time from experimental evidence and that from the model for HC fire curves.*

Looking at the comparison of the model results in terms of spalling time, several considerations could be make. For samples subject to the ISO834 fire curve, shown in the Figure 44, a tendency of the model to overestimate the spalling times is observed.

The results regarding the samples exposed to HC fire curves show that the model provides times closer to those of the experimental results. However, as observed for the depth of spalling, in many cases it does not fully capture the occurrence of the phenomenon (Figure 45).

### 4.4.4 Conclusions about the benchmark

As seen in the previous paragraph, the model defined as "*Coupled buckling instability and crack failure spalling analytical model"* is based on the thermos-mechanics of the spalling phenomenon. The authors have been able to validate it through a comparison with experimental results, showing that it exhibits good predictions. However, they

declare that the applications are limited and therefore it is necessary to apply it to samples for which there are more experimental results. For this reason, an in-depth study has been carried out in the literature, collecting a series of experimental results relating to spalling tests carried out on RC and PC subjected to ISO834 and HC fire curves. Analysing these results compared to the model application results, for both parameters that characterize the spalling (*d* and *t)*, it has been possible to observe that:

- The model predictions in terms of depth are conservative when the structural elements are subject to the ISO834 fire curve, while it is not when the fire curve is the HC, showing a dependence on thermal input;

- The model predictions in terms of time are not conservative when the structural elements are exposed to ISO834, while in the case of HC they are in good agreement with experimental data except when it fails to capture the spalling phenomenon;

The model returns results in terms of depth and spalling time that are not in good agreement with the experimental evidence. This is evident from the comparison of the model results with the results of experimentation conducted on samples of structural elements subjected to ISO834 and HC fire curves. What is highlighted in the benchmark made in this paragraph reflects what the authors have also stated, namely: *The proposed model has limitations and requires further elaboration. Additional full-scale spalling tests are recommended to record the progress over time and crack development during spalling failure... The model does not yet take into account the effect of pore pressure... Further improvements could also come from the introduction of different support conditions in the column spalling model and a better idealization and modelling of the initial crack pattern and its development.*

Considering the above considerations, the following paragraph will present a theoretical correction to the model that will address some of the previously identified modelling

errors.

### 4.4.5 Theoretical correction

Regarding the studied spalling model, after analysing the results of the applications based on experimental findings, it was possible to understand that the model fails to capture unique results in terms of time and depth for each case. The model is indeed closely dependent on the first attempt spalling depth. In particular, it is observed that for initial thickness values close to those of the maximum aggregate (i.e., 16 mm), the iterative process is not activated, and the model indicates the absence of spalling. This is justified by the fact that, in the preliminary part, the exposure time to the fire is determined based on the thickness of spalling, and this exposure time is greater the larger the depth of spalling. By studying all possible cases and varying the initial depth of spalling for incremental depth, it was possible to understand that the model records spalling only up to depths on the order of 50/60 mm.

These observations are not completely at odds with the experimental evidence currently present in the literature, as the order of magnitude of these depths aligns with the typical rebar cover thicknesses in underground structures.

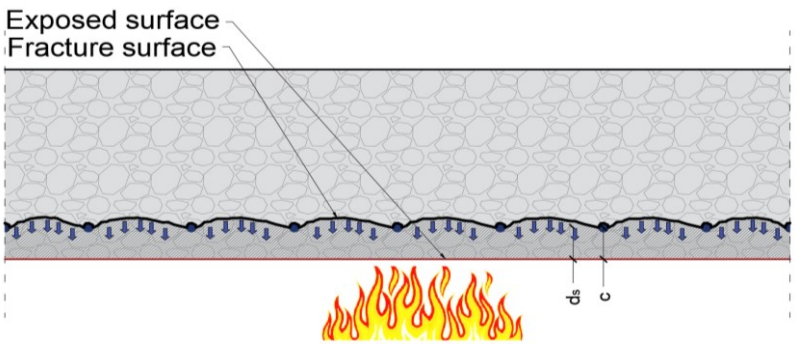


*Figure 46: Extended spalling covering the entire rebar cover.*

The level at which the outermost stell bars are located defines a surface of the cementitious conglomerate characterized by greater discontinuity, thus establishing a preferential fracture surface in the case of spalling (Figure 46).

Based on the aforementioned considerations and the disappointing results provided by the application of the *Coupled buckling instability and crack failure spalling analytical model*, the theoretical application process of the model was analysed, resulting in modifications. In particular, by implementing the model in an automated Python code, it was possible to reverse the logical process, assuming the starting thickness equal to the maximum appreciable spalling depth. As mentioned, the maximum spalling thickness is not fixed; however, literature studies have shown that it generally approximates the reinforcement cover thickness. Starting from this thickness, the entire process characterizing the model is activated, and if it does not satisfy the conditions determining spalling, the process is iterated, starting from a lower spalling thickness, Figure 47 (the reduction was made considering a discretization of the section with a step $\bar{s} = 2\ mm$).

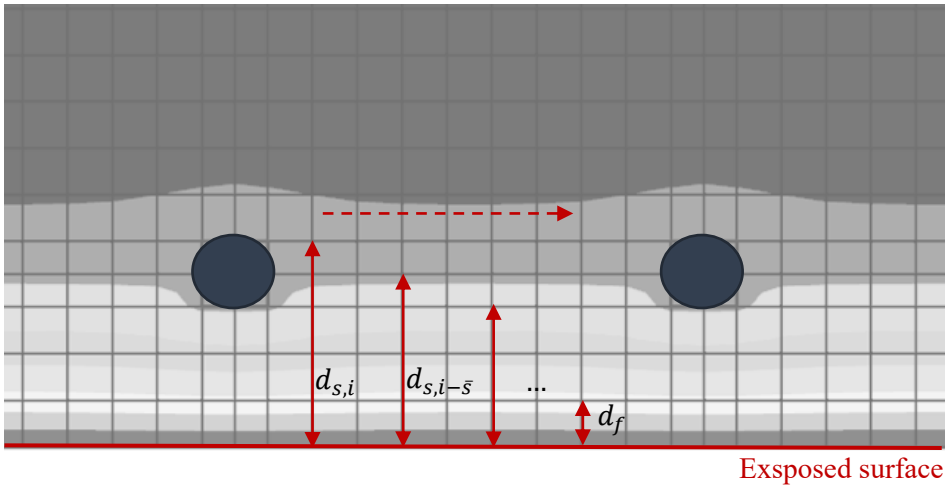


*Figure 47: Schema of the procedural inversion practiced.*

By running the spalling model again with the theoretical correction, it was possible to obtain the results shown in Figure 48 and Figure 49.

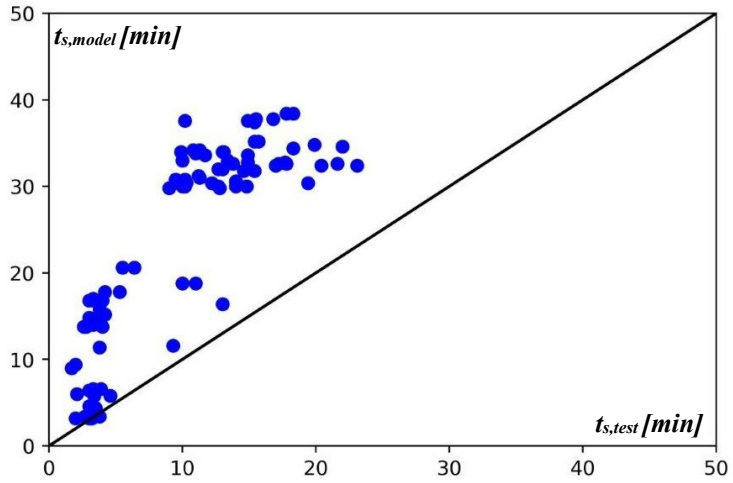


*Figure 48: The benchmark between results of Modified Coupled buckling instability and crack failure spalling analytical model and experimental results in terms of spalling time.*

The results for the specimens subjected to the ISO834 and HC fire curves are presented on the same graph as they assume comparable magnitudes, both in terms of time and depth of spalling.

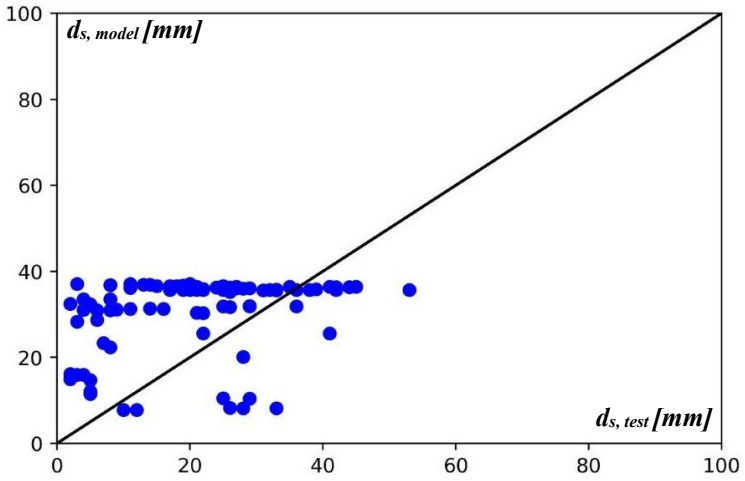


*Figure 49: The benchmark between results of Modified Coupled buckling instability and crack failure spalling analytical model and experimental results in terms of spalling depth.*

Compared to the original model discussed in the previous paragraph, it can be observed that with the applied theoretical modification, the occurrence of spalling can be captured for all the samples, both those subjected to the ISO834 curve and the HC curve. In the results seen in the previous paragraph, it was evident that for many samples subjected to the HC fire curve, it was not possible to capture the occurrence of the phenomenon either in terms of thickness or time (Figure 43 and Figure 45). Furthermore, it can be observed that the values calculated with the modified model, although not perfectly aligned with the experimental results, appear to be more consistent with them. In particular, it can be noted that the spalling depth values are more conservative compared to the previous ones, as the model generally predicts greater spalling depths than those observed experimentally. The same, however, cannot be said for the times. The modified model, in fact, estimates the occurrence times of the phenomenon to be generally longer than those recorded experimentally.

## 4.5 Proposed spalling model

The spalling model treated so far is the *Coupled buckling instability and crack failure spalling analytical model* [53]. It has been seen as said model allows to consider several aspects to which the phenomenon of spalling: *thermal expansion*, *decay of the resistance of the materials*, *moisture content*, *applied external forces etc.*. It was also possible to appreciate the limits of this model through comparisons with experimental results. What has been done, however, observing the latest results, shows that the model is too complex in the application but with poor results in terms of time prediction and spalling depth.

Moreover, by analysing the reports of experimental campaigns made on concrete elements subject to fire, such as [47], it is possible to draw different considerations on the phenomenon of spalling and on how this is modelled. In particular:

a) Spalling generally takes place in an explosive manner and in several events contained in a period of time defined as the *duration* of the spalling phenomenon;

b) The duration of the spalling phenomenon characterizes its surface extension rather than its thickness. During the recorded duration of the experiments, spalling occurred multiple times at different points on the exposed surface. Therefore, we are talking about repetitive spalling but not progressive in thickness;

c) The model discussed in paragraph 4.4.3 considers the piece of concrete subject to spalling as an ideal column subjected to buckling. In doing so, the authors adopt a free buckling length $l_b$ comparable to that of a simply supported beam and related to the initial spalling thickness, as showed in Figure 37. In reality, this is not always the case because the stiffness of the constraint may vary. In this regard, a parametric study is subsequently presented, showing how both the spalling thickness and the spalling time are related to the free buckling length $l_b$;

d) The spalling model studied in the paragraph 4.4.3 shows a strong dependence of the result on the spalling thickness of the first attempt. We have seen that, even when varying the application procedure of the model (theoretical correction in paragraph 4.4.5), initially affecting the greater spalling thicknesses, there remains a strong dependence on $d_{i,1}$.

Starting from the previously seen limitations and the crack and buckling phenomenon occurrence, needed for spalling in the *Coupled Buckling Instability and Crack Failure Spalling Analytical Model*, another model is proposed in this thesis to simplify the procedure for estimating the time and thickness of spalling. This new version is based on a non-iterative procedure that involves analysing the phenomenon through the analytical relationships that model the formation of cracks and the occurrence of instability, as seen in paragraph 4.4.3 but revisited. The new procedure is non-iterative because it does not start from a single spalling thickness. Instead, after discretizing the section into 2 mm

strips, all the pairs of spalling thickness and time $(d_{s,i}; t_{s,i})$ that satisfy the crack formation and buckling occurrence relationships are analysed.

The proposed model has the feature of allowing the calculation of the spalling initial time $t_{s,ini}$. This temporal instance corresponds to the time required for spalling conditions to be reached at the depth of the section corresponding to the maximum aggregate diameter present in the concrete. Subsequently, through a similar procedure, the model allows estimating the maximum spalling depth $d_s$ that can occur, and the corresponding temporal instance defined as the final spalling time $t_{s,fin}$.

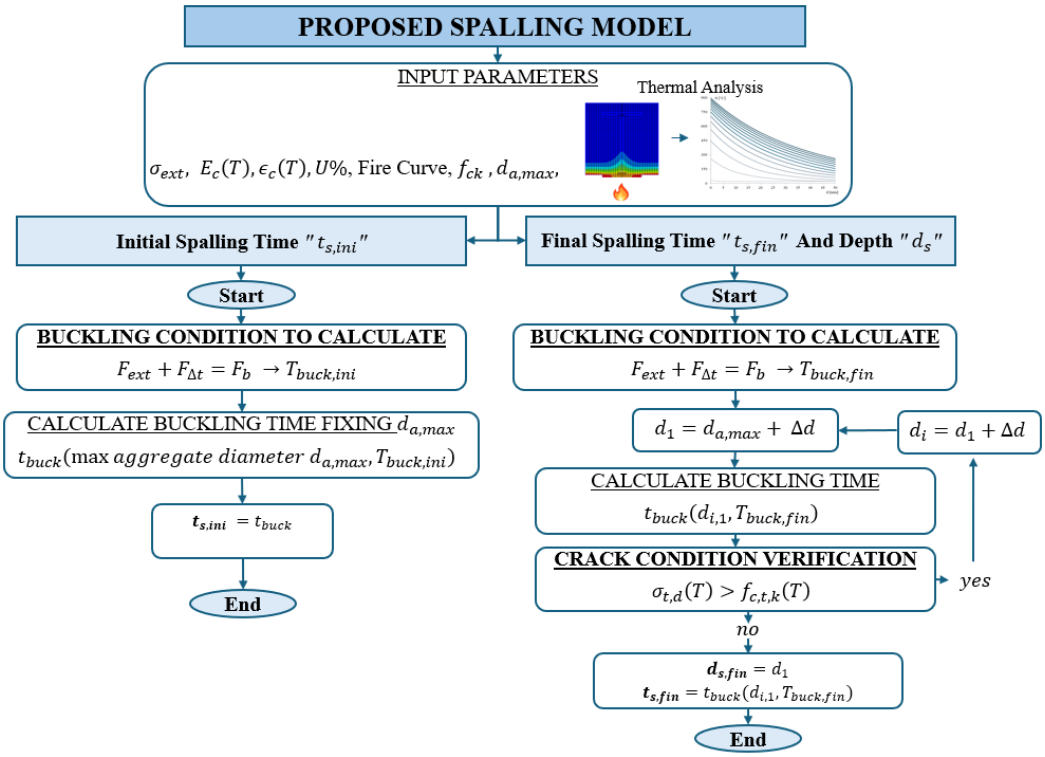


*Figure 50: proposed spalling model flow chart.*

To explain the procedure implemented in Python for the application of the proposed model, please refer to Figure 50, which schematically represents the logical process to

follow. The calculation of the initial spalling time is carried out by verifying only the buckling condition, assuming a spalling thickness equal to the maximum diameter of the aggregate present in the concrete. The cracking condition is indirectly verified, as it has been observed in various applications that for such low spalling depth values, cracking always occurs.

The calculation of the final spalling time and its depth, on the other hand, involves checking both conditions. The proposed spalling method, in fact, requires calculating the average temperature $T_{avg}$ within an initial spalling thickness using the relationship that describes the occurrence of instability, as reported in ( 81 ). In order to do this, it is necessary to know the input parameters, which are the compressive stress due to the external load $\sigma_{ext}$, the Young's modulus of concrete in function of temperature $E_c(T_{avg})$, the function of the thermal deformation function of the concrete $\epsilon_c(T_{avg})$, the moisture content of the concrete U%, the Fire Curve applied and the characteristic strength of the concrete used. Once the average temperature that causes spalling is determined, the next step is to evaluate the fire exposure time necessary for the calculated average temperature to be reached at the studied depth of the section. This allows for the evaluation of the exposure time at which the conditions of instability occur. Once the time instant is known, it is possible to proceed with evaluating the condition for crack formation. If this condition is met, the implemented code proceeds to the next step, which involves studying a new spalling depth, greater than the previous one. For this new depth, a new time instant is evaluated, and the cracking condition is verified. The cycle, as defined, ends at the i-th step when the cracking condition is no longer satisfied, allowing the i-th studied depth to be designated as the maximum spalling depth. The following section will provide a more detailed analysis of the relationships used by the proposed model.

The relationship for which **buckling** occurs is characterized by having the spalling depth and time as direct and indirect unknowns. In equation ( 79 ), we see that the

spalling depth directly influences the calculation of the external force acting, the increase in stress due to thermal expansion, and the calculation of instability resistance. Additionally, it indirectly affects the average temperature within the spalling thickness of a single attempt. The spalling time, on the other hand, indirectly influences the equation by modifying the average temperature, which consequently changes both the thermomechanical properties of the sample and the stress. The basic concept is that for each individual sample analysed, given the same material resistance, external stress, and laws governing the variation of the material's thermomechanical properties, knowing the fire curve and setting a reference spalling depth, there will definitely be a specific point in time that satisfies the buckling relationship described in equation ( 79 ).

$$\sigma_{ext} \cdot b \cdot d_{s,i} + E_c\left(T_{avg}(t_{s,i}, d_{s,i})\right) \cdot \epsilon_c\left(T_{avg}(t_{s,i}, d_{s,i})\right) \cdot b \cdot d_{s,i} > \frac{\pi^2 \cdot E_c\left(T_{avg}(t_{s,i}, d_{s,i})\right) \cdot b \cdot {d_{s,i}}^3}{l_b(d_{s,i})^2 12} \quad (79)$$

Where:

- $\sigma_{ext}$ is the compressive stress close to the exposed surface due to the external load;
- $b$ is the base of analysed section which conventionally assumes a unit value;
- $d_{s,i}$ is the i-th spalling depth;
- $t_{s,i}$ is the i-th spalling time;
- $T_{avg}(t_{s,i}, d_{s,i})$ is the average temperature in the depth $d_{s,i}$ at certain instant of time $t_{s,i}$
- $l_b(d_{s,i}) = 2\, d_{s,i} \cdot \tan 85°$ is the buckling length.

By rewriting equation 79 to explicitly state the free buckling length that characterizes the buckling phenomenon, it is possible to arrive at equation ( 80 ). In this equation, it can be observed how it is possible to simplify it by eliminating the parameter $d_{s,i}$ from each term. Specifically, the direct parameter is eliminated, thus leaving the equation dependent solely on the average temperature term.

$$\sigma_{ext} \cdot b \cdot d_{s,i} + E_c\left(T_{avg}(t_{s,i}, d_{s,i})\right) \cdot \epsilon_c\left(T_{avg}(t_{s,i}, d_{s,i})\right) \cdot b \cdot d_{s,i} = = \frac{\pi^2 \cdot E_c(T_{avg}(t_{s,i}, d_{s,i})) \cdot b \cdot {d_{s,i}}^3}{(2\, d_{s,i} \cdot \tan 85°)^2 12} \quad (80)$$

The simplified equation obtained is shown in ( 81 ), and as can be observed, the dependence on the pair of terms $(t_{s,i}, d_{s,i})$ relates to what is defined as the average temperature in the i-th thickness at the i-th time instant. This simplification allows the buckling condition to be expressed solely as a function of the average temperature, thus obtaining a specific minimum value of this temperature, for each sample/case study, that causes the phenomenon to occur.

$$\sigma_{ext} + E_c\left(T_{avg}(t_{s,i}, d_{s,i})\right) \cdot \epsilon_c\left(T_{avg}(t_{s,i}, d_{s,i})\right) = = \frac{\pi^2 \cdot E_c(T_{avg}(t_{s,i}, d_{s,i}))}{(2 \cdot \tan 85°)^2 12} \quad (81)$$

Defining the minimum average temperature that satisfies the buckling condition seen in equation ( 81 ), it is interesting to observe how, given a fixed average temperature, it is possible to identify various time-depth $(t_{s,i}, d_{s,i})$ pairs that achieve it. Therefore, in the first part of the model, fixing the depth equal to the maximum aggregate diameter the initial spalling time could be determined, as seen in the chart reported in Figure 50.

In addition it is also necessary to assess the occurrence of **cracking** within the concrete depth. This is a prerequisite condition to ensure the premises for buckling. The condition that leads to the occurrence of cracking is described in detail in paragraph 4.4.3, and the equation is provided below ( 82 ).

$$\frac{\left[\sigma_{ext} \cdot b \cdot 2\ d_{s,i} + E_c\left(T_{avg}\left(t_{s,i}, d_{s,i}\right)\right) \cdot \epsilon_c\left(T_{avg}\left(t_{s,i}, d_{s,i}\right)\right) \cdot b \cdot 2\ d_{s,i}\right] \tan(\alpha)}{2d_s \cdot b \cdot \tan 45} > f_{ct} \cdot\ k_{ct}(T_{d_{s,i}}) \rightarrow the\ crack\ occurs \quad (82)$$

Where:

- $f_{ct}$ is the tensile strength of concrete;
- $k_{ct}(T_{d_{s,i}})$ is the fire strength reduction factor in function of temperature at depth $d_{s,i}$.

In relation ( 82 ), it is also possible to observe how the depth $d_{s,i}$ appearing directly in the equation can be simplified. Then, considering b as unitary and $\tan 45° = 1$ the previous equation is modified, with everything expressed as a function of the average temperature at the i-th section depth $d_{s,i}$ at the i-th exposure time $t_{s,i}$ to the fire curve, obtaining the function ( 83 ).

$$\left[\sigma_{ext} + E_c\left(T_{avg}\left(t_{s,i}, d_{s,i}\right)\right) \cdot \epsilon_c\left(T_{avg}\left(t_{s,i}, d_{s,i}\right)\right)\right] \tan(\alpha) > f_{ct} \cdot\ k_{ct}(T_{d_{s,i}}) \quad (83)$$

As seen with the buckling condition, since temperature is a function of the concrete depth under analysis and the exposure time to the fire curve, it is possible to diagram on the time-depth plane all those pairs $\left(t_{s,i}, d_{s,i}\right)$ that satisfy relation ( 83 ) for each sample/case study. At this point, since spalling occurs when the parameters involved satisfy both the buckling and cracking conditions, in time-depth plane, the two curves representing these

conditions overlap. Their intersection identifies the coordinates $(t_s, d_s)$ where both conditions are simultaneously satisfied. The coordinates of this point represent the exposure time at which spalling occurs and the depth within the section affected by the phenomenon. With the aim of making the model more sensitive to the input data derived from the individual case study, this work has studied the influence of the degree of constraint of the ideal column that tends to be subject to buckling (Figure 51).

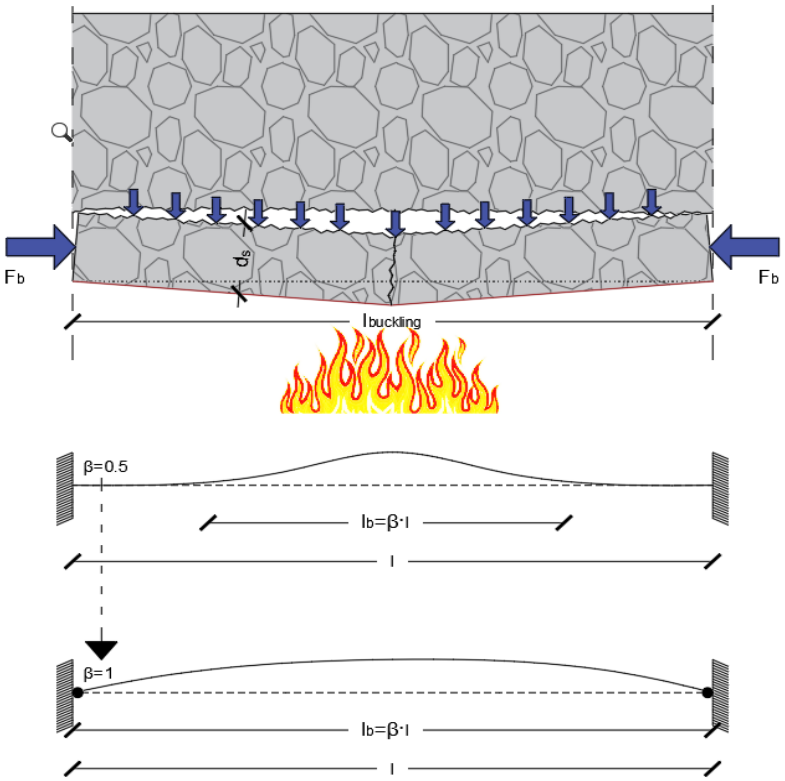


*Figure 51: Two constraint limit schemes for defining the effective length in buckling assessment.*

After the implementation of the new spalling model, it was possible to study the results in relation to the experimental data. In particular, it was possible to apply the model considering different values of the free inflection length, thus obtaining a database of results differentiated according to this parameter.

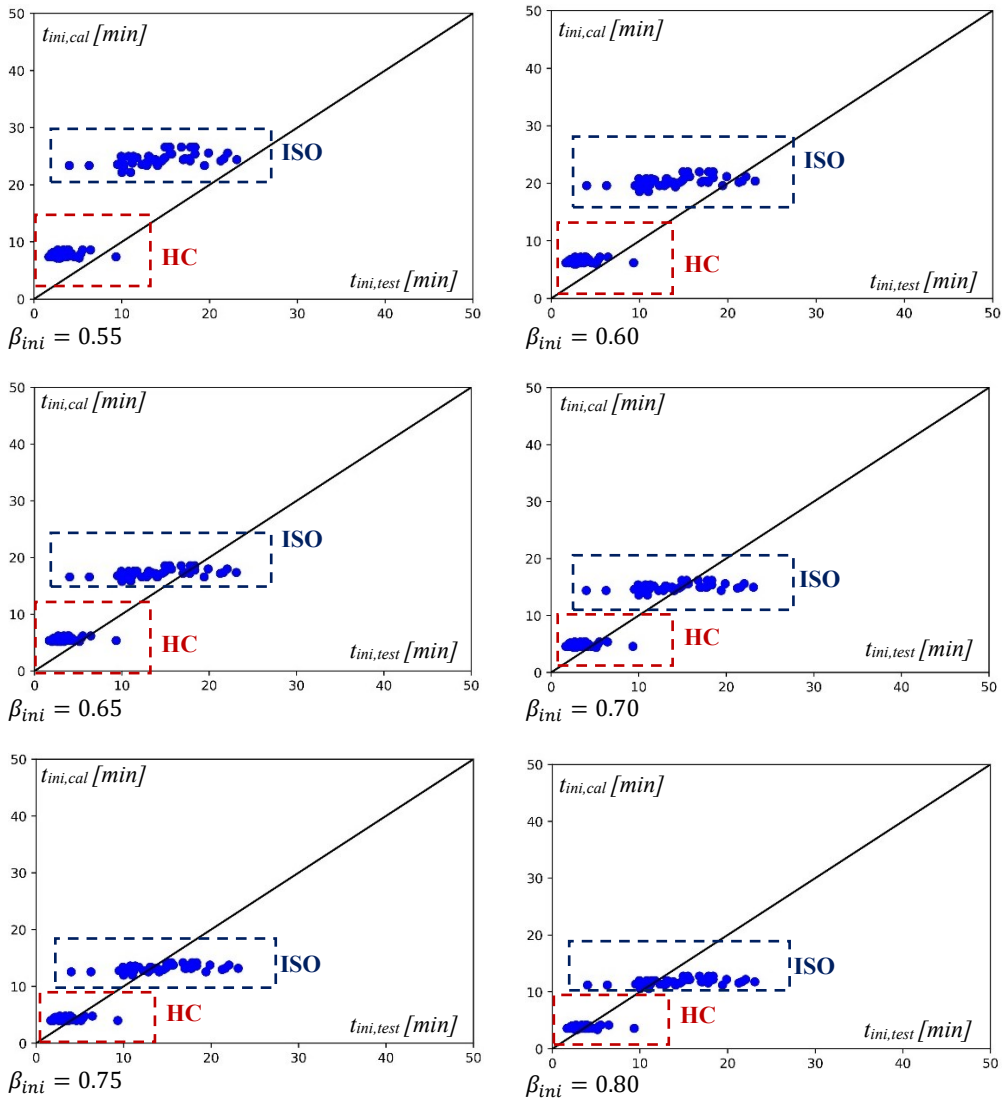


*Figure 52: Analysis of the Influence of the $\beta_{ini}$ Coefficient on the Spalling Initiation Time.*

As can be seen in Figure 52, the coefficient $\beta$, which characterizes the free inflection length, has a significant influence on the results in terms of initial time of spalling. As shown in the previous graphs, with the increase of the $\beta_{ini}$ coefficient (and consequently the decrease in the stiffness of the lateral constraints of the analysed element), the model

provides results that are more consistent with the experimental ones. However, this is true only in the evaluation of the spalling initiation time.

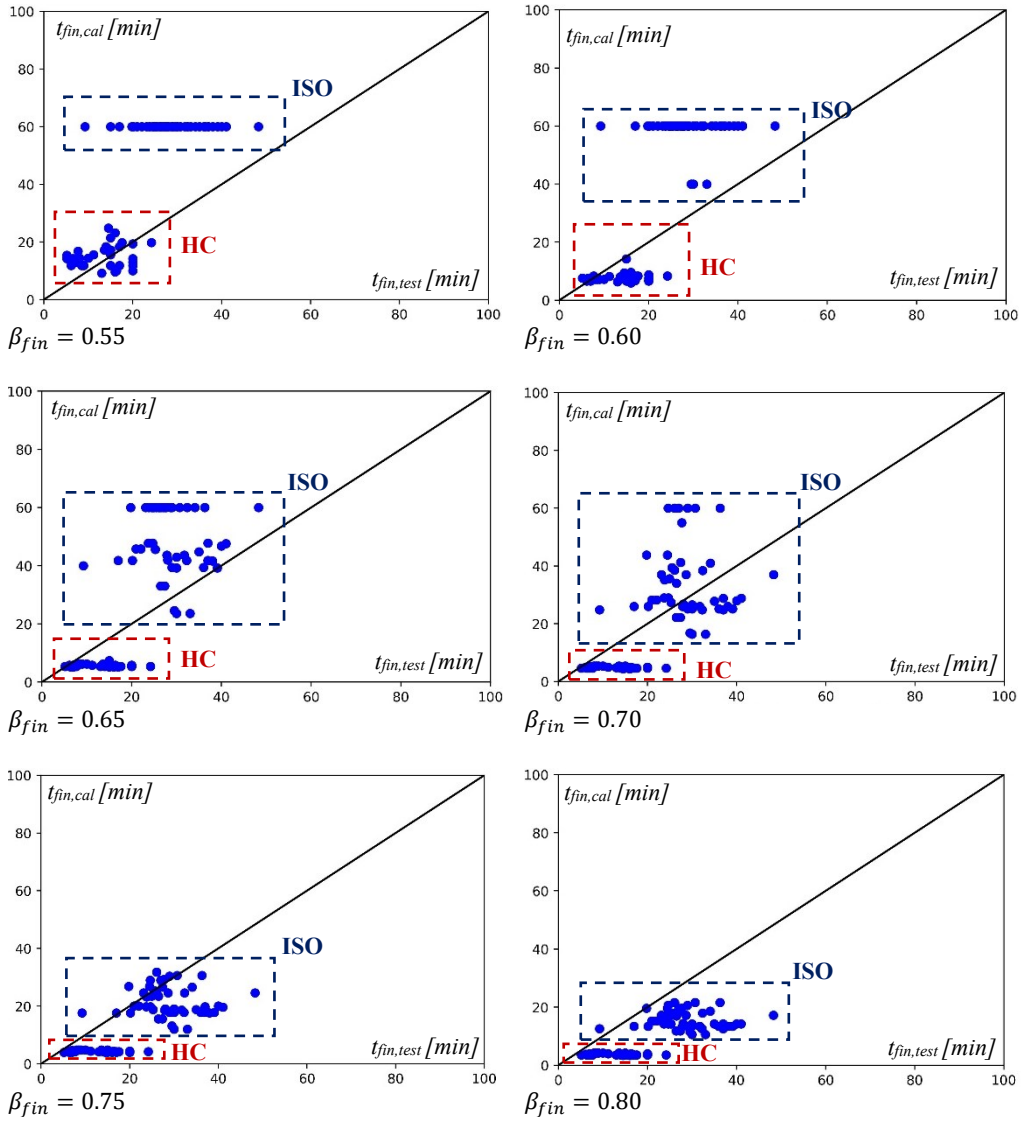


*Figure 53: Analysis of the influence of the $\beta_{fin}$ coefficient on the final spalling time.*

In fact, by observing the graphs in Figure 53, it can be understood that for the samples

subjected to the ISO curve, the influence of $\beta_{fin}$ is the same as that of $\beta_{ini}$.

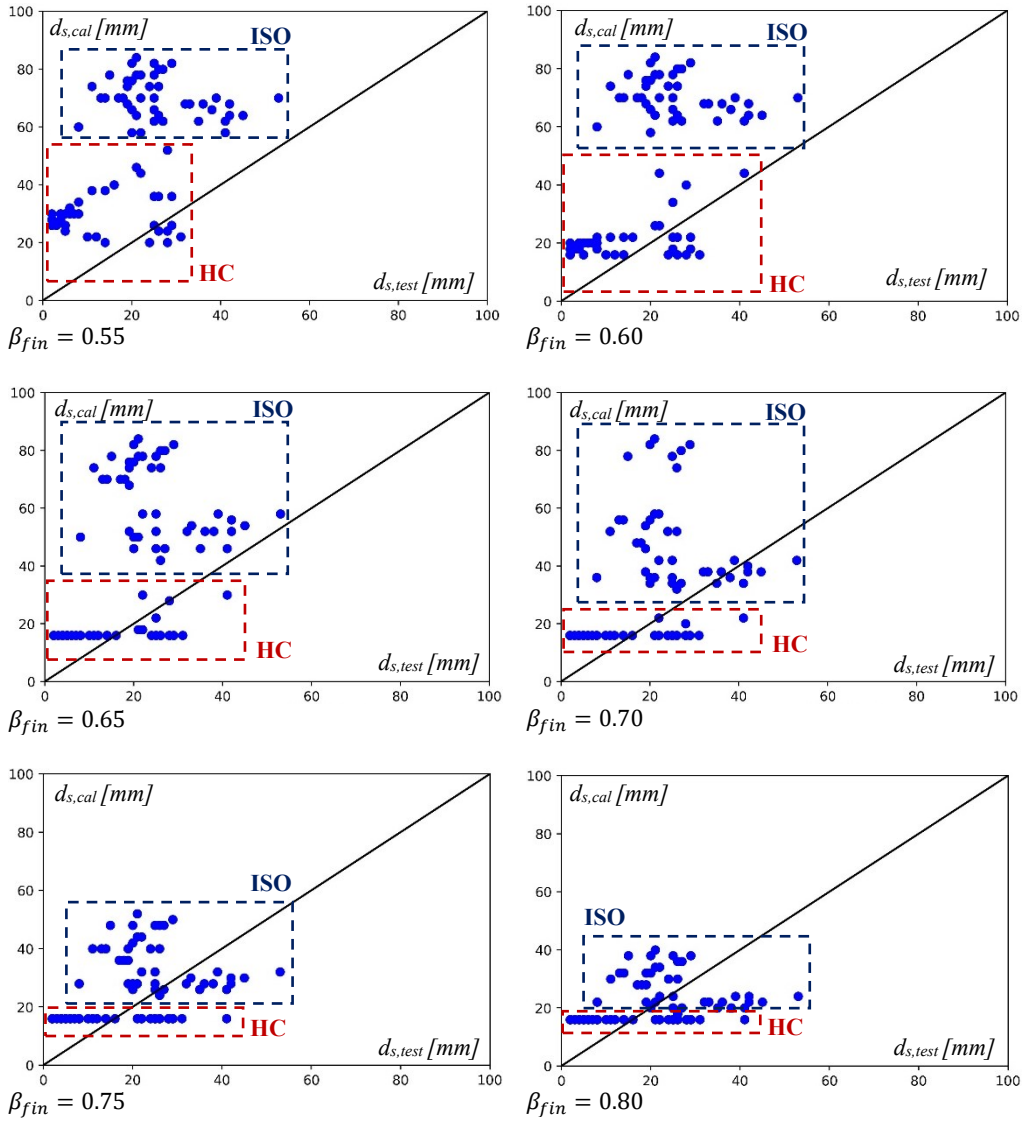


*Figure 54: Analysis of the influence of the $\beta_{fin}$ coefficient on the final spalling depth.*

The samples subjected to the HC curve, on the other hand, exhibit a similar trend in dependence but with worse results as $\beta_{fin}$ increases (as the stiffness of the lateral constraints decreases).

The previous consideration also applies to the values of spalling depth provided by the model. We see that for the elements subjected to the HC fire curve, the constraint assumption that produces the best results is that of a fully fixed element. Conversely, for the samples subjected to the ISO fire curve, the best results are obtained with the assumption of a simply supported element. From the analysed results, it has been understood that it is not possible to assume a unique value for each case study. The first differentiation must be made between $\beta_{ini}$ and $\beta_{fin}$, and subsequently, for both, it is necessary to evaluate a function that allows us to hypothesize them correctly so that the model's results are more consistent with reality. In this regard, an optimization algorithm has been implemented in Python to determine the specific values of $\beta$ that minimize the discrepancy between the experimental results and the calculated ones. Specifically, by constructing an optimization algorithm for the model based on the findings from experimental results, the effective length factor has been parameterized. This parameterization has been particularly applied to the coefficient β, investigating its values within the range (0.5;1). It is noted that the two extreme cases are those of a pinned-pinned column, which corresponds to a coefficient β =1, and a fixed-fixed column, which corresponds to a coefficient β =0.5.

The parameterization was performed by constructing an algorithm in Python that, based on the proposed spalling model, estimates the spalling time (initial and final) and depth for each sample with experimentally known time and depth of spalling by assuming a certain value of β between 0.5 and 1. Subsequently, the algorithm evaluates the mean squared error of the predictions against the experimental results, aiming to minimize it through an iterative process in which β varies. This algorithm allows estimating, for each sample, the value of β that provides the minimum deviation between the calculated and experimentally measured spalling time and depth. It is also specified that, since the proposed model is applicable for evaluating the initial time of the spalling phenomenon, the same optimization of the β value has been performed to estimate the spalling initiation

time. The study of these β values revealed significant variability from specimen to specimen. In particular, a correlation between the β values and the characteristic strength of the concrete used $f_{ck}$ for each specimen was observed (Figure 55).

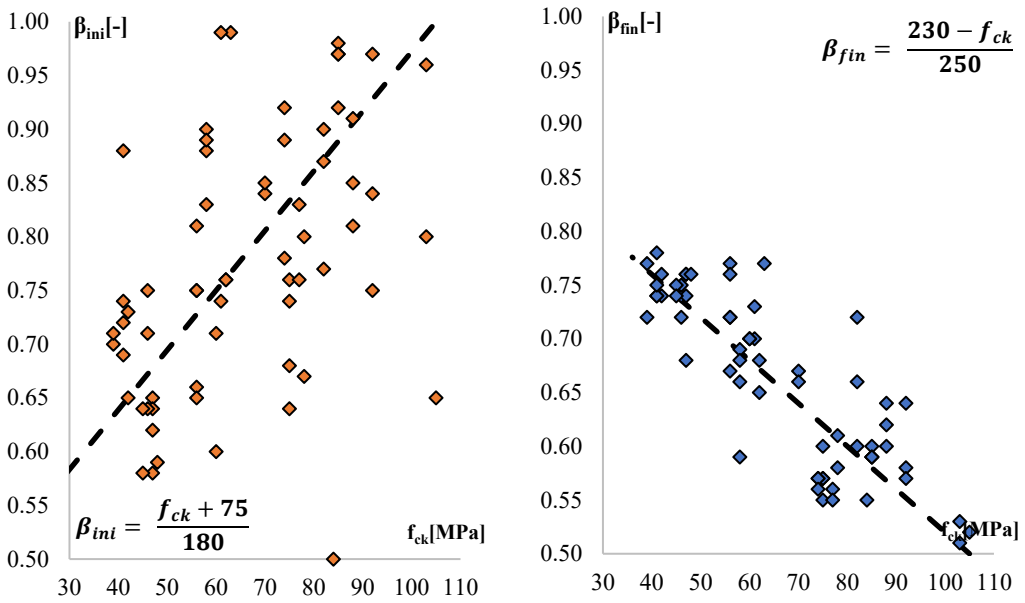


a) b)

*Figure 55: Correlation graphs between the optimal values of $\boldsymbol{\beta}$ and the characteristic strength of the concrete, for $\boldsymbol{\beta_{ini}}$ a) and $\boldsymbol{\beta_{fin}}$ b).*

For these reasons, to increase the precision of the model in evaluating the spalling depth and times, two functions, $\beta_{ini}$ and $\beta_{fin}$, have been introduced in ( 96 ).

$$\beta_{ini} = \frac{f_{ck} + 75}{180}; \qquad \beta_{fin} = \frac{230 - f_{ck}}{250} \tag{84}$$

These functions provide the optimal values of $\beta_{ini}$ and $\beta_{fin}$ based on the varying characteristic strength of the concrete. These values are used to estimate the spalling depth, the initial spalling time, and the final spalling time, as reported in the chart at the Figure 51.

In the following paragraph, the results of applying the proposed spalling model to the samples already studied experimentally are reported and discussed, including a benchmark with the experimental results.

### 4.5.1 Results and benchmarks with experimental data

The previously described model provides much more satisfactory results in terms of the depth and occurrence time of spalling. It is also applicable for evaluating the spalling initiation time, based on the assumption that the minimum thickness of the spalling will be at least equal to the maximum diameter of the aggregate present in the concrete. From this hypothesis, it is indeed possible to apply the entire procedure and determine the corresponding time instant. Subsequently, the integral procedure is applied to obtain the total spalling depth and estimate the time instant when the phenomenon ceases. By knowing the initial and final times, it is also possible to evaluate the duration of the phenomenon $\Delta t$.

First of all, we observe in the graph shown in Figure 56 the comparison between the experimentally measured spalling initiation time $t_{ini,test}$ and the spalling initiation time calculated $t_{ini,cal}$ with the proposed model. Subsequently, following the application of the proposed model as previously discussed, Figure 57 shows the comparison between the calculated spalling end time and the spalling end time measured in the tests. This time instant represents the one calculated with the spalling model analysed by other authors an reported in the paragraph 4.4.3, and it can be observed that the proposed model provides results in terms of timing that are much more in agreement with the experimental ones compared to the previous models. Thanks to the difference between the spalling initiation time and the spalling end time, it is also possible to estimate the duration $\Delta t$, a parameter that emerged in the analysed experimental campaign.

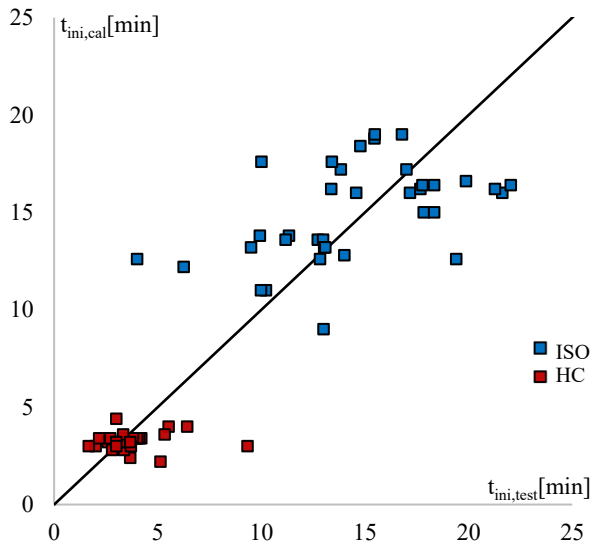


*Figure 56: The benchmark between experimentally measured initiation spalling time $t_{ini,test}$ and the calculated with the proposed model ones $t_{ini,cal}$ .*

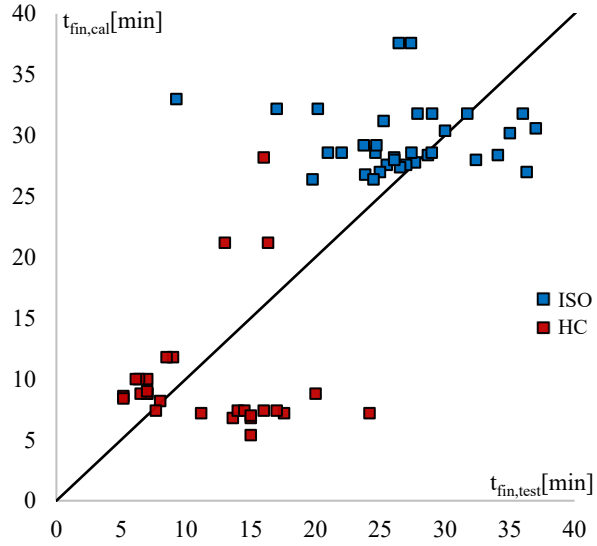


*Figure 57: The benchmark between experimentally measured final spalling time $t_{fin,test}$ and the calculated with the proposed model ones $t_{fin,cal}$ .*

This is shown in Figure 58 and compared with the experimental recordings. From this, it can be observed that for both the specimens subjected to the HC curve and those subjected

to the ISO curve, the results are in excellent agreement with the experimental ones.

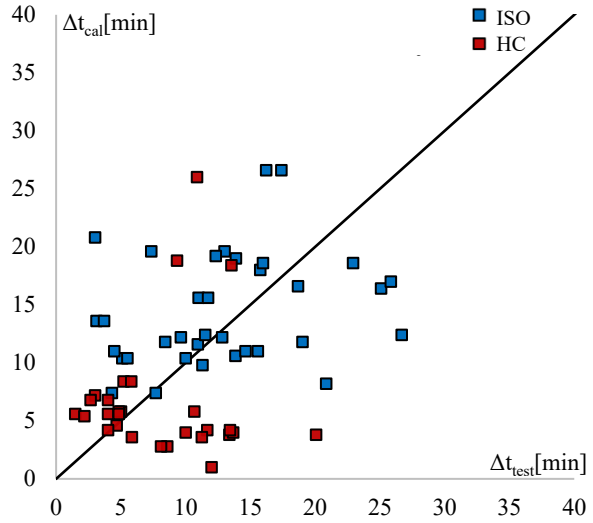


*Figure 58: The benchmark between experimentally measured duration of spalling $\Delta t_{test}$ and the calculated with the proposed model ones $\Delta t_{cal}$ .*

The analysis of the results of the proposed spalling model in terms of spalling depth is also very interesting.

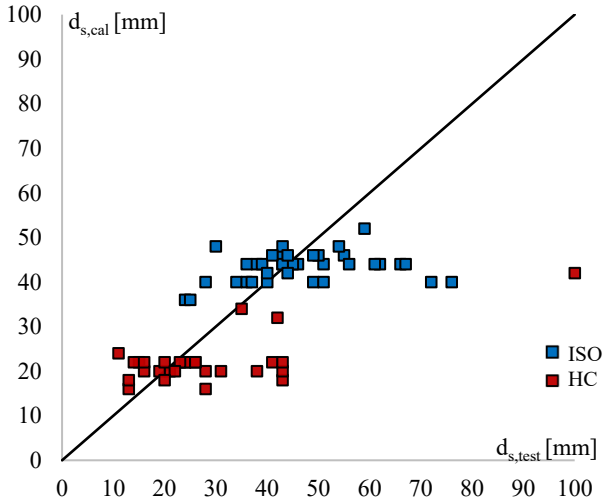


*Figure 59: The benchmark between experimentally measured spalling depth $d_{s,test}$ and the calculated with the proposed model ones $d_{s,cal}$.*

The graph in Figure 59 shows the comparison points of the calculated spalling depth and the measured spalling depth from the analysed experimental campaign. It can be seen

that, compared to the previous model, the results are much more in agreement with the experimental ones, as they are generally lying on the line of equivalence.

From the reported results, it is crucial to reflect on the average deviations that the model returns relative to the quantities it can simulate. We observe that the average deviation between the model's results and the experimental results is 6% in terms of spalling initiation time, 11% in terms of final time, and about 3% in terms of spalling depth. These data indicate that the proposed model, overall, provides excellent results. Despite the model's excellent performance, an in-depth literature review and consideration of the various factors playing a significant role in the spalling phenomenon revealed the high randomness that affects both the predictive model and the actual spalling phenomenon. This reflection led to the study presented in the next paragraph, from which a probabilistic corrective model emerges. This model reduces the error of the proposed spalling model and provides a probabilistic, rather than deterministic, approach to this analysis.

### 4.5.2 Model assumptions and limitations

In theory, the presented spalling model is based on the modelling of two physical phenomena: the formation of the crack and the destabilization of the portion of concrete bounded by the crack and the exposed surface. As observed, these phenomena alone do not fully justify spalling, as it is influenced by a greater number of factors (such as vapor pressure). Nevertheless, they do allow for a satisfactory modelling of spalling, as seen in the previous subsections. In fact, the proposed model is capable of simulating the spalling initiation time, the end time, and the maximum depth, providing results that are largely in good agreement with experimental data. This, theoretically, may suggest that the proposed model has a generalized applicability on a large scale. However, in this work, its applicability was tested in specific cases characterized by defined ranges of mechanical and physical parameters and specific boundary conditions, including fire curves. Therefore, the following summary Table 6 presents all the parameters used in the application

of the model and the ranges of values tested.

*Table 6: Proven validity limits of the proposed model.*

| Fire Curve [-] | Number of exposed sides [-] | Maximum aggregate diameter $d_{max}$ [mm] | External load $\sigma_{ext}$ [MPa] | Moisture Content [Kg/m$^3$] | Concrete Strength $R_{ck}$ [MPa] |
|---|---|---|---|---|---|
| ISO and HC | 1 | ≤ 32 | 0 ÷ 11 | 40 ÷ 66 | 35 ÷ 105 |

It is intuitive to understand that the findings of this work apply only to the cases falling within the limits described above, and that the extension of the results beyond these limits requires further investigation based on experimental data.

### 4.5.3 Model sensitivity analysis

The proposed model was applied to samples tested experimentally and characterized by the variability of certain parameters, such as external tension, concrete resistance, and moisture content. In order to study the model's ability to capture the variability of these parameters, a sensitivity analysis was conducted. This analysis focused on the correlation of the aforementioned parameters with the individual model results, namely the initial spalling time, the final spalling time, the duration, and the depth of the phenomenon. The main results are summarized in the following graphs and related considerations.

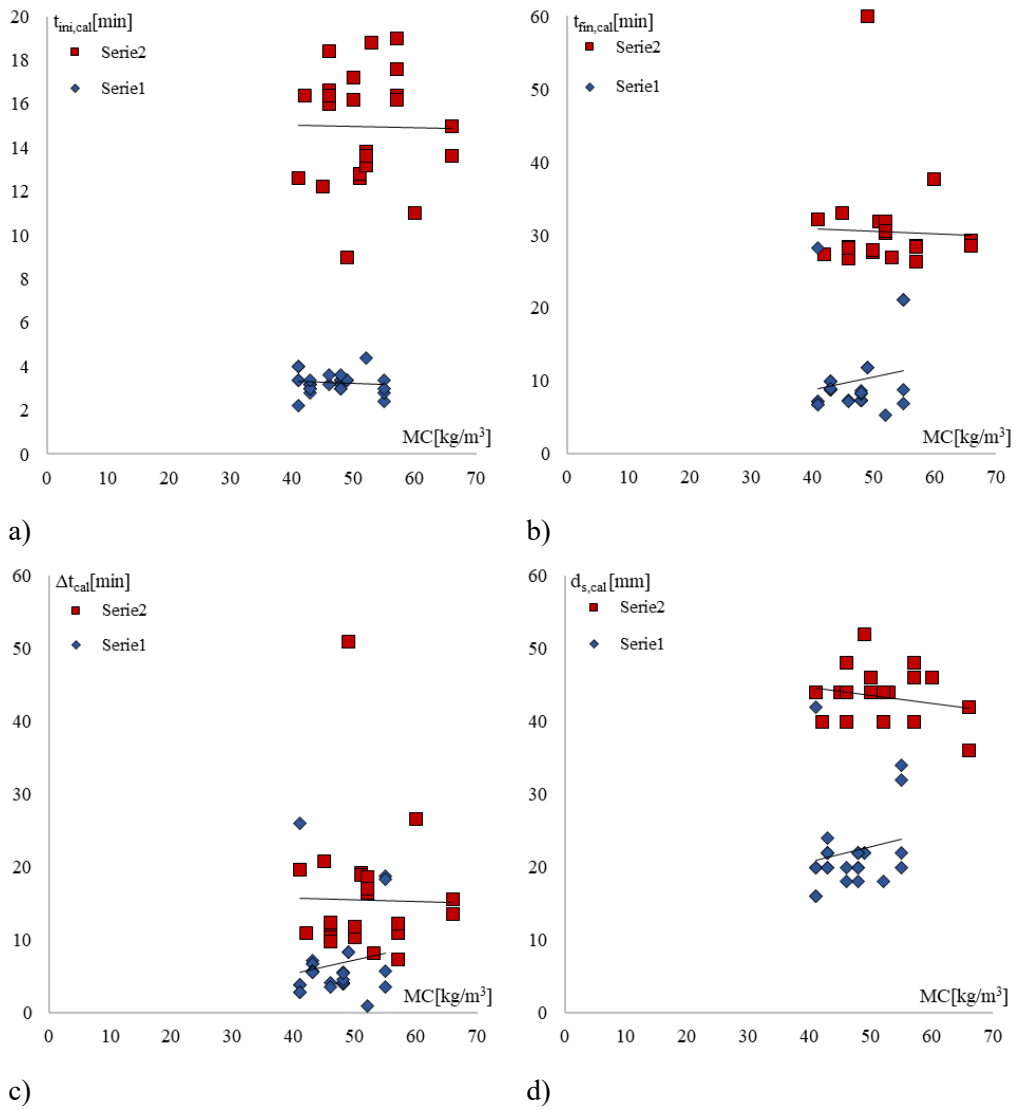


*Figure 60: Representation of the model's sensitivity to the water content, based on the results in terms of initial spalling time a), final spalling time b), spalling duration c), and spalling depth d).*

From the analysis of the model results in terms of initial spalling time, correlated with moisture content, no strong correlation is observed. However, there is a slight tendency for the initial spalling time to decrease as the water content increases. Conversely, the

final spalling time, the spalling duration, and the spalling depth increase with higher water content, especially in the specimens subjected to the HC curve, with a slight opposite trend in those subjected to the ISO curve, as reported in the Figure 60.

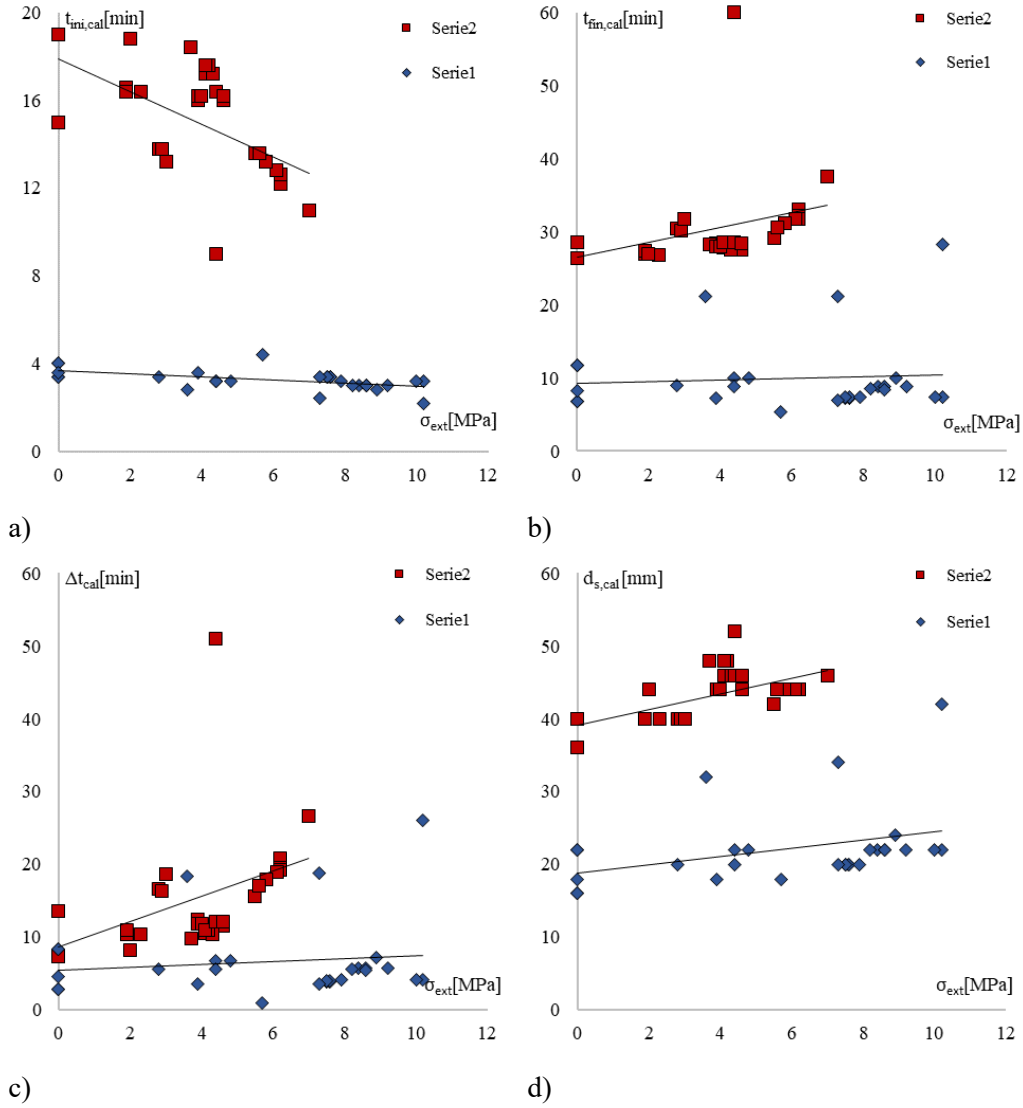


*Figure 61: Representation of the model's sensitivity to the external forces, based on the results in terms of initial spalling time a), final spalling time b), spalling duration c), and spalling depth d).*

From the analysis of the model results in terms of initial spalling time, correlated with external tension, there is a tendency for the onset of spalling to occur earlier as the external tension increases, as reported in the Figure 61.

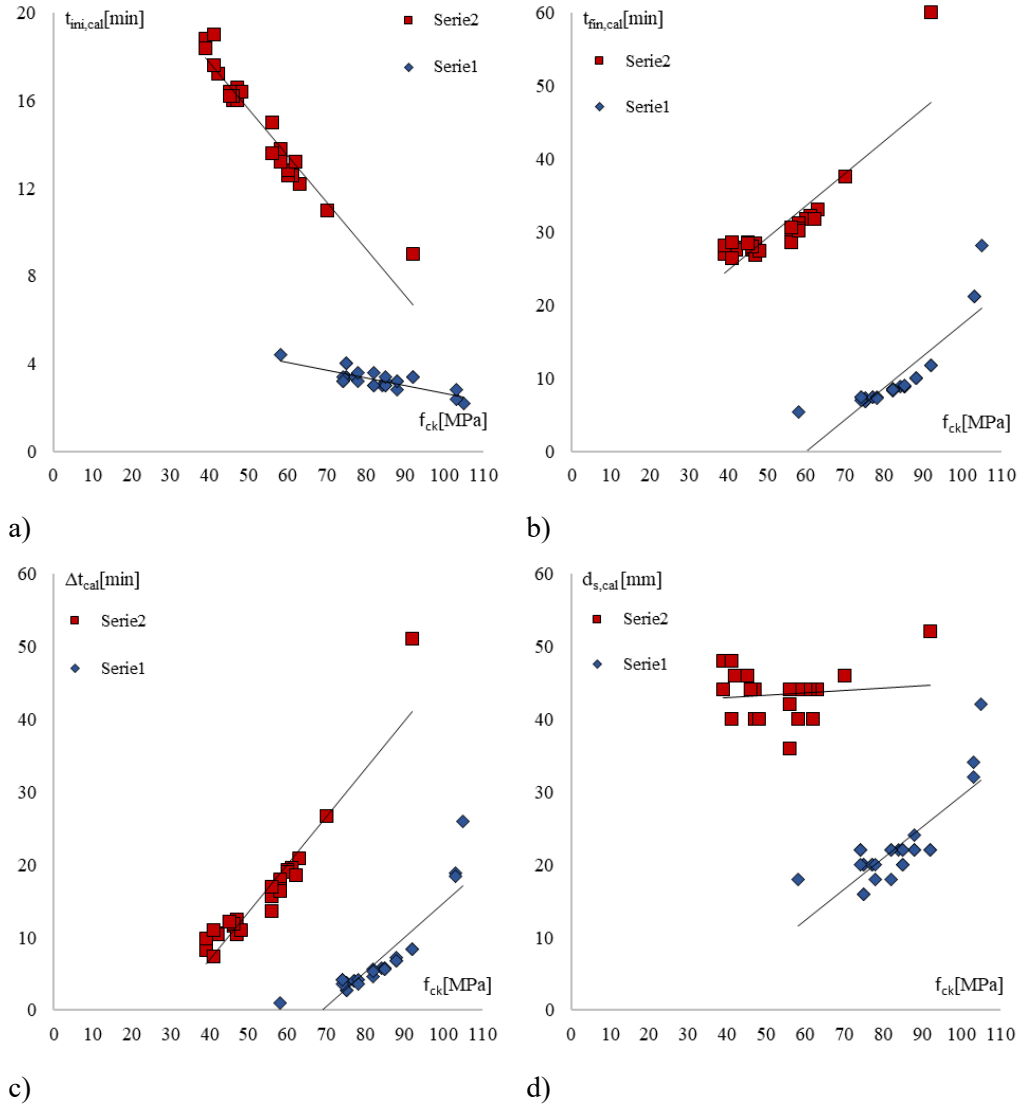


*Figure 62: Representation of the model's sensitivity to concrete strength, based on the results in terms of initial spalling time a), final spalling time b), spalling duration c), and spalling depth d).*

This effect is more evident in the samples subjected to the ISO curve. From the analysis of the model results in terms of final spalling time, duration, and depth, correlated with external tension, there is a tendency for the spalling time to increase as external tension increases. This effect is also more evident in the samples subjected to the ISO curve.

From the analysis of the model results in terms of initial spalling time, correlated with the characteristic strength of the material, there is a tendency for the spalling to begin earlier as the strength increases. This effect is more evident in the samples subjected to the ISO curve. From the analysis of the model results in terms of final spalling time and duration, correlated with the characteristic strength of the material, these increase as the strength increases, for both fire curves. In terms of spalling depth, however, there is a marked incremental trend for the specimens subjected to the HC curve, while it is very slight in the case of the ISO curve, as exposed in the Figure 62.

## 4.6 Proposed spalling model probabilistic correction

The spalling model analysed so far belongs to the circle of deterministic capacity models in structural engineering. These models are typically developed using mechanical relationships based on deterministic input data, calibrated against experimental results.

Consequently, these models fail to explicitly consider the inherent uncertainty in its, leading to biased estimates of capacity. Although deterministic models have been effectively employed for designing secure structures, the demands of contemporary structural engineering, particularly with the introduction of the performance-based design concept, necessitate predictive capacity models that are impartial and explicitly address all prevailing uncertainties.

In the scientific literature, there are several works that, through a Bayesian framework, have led to the development of multivariate probabilistic capacity models for struc-

tural elements that properly account for all prevailing uncertainties, including model errors arising from an inaccurate model form or missing variables, measurement errors, and statistical uncertainty [58]. Over the years, the goal has been set to facilitate their practical use by developing correction terms for existing commonly used deterministic capacity models, rather than creating new capacity models, which adequately address intrinsic bias and uncertainty. Through this approach the proposed model treated in the previous paragraph 4.6 has been upgrading. The probabilistic models and determination of unknown parameters are developed using the formulation presented by [58]. A Bayesian approach is employed to facilitate model updates when additional data become available. The posterior statistics of the parameters are derived through a Monte Carlo simulation, utilizing the procedure outlined by [58]. This procedure can be adapted for parallel computing to decrease computation time [59].

First, this paragraph presents the general formulation of the probabilistic models. Then, the results of the model calibration and the posterior statistics of the unknown model parameters are presented and discussed. Finally, an assessment of the reliability of underground structures in terms of spalling occurrence is proposed, thanks to the application of the probabilistically corrected model.

### 4.6.1 Development of probabilistic models

#### *4.6.1.1 General formulation*

In this framework the *"model"* is a mathematical expression relating more quantities of interest (e.g. moisture content, resistance, stress field, fire curve etc.). The primary objective of the model is to offer a method for forecasting quantities of interest based on specified deterministic or random values of the variables. Based on the general formulation in [58], the probabilistic models are written as exposed in ( 85 ).

$$Y(x, \boldsymbol{\Theta}) = y(x, \boldsymbol{\theta}, \boldsymbol{\lambda}) + \sigma\varepsilon \quad (85)$$

Where **x** is a vector of material, geometric and thermal properties, $\boldsymbol{\Theta} = (\boldsymbol{\theta}, \boldsymbol{\lambda})$ is the set of unknown model parameters, $\sigma\varepsilon$ is the model error in which $\sigma$ is the standard deviation of the model error, $\varepsilon$ is a random variable with zero mean and unit variance. The models are formulated and calibrated under three assumptions:

1. $\sigma$ is independent of **x** (homoskedasticity assumption);
2. $\varepsilon$ follows the normal distribution (normality assumption);
3. the model error can be added to the model (additive assumption.).

Since these three assumptions are generally not satisfied, we apply a variance-stabilizing transformation to approximately meet these assumptions within the data range. The vector of parameter $\boldsymbol{\lambda}$ is used to define the variance stabilizing transformation within a family of possible transformations. One of the transformation available is that proposed by [60] and reported below in the ( 98 ) and the inverse in the ( 99 ).

$$f_\lambda(\cdot) = \begin{cases} \dfrac{(\cdot)^\lambda - (\cdot)^{-\lambda}}{2\lambda} & if\ \lambda \neq 0 \\ l(\cdot) & if\ \lambda = 0 \end{cases} \quad (86)$$

$$f_\lambda^{-1}(\cdot) = \begin{cases} \left(\lambda(\cdot) + \sqrt{1 + \lambda^2(\cdot)^2}\right)^{\frac{1}{\lambda}} & if\ \lambda \neq 0 \\ e^{(\cdot)} & if\ \lambda = 0 \end{cases} \quad (87)$$

Such functions show properties like the well-known power transformation [61], but without the long-standing truncation problem. In this application the $\boldsymbol{\lambda}$=$\lambda$=0 is used.

### *4.6.1.2 Bayesian updating and determination of posterior statistics*

In a Bayesian approach, the unknown model parameters are estimated through

the specific updating rule updating rule reported in the relation ( 100 ).

$$p(\boldsymbol{\Theta}|\mathbf{y}) = \kappa L(\boldsymbol{\Theta}|\mathbf{y})p(\boldsymbol{\Theta}) \quad (88)$$

Where $p(\boldsymbol{\Theta}|\mathbf{y})$ is the posterior distribution that reflects the updated state of information about $\boldsymbol{\Theta}$, $L(\boldsymbol{\Theta}|\mathbf{y})$is the likelihood function which captures the information from the data vector of *n* observations, $\mathbf{y}' = (y_1, y_2, \ldots, y_n)$, $p(\boldsymbol{\Theta})$ is the prior distribution which represents the information available before collecting the data, and $\kappa = [\int L(\boldsymbol{\Theta}|\mathbf{y})p(\boldsymbol{\Theta})d\boldsymbol{\Theta}]^{-1}$ is the normalizing factor. More specifically, the likelihood function is proportional to the probability of seeing the data. In the [58] the authors give a general formulation of the likelihood function that considers different types of data (i.e., equality data - when the quantity of interest is measured, and lower-/upper- bound data - when a smaller or larger value is measured).

The computation of posterior statistics can be very complex, especially when a large number of parameters is to be determined. In order to simplify this procedure the authors in [58] give an important sampling algorithm that allows to compute a common integral *I* which provides the desired posterior statistics. The general form of the integral *I* is reported in ( 101 ).

$$I = \int B(\boldsymbol{\Theta})d\boldsymbol{\Theta} \quad (89)$$

where the integrand is $B(\boldsymbol{\Theta}) = w(\boldsymbol{\Theta})L(\boldsymbol{\Theta})p(\boldsymbol{\Theta})$. If $w(\boldsymbol{\Theta}) = 1$ is selected we obtain $I = 1/\kappa$. If $w(\boldsymbol{\Theta}) = \kappa\boldsymbol{\Theta}$ is selected we have the mean$I = \mathbf{M}_{\boldsymbol{\Theta}}$, and finally if$w(\boldsymbol{\Theta}) = \kappa\boldsymbol{\Theta}\boldsymbol{\Theta}'$, then $I = \mathbb{E}[\boldsymbol{\Theta}\boldsymbol{\Theta}']$, from which we can determine the covariance matrix $\Sigma_{\boldsymbol{\Theta}\boldsymbol{\Theta}} = \mathbb{E}[\boldsymbol{\Theta}\boldsymbol{\Theta}'] - \mathbf{M}_{\boldsymbol{\Theta}}\mathbf{M}'_{\boldsymbol{\Theta}}$. By using an importance sampling density$S(\boldsymbol{\Theta})$, the Bayesian integrand can be modified as showed in the relation.

$$I = \int \left[\frac{B(\boldsymbol{\Theta})}{S(\boldsymbol{\Theta})}\right] S(\boldsymbol{\Theta}) d\boldsymbol{\Theta} \quad (90)$$

Considering $N$ total random realizations, we have the estimation of the previous relation as the relation ( 91 ).

$$\bar{I} = \frac{1}{N}\sum_{i=1}^{N}\frac{B(\boldsymbol{\Theta}_i)}{S(\boldsymbol{\Theta}_i)} \quad (91)$$

As a termination criterion, it's possible to set that the maximum coefficient of variation (COV), expressed as reported in ( 92 ), be sufficiently small (e.g., less than 0.02).

$$\mathrm{COV}\left(\frac{\boldsymbol{\Theta}}{\kappa}\right) = \frac{\sqrt{\frac{1}{N}\sum_{i=1}^{N}\left[\frac{\boldsymbol{\Theta}_i L(\boldsymbol{\Theta}_i) p(\boldsymbol{\Theta}_i)}{S(\boldsymbol{\Theta}_i)}\right]^2 - \left\{\frac{1}{N}\sum_{i=1}^{N}\left[\frac{\boldsymbol{\Theta}_i L(\boldsymbol{\Theta}_i) p(\boldsymbol{\Theta}_i)}{S(\boldsymbol{\Theta}_i)}\right]\right\}^2}}{\frac{1}{N}\sum_{i=1}^{N}\left[\frac{\boldsymbol{\Theta}_i L(\boldsymbol{\Theta}_i) p(\boldsymbol{\Theta}_i)}{S(\boldsymbol{\Theta}_i)}\right]} \quad (92)$$

## 4.6.2 Formulation of probabilistic models for the time of occurrence and depth of spalling

### *4.6.2.1 Formulation of the probabilistic model*

In this probabilistic model we propose to define $\xi$ as the generic spalling property (e.g., $\xi$ = ISO,$t$ for the time of spalling occurrence in case of exposure to the ISO curve, $\xi$ = ISO,$d$ for the related depth of spalled concrete). On the basis of the idea of [58], the probabilistic model can assume a formulation expressed by the following equation:

$$\ln\left[\xi\left(\mathbf{x}, \boldsymbol{\Theta}_\xi\right)\right] = y_\xi\left(\mathbf{x}, \boldsymbol{\Theta}_\xi\right) = \hat{y}_\xi(\mathbf{x}) + \gamma_\xi\left(\mathbf{x}, \boldsymbol{\theta}_\xi\right) + \sigma_\xi \varepsilon \quad (93)$$

Where $\boldsymbol{\Theta}_{\xi} = (\boldsymbol{\theta}_{\xi}, \sigma_{\xi})$ is a global set of unknown parameters, in which $\sigma_{\xi}$ is the standard deviation of the model error and $\boldsymbol{\theta}_{\xi}$ represents the subset of the unknown parameters. The expression $\hat{y}_{\xi}(\mathbf{x}) = \ln[\hat{\xi}(\mathbf{x})]$ is the deterministic model and $\gamma_{\xi}(\mathbf{x}, \boldsymbol{\theta}_{\xi})$ is the correction term.

#### *4.6.2.2 Deterministic model*

The proposed probabilistic correction model is applied to a deterministic model capable of simulating the spalling phenomenon in terms of initial time, duration, and depth of spalling. These results are made possible through the application of the model proposed in paragraph 4.5. To summarize, the input parameters for the model are stress due to external load, stress due to the thermal expansion restrained, mechanical and thermal properties of materials, geometry and the fire curve applied on the structural elements. The calculation procedure of the model is summarized in the chart shown in Figure 50. As mentioned earlier, the proposed deterministic spalling model, even based on comparisons with experimental findings in paragraph 4.5.1, exhibits a series of errors and uncertainties that lead to a deviation from the results. Therefore, in order to make the model more reliable, probabilistic corrective model is applied, based on experimental findings, obtaining the results exposed in the following paragraphs.

#### *4.6.2.3 Models' corrections*

As seen in the paragraph 4.6.2.1 the first step related to the probabilistic correction is the definition of the correction terms $\gamma_{\xi}(\mathbf{x}, \boldsymbol{\theta}_{\xi})$. Referring again to [58], the correction terms could be written as a complete first order polynomial ( 94 ).

$$\gamma_{\xi}(\mathbf{x}, \boldsymbol{\theta}_{\xi}) = \boldsymbol{\Theta}_{\xi}^{T}\mathbf{h}(\mathbf{x}) = \sum_{i=0}^{n} \boldsymbol{\theta}_{\xi,i} + h_i(\mathbf{x}) \qquad (94)$$

Where $\mathbf{h}$ is a vector that contain the explanatory functions $h_i(\mathbf{x})$ which could be obtained

through the transformation reported in equations ( 86 ) and ( 87 ). This transformation could be used to a set of basis functions expressed as $\eta_{k,i}(\mathbf{x}_k)$, that are equal to ( 95 ).

$$h_i(\mathbf{x}) = \ln\left[\eta_i(\mathbf{x})\right] \quad (95)$$

The development of the proposed probabilistic model needs to set the first candidate explanatory function $h_o(\mathbf{x}) = 1$, in order to capture the potential bias of the deterministic models of each of the two components, that is not affect by $\mathbf{x}$. To thoroughly examine potential biases linked to each component of $\mathbf{x}$, we additionally evaluate $\eta_1(\mathbf{x}) = \sigma_c/\mathrm{f}_c$ , $\eta_2(\mathbf{x}) = u$ and $\eta_3(\mathbf{x}) = \mathrm{t}_{28}/\mathrm{t}_{Age}$.

#### *4.6.2.4 Model selection*

The set of available data $(\boldsymbol{y}_\xi, \mathbf{x})$ for each sample can help simplify the model through a *stepwise deletion process*. This process was developed in [58] and it is applicable to all types of data. The simplification process involves removing terms with little influence, resulting in a more streamlined form of the model. Diagnostic plots at each step of the process, as indicated by [62], lead to confirm the normality assumption of the model error. In particular, the stepwise deletion process consists in the steps exposed below:

1. Starting from the indication of [63], the posterior mode and the related approximation of covariance matrix ( 96 ) of the parameters $\boldsymbol{\Theta}_\xi$ could be compute;

$$\sum_{\boldsymbol{\Theta}_\xi, \boldsymbol{\Theta}_\xi} -\left\{\nabla\nabla \ln\left[L(\boldsymbol{\Theta}_\xi|\mathbf{y}_\xi)p(\boldsymbol{\Theta}_\xi)\right]\right\}^{-1} \quad (96)$$

2. Identify the term $h_i(\mathbf{x})$ for which the coefficient $\boldsymbol{\theta}_\xi$ exhibits the highest coefficient of variation (C.o.V.). This particular term is considered the least informative among all the explanatory functions, and there is an option to omit it from the correction

term $\gamma_{\xi}(\mathbf{x}, \boldsymbol{\theta}_{\xi})$;

3. Evaluate the reduced model by examining whether the value of $\sigma_{\xi}$ has not experienced an unacceptable increase. If the increase is deemed acceptable, accept the reduced model and proceed to repeat steps **1** and **2** for additional reductions. However, if the performed reduction leads to an undesirable increase in $\sigma_{\xi}$, maintain the model in its original form before the reduction, as it is considered as parsimonious as possible;

4. Calculate the posterior statistics of the parameters $\boldsymbol{\Theta}_{\xi}$ as outlined in 4.6.1.2. It is important to highlight that the determination of the unacceptability of the increase in $\sigma_{\xi}$ is contingent upon the desired level of accuracy and, concurrently, parsimony for the specific problem at hand.

## 4.6.3 Calibration procedure for proposed probabilistic model

### *4.6.3.1 Datasets used to calibrate the probabilistic models*

In order to calibrate the probabilistic models its necessary to individuate the database based on the experimental tests results. The experimental campaign referred to is discussed in paragraph 4.2. At the SP Technical Research Institute of Sweden, an extensive experimental study was conducted on the behavior of self-compacting concrete when exposed to fire. Over 200 fire tests were performed on about 50 types of self-compacting concrete, examining factors such as compressive load, fire curve, and concrete admixture. Results showed that orthogonal load levels did not significantly influence spalling, whereas membrane pressure did. The tests used small slabs (600 x 500 x 200 mm) without reinforcement, except for post-stress bars for applying external compressive load. Tests were conducted in a small furnace with a clear opening of 500 x 400 mm, with

specimens placed horizontally and exposed to fire on one side. Spalling depth was measured in a grid pattern, excluding boundary measurements due to uncertainty. The results used are summarized in Table 3 exposed in the paragraph 4.4.1 and they represent the basis for calibrating the probabilistic correction model we are applying.

#### *4.6.3.2 Bayesian updating, definition of the likelihood function and prior distribution*

Defined the data set to calibrate the probabilistic model its necessary, for every data, to perform the Bayesian update using the rule written in ( 97 ).

$$p(\boldsymbol{\Theta}_\xi|\mathbf{y}_\xi) = k_\xi L(\boldsymbol{\Theta}_\xi|\mathbf{y}_\xi)p(\boldsymbol{\Theta}_\xi) \quad (97)$$

Where $p(\boldsymbol{\Theta}_\xi|\mathbf{y}_\xi)$ is the posterior distribution of the unknown parameters $\boldsymbol{\Theta}_\xi$, $L(\boldsymbol{\Theta}_\xi|\mathbf{y}_\xi)$ is the likelihood function, $p(\boldsymbol{\Theta}_\xi)$ is the prior distribution and ( 98 ) is the normalizing factor.

$$k_\xi = \left[\int L(\boldsymbol{\Theta}_\xi|\mathbf{y}_\xi)p(\boldsymbol{\Theta}_\xi)d\boldsymbol{\Theta}_\xi\right]^{-1} \quad (98)$$

In the case treated the values of *spalling time* $\mathrm{t}_s$ and *spalling depth* $\mathrm{d}_s$ lead to the expression of *l-th* residual $r_{\xi,l}$ related to the transformed reading $y_{\xi,l}$, reported in the relation ( 99 ).

$$r_{\xi,l}(\boldsymbol{\Theta}_\xi) = y_{\xi,l} - \hat{y}_\xi(\mathbf{x}_l) - \gamma_\xi(\mathbf{x}_l, \boldsymbol{\theta}_\xi) \quad (99)$$

Where

$$r_{\xi,l}(\boldsymbol{\Theta}_\xi) = \sigma_\xi \cdot \varepsilon_l \quad (100)$$

Thanks to the assumption of statistically independent observations it's possible to obtain

the general form of likelihood function as reported in ( 101 ).

$$L(\boldsymbol{\theta}_{\xi}, \sigma_{\xi} | y_{\xi}) \propto \prod_{l} P[\sigma_{\xi} \varepsilon_{l} = r_{\xi,l}(\boldsymbol{\theta}_{\xi})] \qquad (101)$$

Then, considering that $\varepsilon$ has a *standard normal distribution*, the relation ( 101 ) could be expressed as reported in ( 102 ).

$$L(\boldsymbol{\theta}_{\xi}, \sigma_{\xi} | y_{\xi}) \propto \prod_{l} \left\{ \frac{1}{\sigma_{\xi}} \varphi \left[ \frac{r_{\xi,l}(\boldsymbol{\theta}_{\xi})}{\sigma_{\xi}} \right] \right\} \qquad (102)$$

Where $\varphi$ represents the *standard normal probability density function*.

Given a non-informative prior distribution for the parameters $\boldsymbol{\theta}_{\xi}$, following the approach in [64], it can be demonstrated that the prior is locally uniform. Additionally, in accordance with [58], for $\sigma_{\xi}$, we adopt a prior distribution $p(\sigma_{\xi}) \propto \frac{1}{\sigma_{\xi}}$. Consequently, the prior distribution takes the form as described in the relation ( 103 ).

$$p(\boldsymbol{\Theta}_{\xi}) \propto \frac{1}{\sigma_{\xi}} \qquad (103)$$

### 4.6.4 Calibrated probabilistic models

The results of the stepwise deletion and the estimation of the posterior statistics for the parameters $\boldsymbol{\Theta}_{\mathbf{ISO,t}}$ and $\boldsymbol{\Theta}_{\mathbf{HC,t}}$ are presented here, considering two sets of data obtained from tests conducted on the ISO and HC curves (hereafter described as Fire Curves FC), for the estimation of the spalling time occurrence and spalling depth.

#### *4.6.4.1 Probabilistic model for the initiation spalling time*

Initially, with the complete model incorporating all candidate explanatory functions and utilizing the first set of data ($\mathbf{y}_{\mathrm{t_{ini}}}$, $\mathbf{x}$) regarding the specimens subjected at first to ISO curve and then to HC curve, it is observed that the parameter $\theta_1$ exhibits the largest Coefficient of Variation (C.o.V.); to simplify the model, the term $\frac{\sigma_{ext}}{fc}$ is then dropped. Subsequently, the reduced model is assessed, and the stepwise deletion process is repeated. After four steps, the model selection process identifies that the explanatory basis functions do not alter significantly the posterior mode standard deviation $\sigma$. Figure 63 provides a summary of the stepwise deletion, displaying the C.o.V. values of the model parameters and the posterior mode of the model standard deviation σ. The posterior statistics, referred to stepwise deletion process above, was reported in the Table 7, and it define the following form of the probabilistic model (104 ) and ( 105 ).

$$\mathrm{y}_{\mathrm{t_{ini}}}\left(\mathbf{x}, \boldsymbol{\Theta}_{\mathbf{t_{ini}}}\right) = ln\left[\mathrm{t}_{\mathrm{ini}}\left(\mathbf{x}, \sigma_{\mathrm{t_{ini}}}\right)\right] \quad (104)$$

$$\ln\left[t(\mathbf{x}, \sigma_{\mathrm{t_{ini}}})\right] = ln(\hat{t}_{\mathrm{ini}}) + \sigma_{\mathrm{t_{ini}}}\varepsilon \quad (105)$$

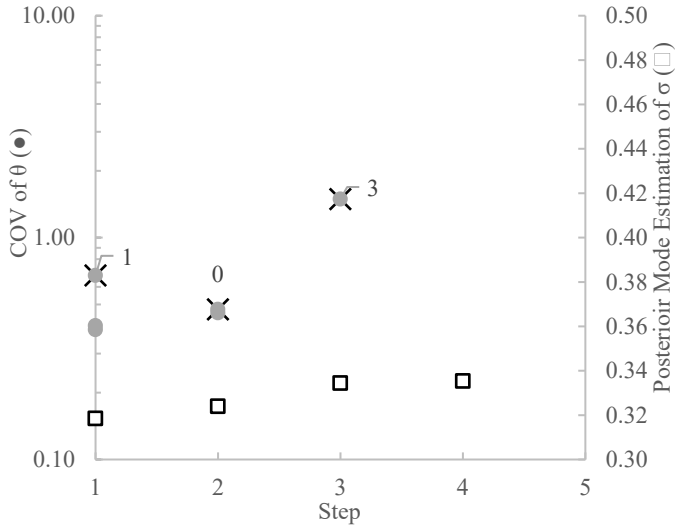


*Figure 63: Stepwise deletion process of the initiation time of spalling occurrence, using the set of experimental data.*

*Table 7: Posterior statistics of parameters in the model of initiation time of spalling occurrence.*

| | $\sigma_{t_{ini}}$ |
|---|---|
| Mean | 0.34 |
| SD | 0.029 |

A comparison between the measured and predicted initiation time of spalling ratio for specimens, on both deterministic Figure 56 and probabilistic corrected models Figure 64, is presented. In an ideal scenario, for a perfect model, any comparison point of results should align along the 1:1 dashed line.

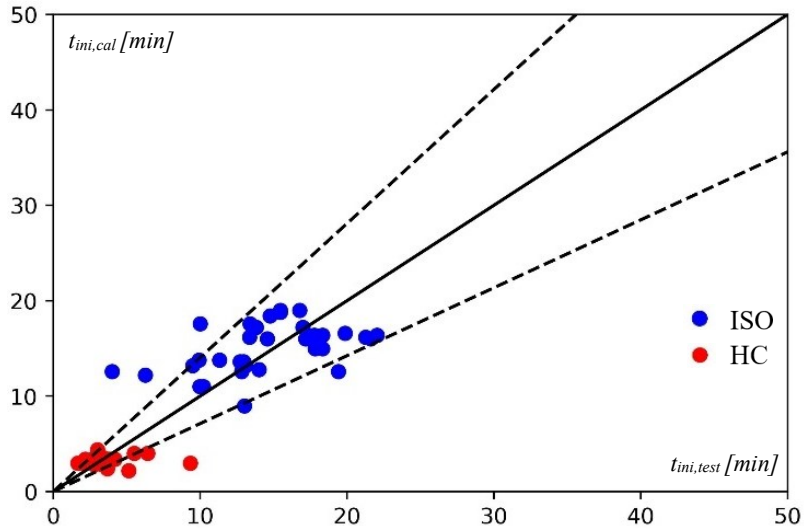


*Figure 64: Comparison between experimental and probabilistic model of initiation spalling time.*

It is possible to observe how, through probabilistic correction, corrected results of the deterministic model can be obtained using parameters based on experimental findings.

### *4.6.4.2 Probabilistic model for the spalling duration*

As for the initiation spalling time, also for the duration the stepwise deletion has

been applied. Thaks this process the member reduction of elements of $\boldsymbol{\Theta_{\Delta t}}$ for the spalling duration has been done. The graph in the Figure 65 summarizes the stepwise deletion process. The posterior statistics, reported in Table 4, define the following form of the probabilistic model described in (106 ) and ( 107 ).

$$y_{\Delta t}(\mathbf{x}, \boldsymbol{\Theta}_{\Delta t}) = ln[\Delta t(\mathbf{x}, \boldsymbol{\Theta}_{\Delta t})] \quad (106)$$

$$\ln[\Delta t(\mathbf{x}, \boldsymbol{\Theta}_{\Delta t})] = \ln(\widehat{\Delta t}) + \theta_{\Delta t,1} \frac{\sigma_c}{f_c} + \theta_{\Delta t,2} u + \sigma_{\Delta t} \varepsilon \quad (107)$$

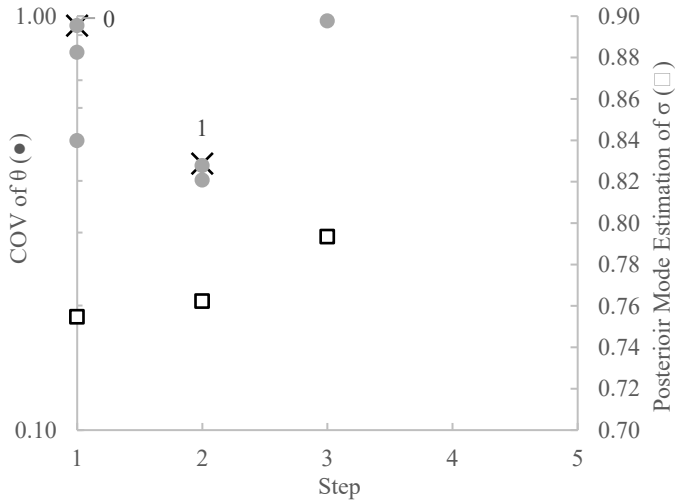


*Figure 65: Stepwise deletion process of the spalling duration.*

*Table 8: Posterior statistics of parameters in the model of the spalling duration.*

| | $\boldsymbol{\theta_{\Delta t,1}}$ | $\boldsymbol{\theta_{\Delta t,2}}$ | $\boldsymbol{\sigma_{\Delta t}}$ |
|---|---|---|---|
| Mean | - 0.01 | 5.23 | 0.81 |
| SD | 0.009 | 6.927 | 0.076 |
| **Correlation Coefficient** | | | |
| $\boldsymbol{\theta_{\Delta t,2}}$ | - 0.959 | | |
| $\boldsymbol{\sigma_{\Delta t}}$ | - 0.047 | - 0.062 | |

Following the application of stepwise deletion and the evaluation of correlation coefficients, it is possible to apply the optimized probabilistic model to the duration of spalling as well. This application yields new values for the duration of the spalling phenomenon, corrected with a probabilistic term that makes them even more consistent with the experimental results, as shown in Figure 66.

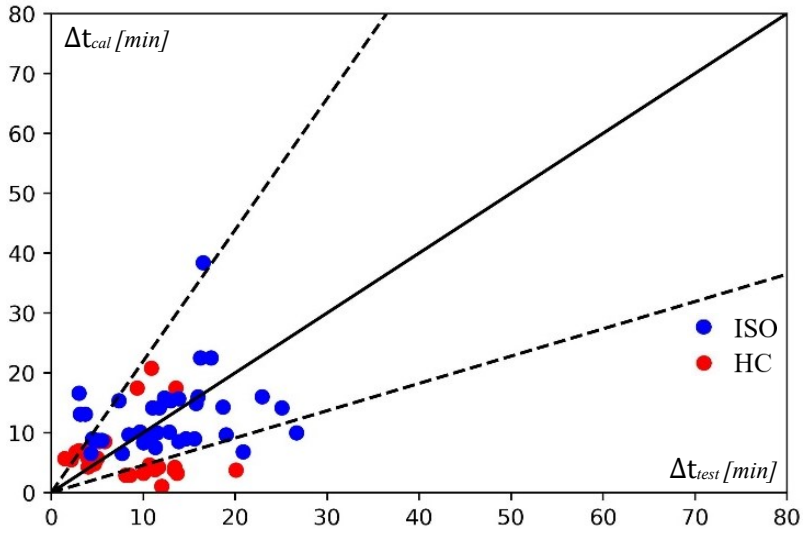


*Figure 66: Comparison between experimental and probabilistic model of spalling duration.*

### *4.6.4.3 Probabilistic model for the spalling depth*

As for the spalling initiation time and duration, the stepwise deletion is performed to reduce number of elements of $\boldsymbol{\Theta_d}$ regarding the depth of spalling. The stepwise deletion process could be summarized in the graph reported in Figure 68 while the posterior statistics results in the Table 9. These results allow for the definition of the present probabilistic model described in equations (108 ) and ( 109 ).

$$\mathrm{y_d}(\mathbf{x}, \boldsymbol{\Theta_d}) = ln[\mathrm{d}(\mathbf{x}, \boldsymbol{\Theta_d})] \tag{108}$$

$$\ln[\mathbf{d}(\mathbf{x}, \boldsymbol{\Theta_d})] = \ln(\hat{\mathrm{d}}) + \theta_{\mathrm{d},1}\frac{\sigma_c}{f_c} + \theta_{\mathrm{d},2}u + \sigma_{\mathrm{d}}\varepsilon \tag{109}$$

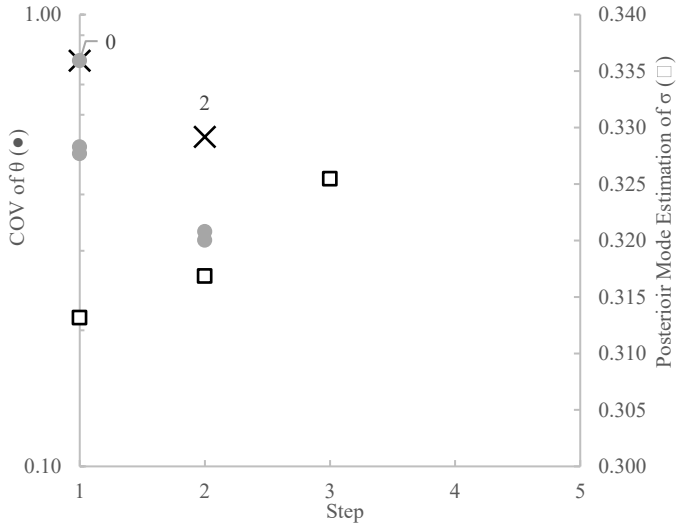


*Figure 67: Stepwise deletion process of the spalling depth.*

*Table 9: Posterior statistics of parameters in the model of the spalling depth.*

| | $\theta_{d,1}$ | $\theta_{d,2}$ | $\sigma_d$ |
|---|---|---|---|
| **Mean** | 2.82 | - 2.78 | 0.33 |
| **SD** | 0.918 | 1.553 | 0.030 |
| **Correlation Coefficient** | | | |
| $\theta_{d,2}$ | - 0.832 | | |
| $\sigma_d$ | - 0.021 | 0.010 | |

Following the application of stepwise deletion and the evaluation of correlation coefficients, it is possible to apply the optimized probabilistic model to the spalling depth as well. This application yields new values for the spalling depth, corrected with a probabilistic term that makes them even more consistent with the experimental results, as shown in Figure 68.

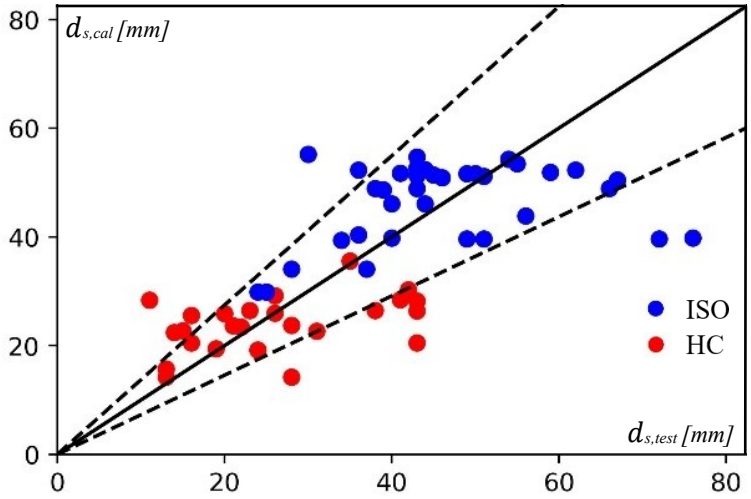


*Figure 68: Comparison between experimental and deterministic model spalling depth.*

Comparing the graphs of the deterministic model, the probabilistically corrected model, and the experimental results shows an improvement with the probabilistic correction. This is evidenced by the reduction in bias between the calculated and experimental results. However, the improvement is not very pronounced, especially regarding the spalling time. This outcome was predictable following the stepwise deletion process. We observed that many of the experimental calibration parameters do not have a significant correlation with the recorded spalling results. This is understandable since many parameters govern the phenomenon, and only some were recorded during the experimental phase. Therefore, by calibrating the presented probabilistic models on experimental results richer in information and correlations, we could achieve more satisfactory corrections that reduce the bias between the experimental evidence and the modelling results in terms of spalling time and depth.

## 4.7 Reliability from spalling point of view

The probabilistic spalling models, developed in the previous sections, can be applied to assess the fragility function to estimate the probability of spalling occurrence for any type of concrete tunnel linings subjected to fire described by ISO and HC curves, with specified geometry, applied forces, mechanical and thermal properties. The computational framework for this purpose is described in [58].

As previously mentioned in paragraph 4.2, we will examine the specimens outlined in the report on the experimental campaign, which feature geometries, external forces, and material properties that reflect those of modern RC underground structures.

The fragility is the conditional probability of failure given one or more measures of demand $(d)$. The predictive fragility estimate $\tilde{P}(d)$ is the expected fragility estimate with respect to the distribution of the model parameters $\boldsymbol{\Theta}$. This estimate considers the effect of epistemic uncertainties (uncertainty in the model parameters) in an average sense. Confidence bounds at specified probability levels provide an explicit account of the variability in the fragility estimate due to epistemic uncertainties.

The predictive probability of occurrence of the spalling phenomenon in each time of exposure to the ISO/HC curve can be calculated as reported in ( 110 ).

$$\tilde{P}(E_I|\, t) = \tilde{P}\left[t_{\text{ini}}\left(\boldsymbol{\Theta}_{t_{\text{ini}}}, \mathbf{x}\right) - t \le 0 \middle| t\right] = \\ = \int_{t_{\text{ini}}\left(\boldsymbol{\Theta}_{t_{\text{ini}}}\mathbf{x}\right)-t\le 0} f\left(\boldsymbol{\Theta}_{t_{\text{ini}}}, \mathbf{x}\right) d\boldsymbol{\Theta}_{t_{\text{ini}}} d\mathbf{x} \qquad (110)$$

The predictive probability of exceedance of a certain pre-set limit of spalling depth in a given period of fire exposure can be calculated as exposed in the relation ( 111 ).

$$\tilde{P}\{[(d_{\lim} - d(\boldsymbol{\Theta}_d, \mathbf{x}) \leq 0) \cap (t_{\text{ini}}(\boldsymbol{\Theta}_{t0}, \mathbf{x}) + \Delta t(\boldsymbol{\Theta}_{\Delta t}, \mathbf{x}) - t \leq 0)] | t_{\text{ini}}(\boldsymbol{\Theta}_{t_{\text{ini}}}, \mathbf{x}) \leq t, t\} =$$
$$= \frac{\tilde{P}\{[(d_{\lim} - d(\boldsymbol{\Theta}_d, \mathbf{x}) \leq 0) \cap (t_{\text{ini}}(\boldsymbol{\Theta}_{t_{\text{ini}}}, \mathbf{x}) + \Delta t(\boldsymbol{\Theta}_{\Delta t}, \mathbf{x}) - t \leq 0) \cap (t_{\text{ini}}(\boldsymbol{\Theta}_{t_{\text{ini}}}, \mathbf{x}) - t \leq 0)] | t\}}{\tilde{P}\{[(t_{\text{ini}}(\boldsymbol{\Theta}_{t_{\text{ini}}}, \mathbf{x}) - t \leq 0)] | t\}} \quad (111)$$

As the event $\left(t_{\text{ini}}(\boldsymbol{\Theta}_{t_{\text{ini}}}, \mathbf{x}) + \Delta t(\boldsymbol{\Theta}_{\Delta t}, \mathbf{x}) - t \leq 0\right)$ is a subset of $\left(t_{\text{ini}}(\boldsymbol{\Theta}_{t_{\text{ini}}}, \mathbf{x}) - t \leq 0\right)$, their intersection is exactly $\left(t_{\text{ini}}(\boldsymbol{\Theta}_{t_{\text{ini}}}, \mathbf{x}) + \Delta t(\boldsymbol{\Theta}_{\Delta t}, \mathbf{x}) - t \leq 0\right)$ and therefore Equation ( 111 ) can be written as exposed in ( 112 ).

$$= \frac{\tilde{P}\{[(d_{\lim} - d(\boldsymbol{\Theta}_d, \mathbf{x}) \leq 0) \cap (t_{\text{ini}}(\boldsymbol{\Theta}_{t_{\text{ini}}}, \mathbf{x}) + \Delta t(\boldsymbol{\Theta}_{\Delta t}, \mathbf{x}) - t \leq 0)] | t\}}{\tilde{P}\{[(t_{\text{ini}}(\boldsymbol{\Theta}_{t_{\text{ini}}}, \mathbf{x}) - t \leq 0)] | t\}} \quad (112)$$

The numerator of Equation ( 112 ) can be seen as a bivariate reliability problem, having respectively $g_1(\boldsymbol{\Theta}_d, \mathbf{x}) = d_{\lim} - d(\boldsymbol{\Theta}_d, \mathbf{x})$ and $g_2(\boldsymbol{\Theta}_{t_{\text{ini}}}, \boldsymbol{\Theta}_{\Delta t}, \mathbf{x}) = t_{\text{ini}}(\boldsymbol{\Theta}_{t_{\text{ini}}}, \mathbf{x}) + \Delta t(\boldsymbol{\Theta}_{\Delta t}, \mathbf{x}) - t$ as limit state functions, corresponding to two different generalized reliability indexes $\beta_1(\boldsymbol{\Theta}_d, \mathbf{x})$ and $\beta_2(\boldsymbol{\Theta}_{t_{\text{ini}}}, \boldsymbol{\Theta}_{\Delta t}, \mathbf{x})$. Thus, the mentioned predictive probability of exceedance of a certain pre-set limit of spalling depth in a given period of fire exposure can be calculated as $\Phi_2(-\boldsymbol{\beta}, \mathbf{R})$, where is the vector $\boldsymbol{\beta} = (\beta_1, \beta_2)$ and $\mathbf{R}$ is the related correlation matrix. Such a reliability problem is addressed in the following using the First Order Reliability Method (FORM).

In Chapter 5, the application of the probabilistic approach for calculating structural reliability in terms of spalling is presented through a case study, illustrating the resulting fragility curves.

Chapter 5

# Fire induced damage states assessment: application on specific underground structure

In this chapter, the application of the calculation methodology for damage limit states, including the assessment of the extent of spalling, will be presented for a specific real case study of a large underground cavern. This cavern is part of the research infrastructure managed by the European Organization for Nuclear Research. The proposed methodology exposed in the previous chapters serves as a vital tool for assessing the potential damage caused by fire within a real cavern. Its primary objective is to discern the anticipated level of damage to the underground structure through the meticulous analysis of smoke temperatures and the execution of advanced thermo-mechanical analyses. This cavern serves as the primary housing for the ATLAS detector, a cornerstone experiment conducted at the European Centre for Nuclear Research (CERN). Operating as one of the two general-purpose detectors within the Large Hadron Collider (LHC), the ATLAS experiment delves into a diverse array of physics inquiries, ranging from the exploration of the elusive Higgs boson to the scrutiny of extra dimensions and hypothetical particles that may compose dark matter. Positioned strategically at one of the four particle collision points within the intricate LHC tunnel complex, the ATLAS detector boasts a suite of sophisticated and high-cost instrumentation. Consequently, safeguarding the

structural integrity of this cavern in the event of a fire is not only critical but paramount for ensuring the safety and continuity of operations. The subterranean expanse at this collision point encompasses the central ATLAS cavern, UX15, intricately linked to the auxiliary service caverns USA15 and US15, along with the access shafts PX16 and PX14. Given the intricacies of this spatial configuration, it becomes imperative to conduct a thorough and comprehensive assessment of potential fire damage. This proactive approach is essential to uphold the operational integrity and safety protocols of the entire facility, thereby mitigating risks and ensuring uninterrupted scientific endeavours.

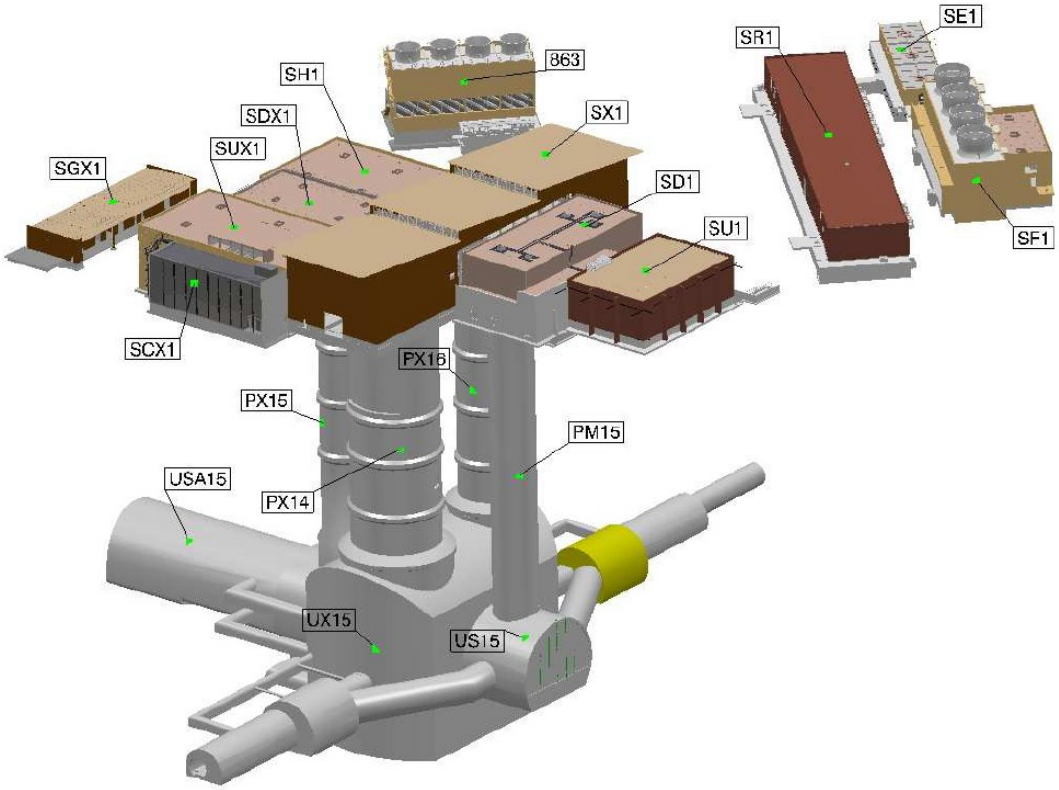


*Figure 69: The ATLAS underground and surface facilities(https://edms-service.web.cern.ch/faq/EDMS/pages/).*

### 5.1.1 Description of analysed structure

The underground structure under evaluation is an artificial cavern located approximately 50 meters below ground level, constructed with cast-in-place reinforced concrete. It represents a unique example of engineering for underground infrastructure within a complex dedicated to housing the world's largest particle detector, associated with the Large Hadron Collider (LHC), known as ATLAS (Figure 69). The specific cavern of interest is named UX15. This cavern stands out due to its impressive dimensions: an internal volume of 47.213,00 $m^3$ with a semi-rectangular footprint measuring approximately 52.9 m x 30 m in plan, and walls approximately 34.9 m high.

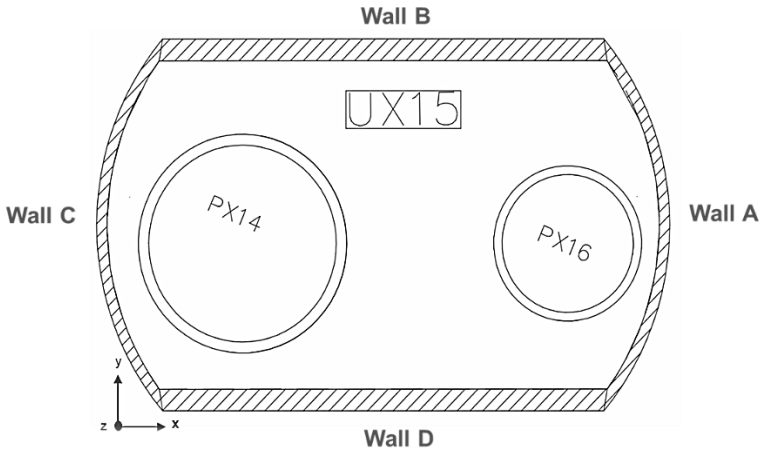


*Figure 70: UX 15 Secondary lining plane scheme.*

Covering the aforementioned volume is a vault characterized by two off-centered openings designed to connect the cavern with vertical shafts, named PX 14 and PX 16, with diameters of 18 m and 14 m respectively, linking the underground volume with surface facilities. The construction of the cavern involved a series of complex excavation and building operations divided into phases. Initially, excavation began from the surface, involving the construction of the aforementioned shafts. Once the desired depth was

reached, excavation proceeded from within these shafts to create the sub-volume necessary for constructing the vault.

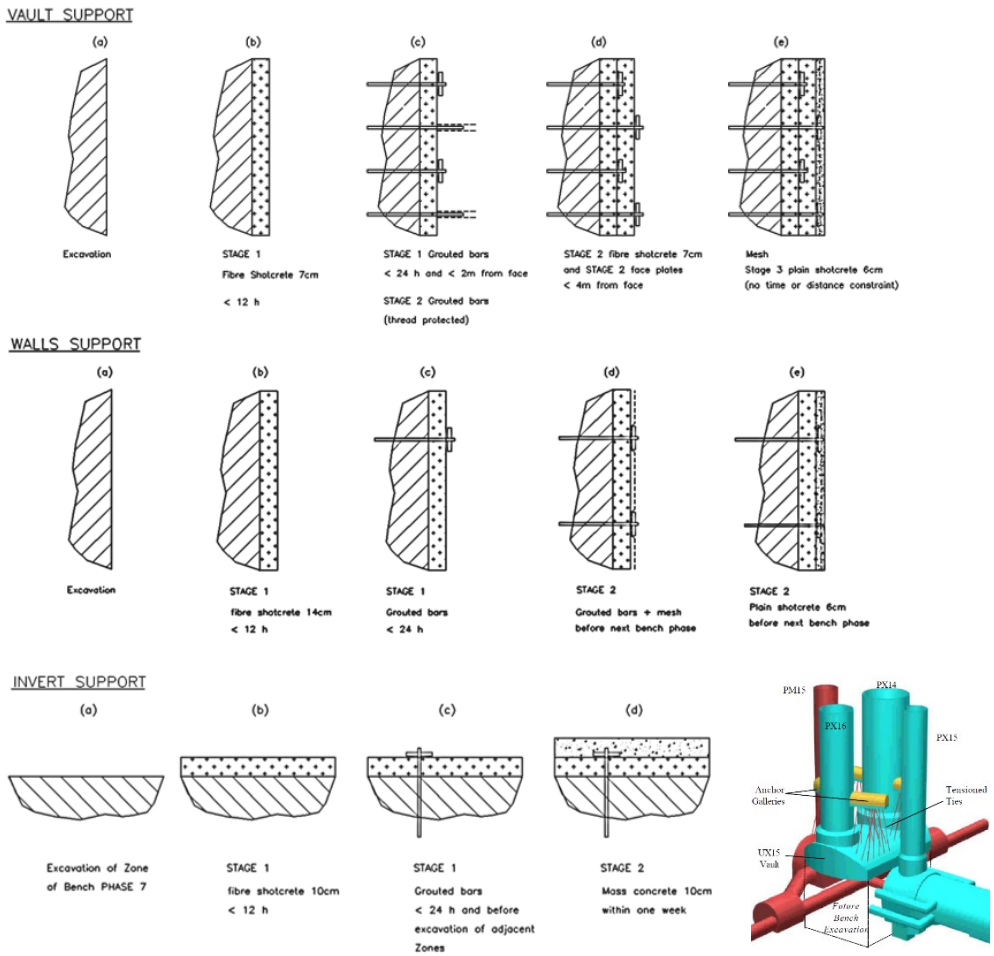


*Figure 71: The construction stages of UX15 primary lining and schematization of vault anchors (https://edms-service.web.cern.ch/faq/EDMS/pages/).*

The vault itself was excavated in multiple phases, during which injections of reinforced concrete with reinforcing bars were applied to stabilize the surrounding ground directly in contact with the vault. Subsequently, a primary lining was installed, encapsulating the

heads of the anchors and creating the initial reinforced concrete vault. This was followed by the construction of a secondary vault lining, also executed through a complex procedure involving temporary anchorage to anchoring blocks located in horizontal service tunnels positioned halfway down the shaft depth (Figure 71). Upon completion of the vault, the excavation and construction of the cavern commenced through seven distinct phases, during which a stratified and anchored primary lining was installed, followed by the secondary lining. This procedure resulted in the creation of an underground structure characterized by a double-layered reinforced concrete lining: the primary lining, approximately 200 mm thick, originally anchored with grouted bolts in the surrounding terrain, and the secondary lining, varying in thickness from 1 to 2 m.

*Table 10:Geometrical and mechanical features of ATLAS Cavern secondary lining.*

| Wall [-] | Thickness [cm] | Reinforcement in both direction [mm/mm] | |
|---|---|---|---|
| Vault | 130 | Φ 32/200 | |
| A | 100 | Φ 32/200 | |
| B | 200 | Φ 32/200 | |
| C | 100 | Φ 32/200 | |
| D | 200 | Φ 32/200 | |
| **Wall [-]** | **Cover [mm]** | **Grade of steel [-]** | **Grade of Concreate [-]** |
| Vault | 75 | | |
| A | 75 | | |
| B | 75 | B450C | C35/45 |
| C | 75 | | |
| D | 75 | | |

It is important to note that after the completion of the vertical structures of the cavern and the base slab, the temporary tiebacks supporting the vault were removed, thereby transferring the entire load of the vault to the vertical walls of the cavern. The cavern is designed with two curved walls, two flat walls, the vault, and the invert, with the primary and secondary linings disconnected from each other. This aspect may influence the as-

sessment of the structure's vulnerability in case of fires, primarily involving the secondary lining. Every part of the cavern, including the walls and the vault, is reinforced with a double regular mesh of steel rebars to ensure structural strength. The most relevant structural details of ATLAS secondary lining for thermomechanical modelling are reported in Table 10. Additionally, holes located on all sides of the cavern allow for connections to surrounding service tunnels, where various instruments contributing to the operation of ATLAS are located. The study of the original design elaborations and the as-built specifications has enabled the understanding of the necessary construction details for accurate thermo-mechanical modelling of the cavern.

### 5.1.2 Fire modelling by FDS

The fire resistance assessment of the structure studied in this chapter involves the application of a performance-based approach. As seen in paragraph 2.1.1, the starting point for applying this approach is the identification of the design fire described through a natural fire curve. In this paragraph, the description of the identification and CFD modeling of fire scenarios used in the UX15 cavern, carried out by the FSE team of the HSE section of CERN, is provided. To identify the design fire, it is necessary to know in detail the geometry of the compartment, the openings present in it, the type of activity exercised, the quantity, distribution, and type of combustible material present (in order to define the fire load $q_f$). In any quantitative fire assessment, it is also important to characterize the fire by means of a heat release rate (HRR) curve and yields of soot and combustion species as seen in the paragraph 2.1.1. This description of the time evolution of the considered fire is known in literature as “design fire”. As seen, there are several models that can be used to estimate a natural fire curve; among these, the model used in this study is the field or CFD model (described in the paragraph 2.1.2.4). This model, being numerical, requires the assistance of dedicated software, in our case, FDS. The aforementioned characterization of the design fire allows the compilation of the necessary data

as input into the CFD software, such as the definition of the HRR curve, the fire surface area, the geometry of the compartment, and the thermal characteristics of the materials present. Combining a design fire with appropriate boundary conditions results in a specific fire scenario.

In this case, it is necessary to clarify that the studies required to identify possible fire scenarios, the type and quantity of combustible material, the location of the fire, and the parameters needed to model and validate each specific fire scenario were conducted by the FSE team of the HSE section at CERN. These studies were specifically initiated to investigate the spread of potential radioactive smoke within and outside the work environments. Therefore, further details on thermofluidic dynamic modelling and fire validation can be found in [65]. The contribution made in this work, however, was to implement and localize the Adiabatic Surface Temperature (AST) devices in the every fire models to detect the temperatures of exposed structural surfaces and to restart the analyses. Subsequently, it was possible to carry out post-processing of the data, obtaining surface temperature curves of the structural elements at various points of interest. Inside the cavern, the main sources of ignition for a fire are the large quantities of cables present, specifically the materials used for their cabling, the electrical panels, and the handling and lifting equipment (such as aerial platforms). The main aspects considered in the selection of the representative fire scenarios are: location of the fire ignition source, fuel load (fuel package of origin and items exposed to secondary ignition) and fire growth. The scenarios with the greatest potential impact on the structure are:

1. *Cable tray fire* outside the detector (ATLAS):

   This scenario represents a fire developing in the cable trays located outside the detector. The HRR was calculated by [65], which allows for an accurate determination of the heat release rate.

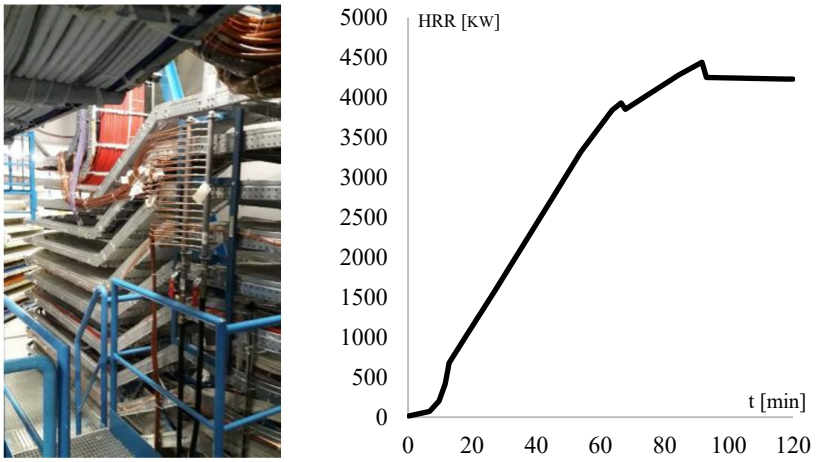


*Figure 72: Example of Cables and corresponding HRR curve in cave UX15.*

For the characterization of this scenario, four heavily-loaded, stacked cable trays with a density of 2500 kg/m$^3$, containing 5 cm of plastic cables, were considered. This configuration represents a critical situation, as the presence of a large amount of highly flammable plastic material can lead to rapid fire growth. Additionally, the stacked cable trays can facilitate the propagation of flames from one level to another;

2. *Rack fire* (group of electrical cabinets): The electrical rack fire was modelled using the method developed by [65], which employs bibliographical data, rack geometrical distribution, and rack specificities (such as the combustible load inside the racks or the door position) to determine the HRR. For this scenario, four cabinets arranged two by two in two rows were considered (see Figure 73);

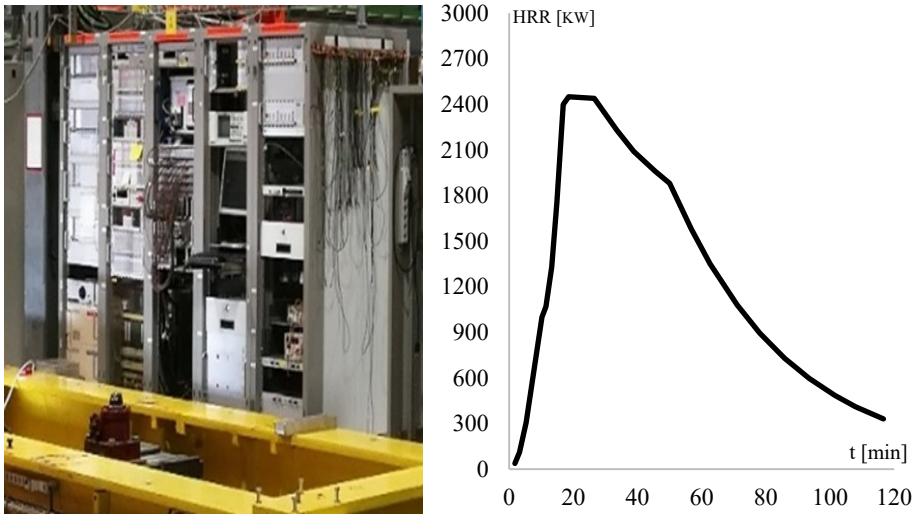


*Figure 73:Example of Electrical Rack and corresponding HRR curve in cave UX15.*

3. *Lifting platform fire*: this lifting platform contains a significant number of combustible materials, including the rubber of the tires, the hydraulic oil for the jacks, and the diesel emergency tank, in particular, 1.7 litters of oil (primary fuel) and 100 litters of diesel (secondary fuel). A composite HRR curve was developed, starting with rapid growth, leading to a plateau from a pool fire caused by the combustible liquids present, to which the HRR curve for the tires is added. The resulting HRR curve is shown in Figure 74.

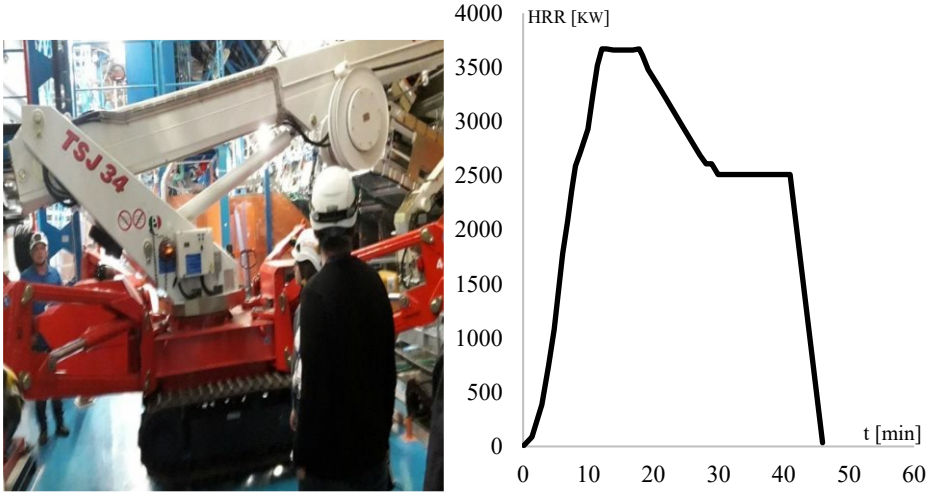


*Figure 74: Lifting platform and corresponding HRR curve in cave UX15.*

Cable insulation is recognized as the most common combustible source at CERN premises, due to the vast presence of cables in surface and underground tunnels, shafts, and caverns at CERN. Computational Fluid Dynamics (CFD) and LES modelling with Fire Dynamics Simulator (FDS shown in paragraph 2.1.2.4) are used. Once the HRR curve and the area affected by the combustible material are defined, it is possible to model in FDS a solid element that releases heat from the external surface following the HRR curve. The three-dimensional model in FDS was created by the aforementioned FSE team of HSE unit at CERN to evaluate possible leaks of radioactive fumes resulting from the mentioned fire scenarios. Therefore, to use these thermos-fluid dynamics models for the purposes connected to this thesis work, it was necessary to implement virtual temperature recording devices in the model. As mentioned in the chapter dedicated to fire modelling, some of these instruments are installed near the surface exposed to the fire and allow the recording of the Adiabatic Surface Temperature (AST). The Adiabatic Surface Temperature is defined as the temperature of a surface that cannot absorb or lose heat to the environment, and it is a parameter that can be used as input for thermomechanical analyses (yellow dots in Figure 75). In other words, this is the highest theoretical temperature

a surface can experience under certain boundary conditions, making it a conservative and appropriate input parameter for structural analysis.

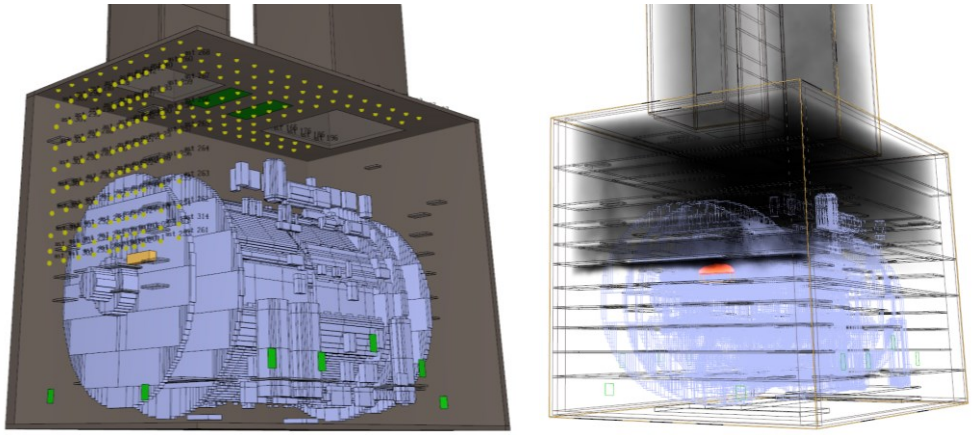

*a) FDS model in pre-processing phase* *b) FDS model in post-processing phase*

*Figure 75: the 3D representation of ATLAS cavern model performed in FDS (in yellow the AST devices).*

Once all the thermal and geometric parameters of the model are defined and the fire input data are inserted, it is possible to start the advanced thermos-fluid dynamics analysis, which allows, for each defined time interval, the evaluation of the temperature (and more) at various points in the calculation volume. As previously mentioned, given the large size of the compartment and the relatively localized nature of the combustible material, the described scenarios pertain to localized fires. For each scenario, temperatures were recorded at various points of each individual compartment element. This allowed for the determination of the most severe fire curve, describing the maximum heating of each element due to the different fire scenarios. From a thermomechanical perspective, by applying the AST, the procedure was simplified by using the most severe fire curve for each structural element for each scenario.

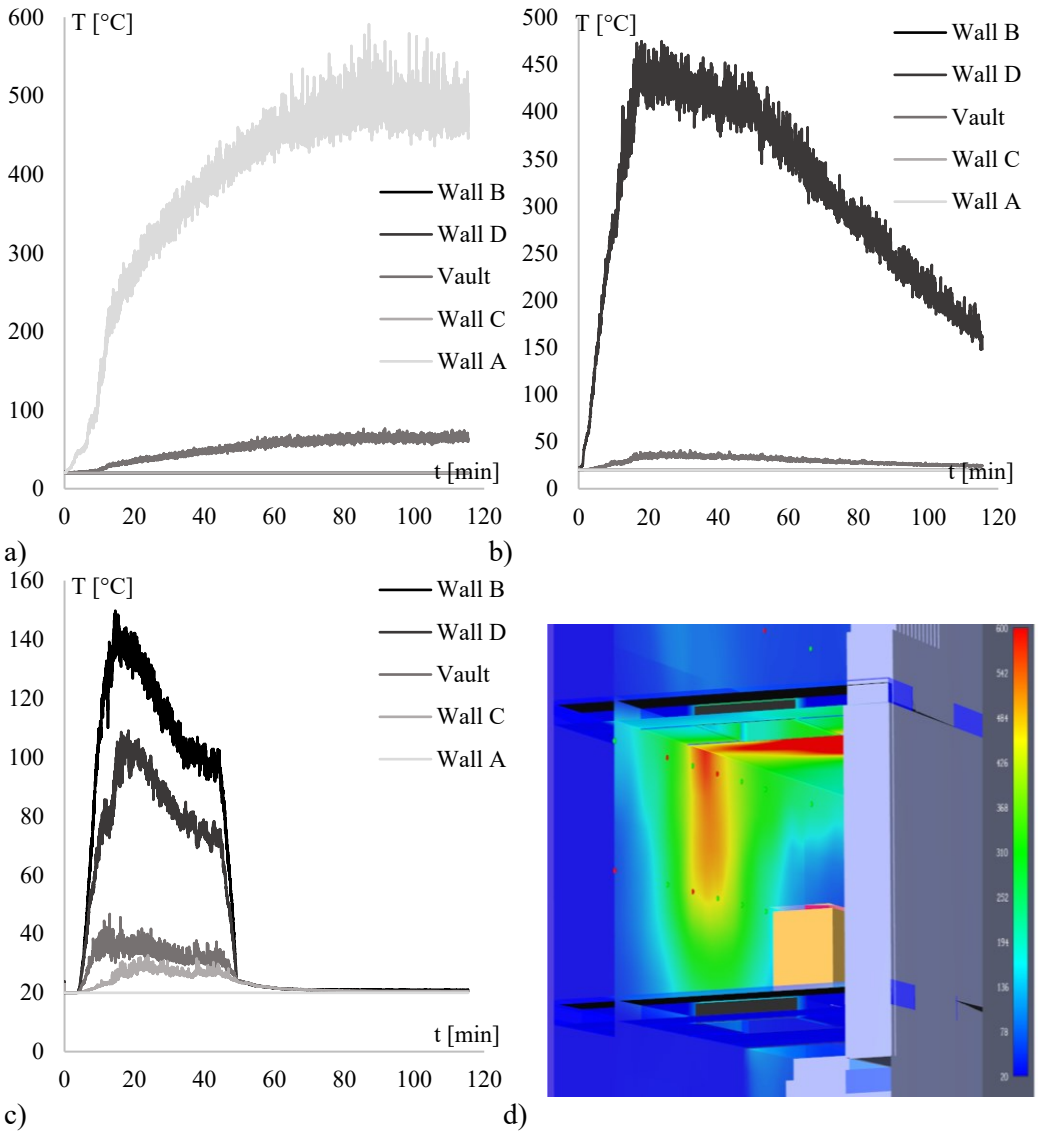


*Figure 76: a), b), c) Fire curves for each scenario and each element; d) graphical result of the FDS.*

The fire curves recorded on the walls directly exposed to each individual fire scenarios are shown in the Figure 76. The fire curves represent the evolution of thermal stress to

be applied as a boundary condition to each structural element, allowing for its thermal analysis.

### 5.1.3 Thermomechanical modelling by SAFIR

Following the thermos-fluid dynamics simulation of the individual fire scenarios that could occur inside the ATLAS cavern, the fire curves to be used as thermal input for the thermomechanical analysis of the structure's lining are now known. It is important to note that in this case, the fire resistance analysis was conducted considering only the secondary lining of the tunnel, as it is disconnected from the main lining and is directly exposed to thermal stress in the event of a fire. As discussed in Section 2.2 dedicated to thermomechanical modelling, knowing the fire curve, the first step is to evaluate, through a thermal analysis, the temperature variations within the structural element induced by the heating of one or more external surfaces. In this case, the analysis was conducted using the specialized software SAFIR. Dealing with flat elements, the considered section model is TSH, described in the manual related to thermal analysis. The numerical analysis involves solving the one-dimensional heat transfer equation. Since the element is symmetric, the analysis is performed on a section of unit width, which benefits from adiabatic lateral surfaces. To capture the temperature variations as a function of the depth of the section from the surface exposed to the fire, a differentiated discretization of the sections was performed. Specifically, in the mesh definition, a step size of 2 mm was chosen up to a thickness of approximately 100 mm, with a denser mesh near the reinforcement bars to calculate the temperature at their centre. The choice of such a fine mesh size is also due to the possibility of using the same thermal model to estimate the extent of potential spalling. The figures below show the graphs of temperature profiles at different depths in the section, highlighting the curve that describes the temperature evolution in the steel reinforcement bars.

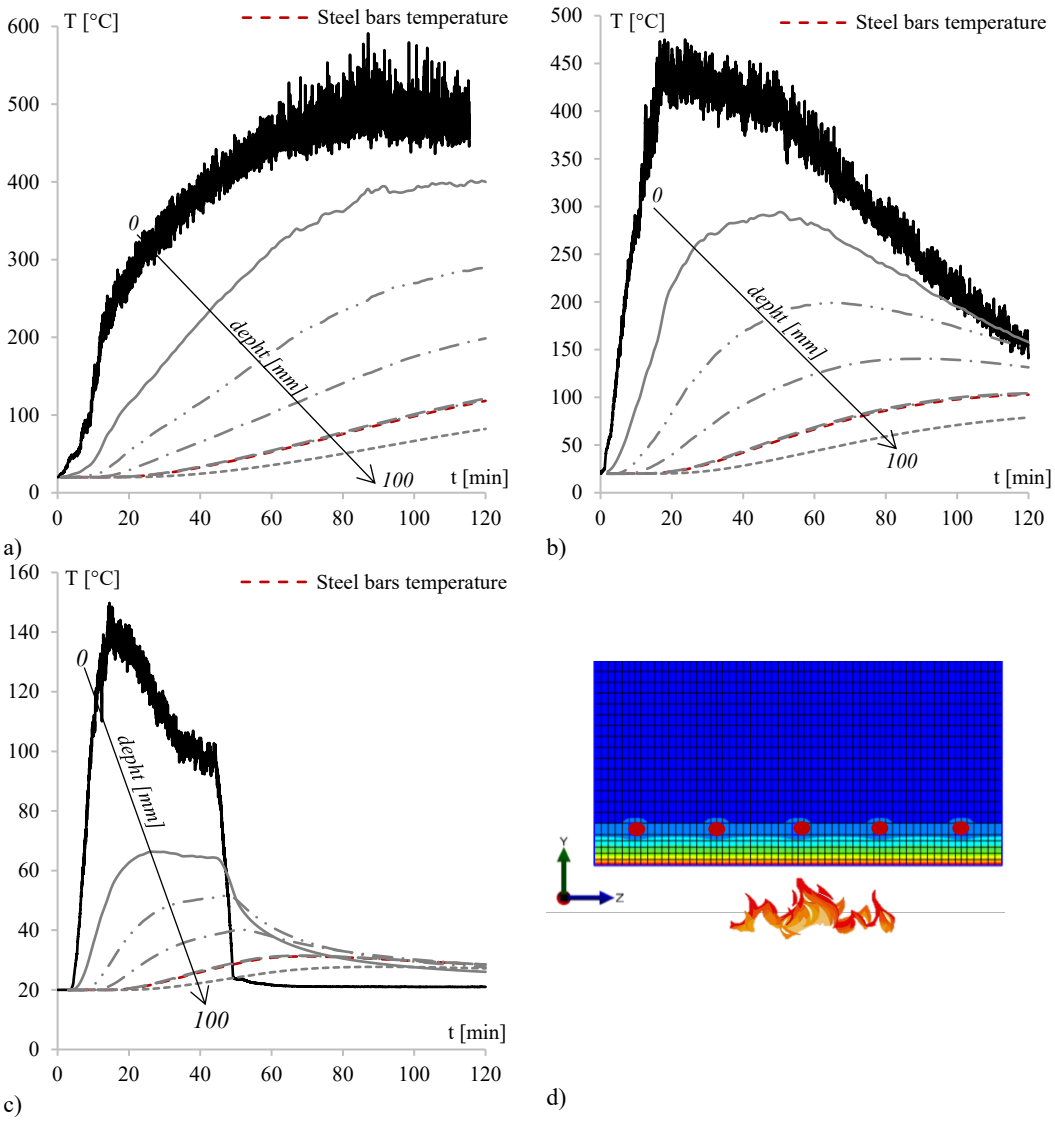


*Figure 77: The temperature distributions in the R.C. section subjected to a) cable tray fire, b) rack fire and c) lifting platform fire; d) example of model of R.C. section subjected to fire.*

Through the analysis of the temperatures within the section, and particularly the maximum temperature reached by the reinforcing bars during fire exposure, it can be observed that 200 °C is never exceeded. This is a significant aspect, as it should be noted that the

strength of steel begins to decrease at 400 °C. Therefore, it can be assumed that, for the temperatures resulting from the fires under consideration, there will be no reduction in load-bearing capacity (a condition verified in the following paragraph). After the thermal modelling of the different sections belonging to the walls and the vault of the cavern, we proceeded to the mechanical modelling by constructing a three-dimensional model made of shell elements.

Knowing the temperature evolution in the sections due to the design fires, it was possible to evaluate the residual structural capacity of the secondary lining of the cavern structure. Advanced thermomechanical analyses were performed on the entire secondary lining of the cavern using SAFIR models. The entire structure was modelled due to its complex geometry, characterized by the absence of symmetries, and to consider the hyperstatic effects induced by the fire (Figure 78). Since the primary and secondary linings are not connected, only the secondary lining was modelled. The modelling was done using only shell elements, and the mesh size was optimized to ensure a sustainable computational load while guaranteeing result independence from the mesh size. The dead loads were applied without considering the interaction with the surrounding ground, as the secondary lining structure appears disconnected from the primary one. The advanced finite element method was used. Shell element modelling was chosen as it is deemed more suitable for the purpose; studies in the literature recommend them for their relatively conservative thermal predictions, their accuracy in displacement predictions, and their reasonable computational load. Given the excessive size of the cavern's base slab and the review of the structural design details reported in the *as-built* documents retrieved on site, it was possible to understand that the vertical walls of the structure can be assumed to be fixed at the base, omitting the modelling of the base slab.

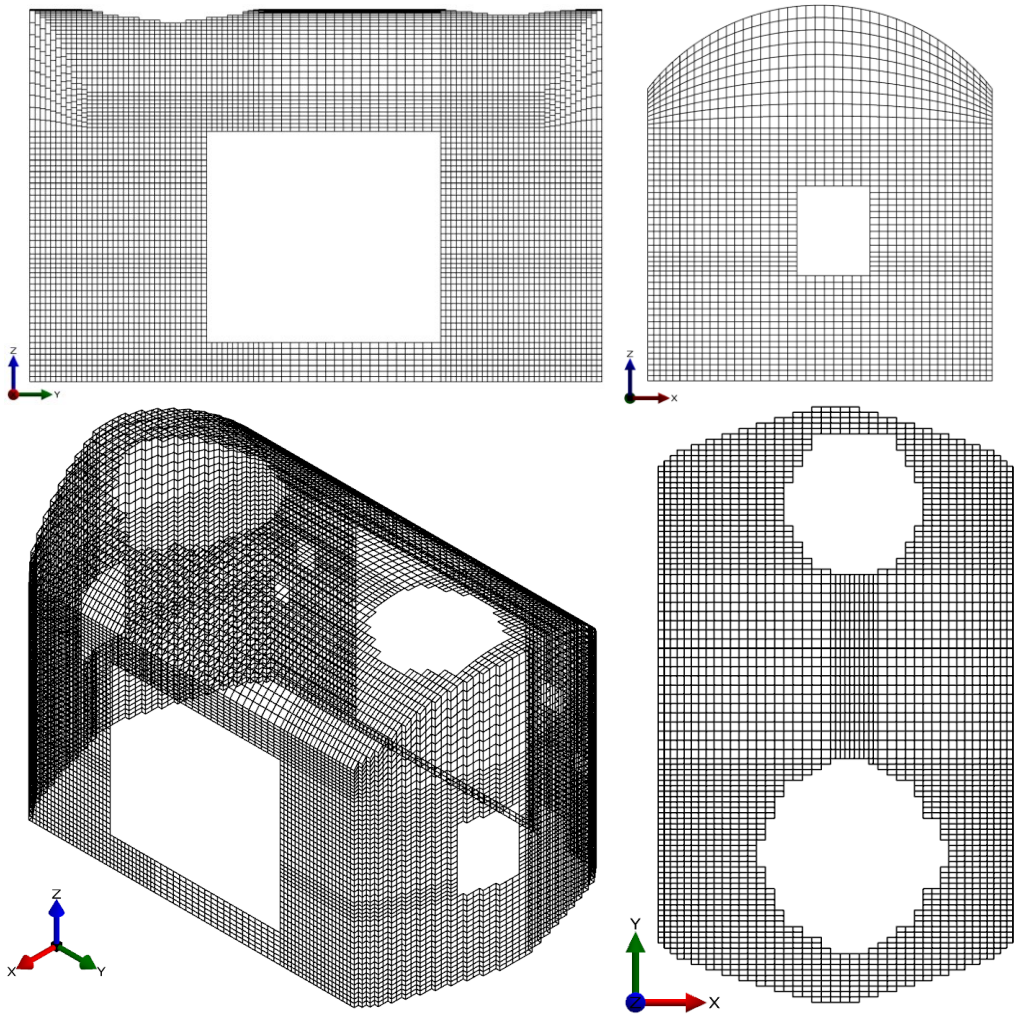


*Figure 78: 3D thermo-mechanical model of UX15 Cavern in SAFIR.*

For thermomechanical purposes, the base slab has low relevance, except for the constraint regime it imposes on the vertical walls of the cavern. From the structural data, it was also possible to understand that the vault has a continuity constraint with the vertical walls, while all the surrounding service galleries and shafts are joined to the structure in question, providing only a translational constraint at the boundary points but without flexural

continuity (Figure 79).

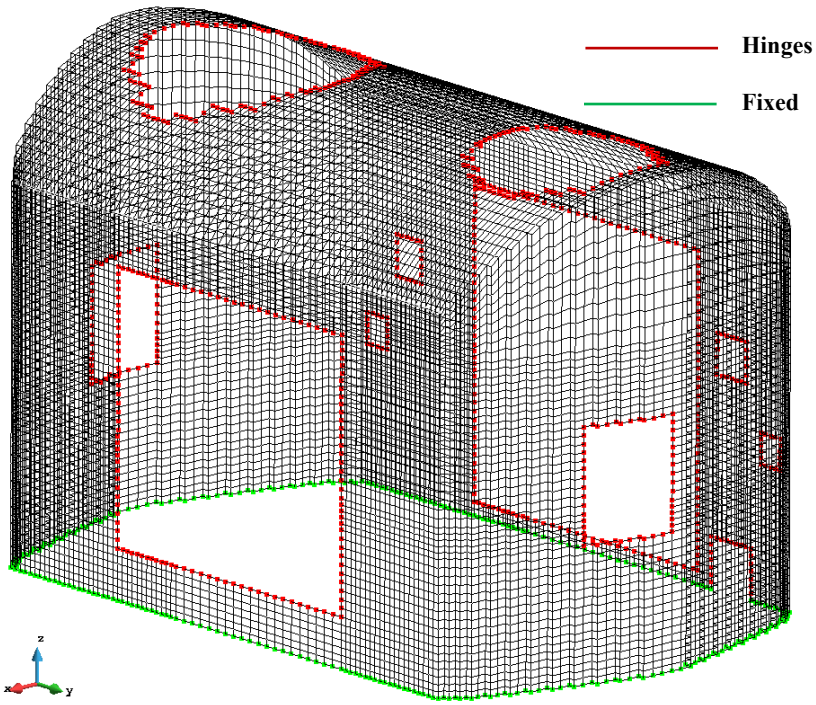


*Figure 79: 3D Model with constrains explicated.*

The thermomechanical modelling of the cavern in SAFIR was designed by differentiating the exposure zones and assigning each of these the maximum temperature recorded in that zone thanks to the thermo-fluid dynamics model. In this way, an attempt was made to achieve the highest modelling accuracy while maintaining computational sustainability. Once the model was defined, advanced thermomechanical analyses were performed for the cavern under different fire scenarios, obtaining the stresses in terms of displacement, membrane forces and bending moments on the shell elements.

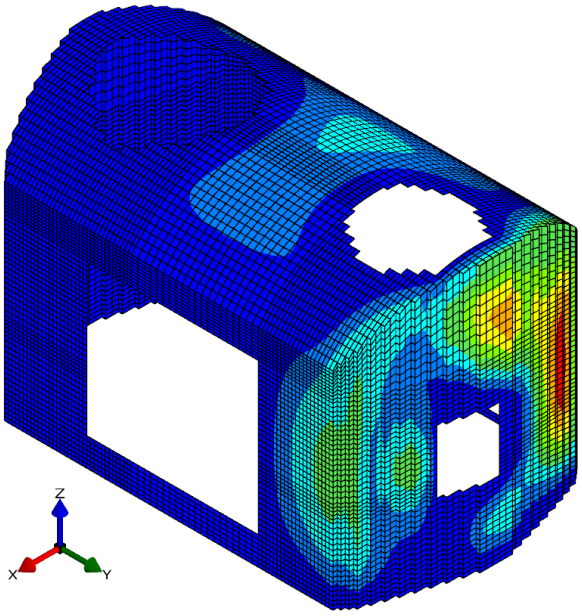


**1-Cable tray fire**

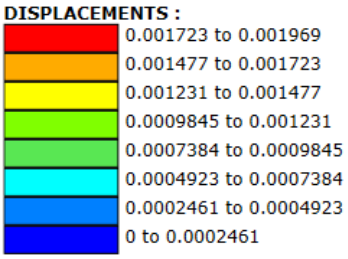


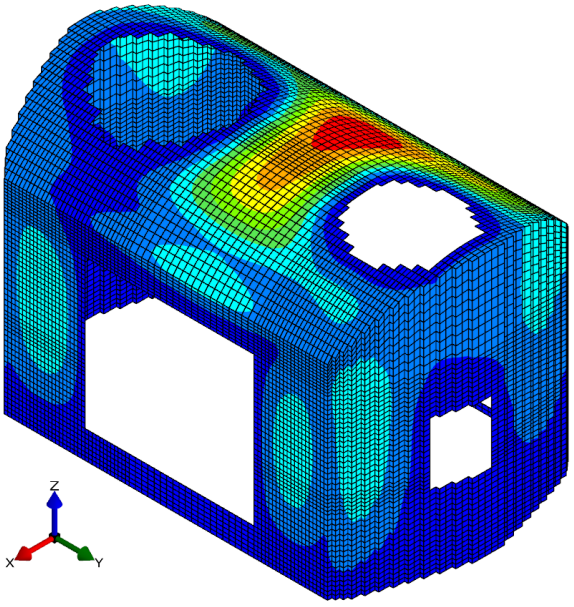


**2-Rack fire**

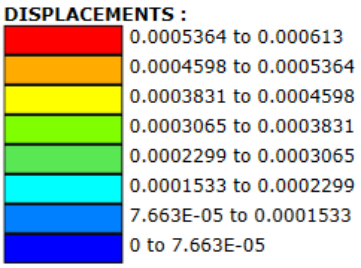

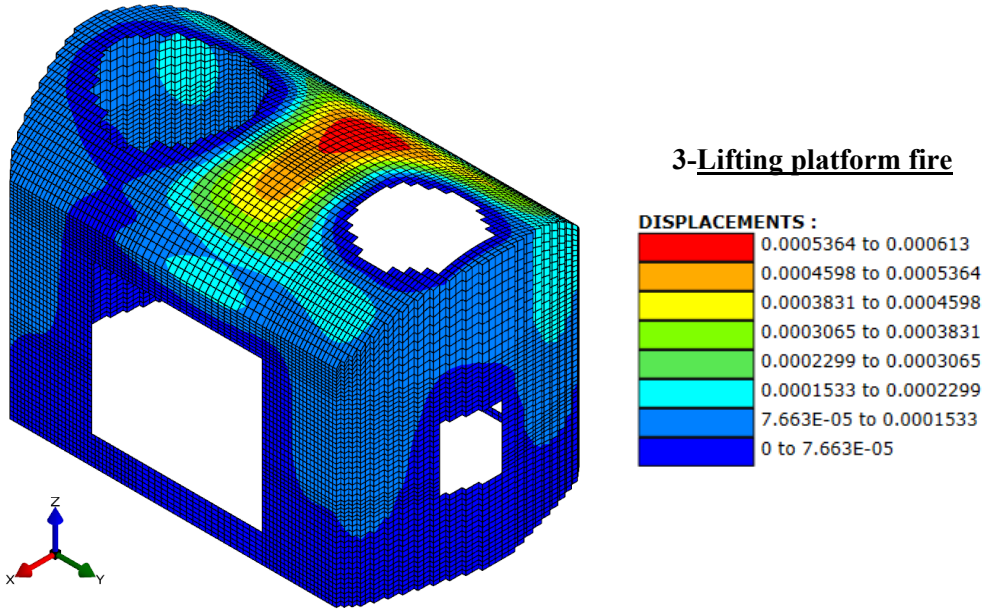


*Figure 80: Displacements mapping of 3D thermomechanical model of UX 15 for each scenarios at maximum temperature instant of time.*

As shown in Figure 80, the design fires do not cause excessive deformations of the cavern lining. In the next paragraph, the load-bearing capacities of individual structural elements will be analysed using the methodology outlined in Chapter 3, also assessing the possibility of spalling phenomena occurring.

### 5.1.4 Verification procedures

As seen in the chapter 3, knowing the structural features and the design fires that can occur it is possible to estimate the damage state correlated to the event. The first step is to assess the occurrence of the spalling phenomenon and its extent, which can be crucial in determining the damage state and the associated performance level.

As seen in paragraph 3.2.1, initially it is possible to analyse the fire curve applied to the structural element and assess the potential for spalling. This can be done by comparing

the temperature-rise rate curve, correlated with the fire curve, with the region of the plane containing the pairs (temperature-rise rate) for which spalling has been experimentally observed. Below is the overlap between the experimental graphs shown in the previous mentioned section and the characteristic curve of the most severe fire scenario for the case study analysed.

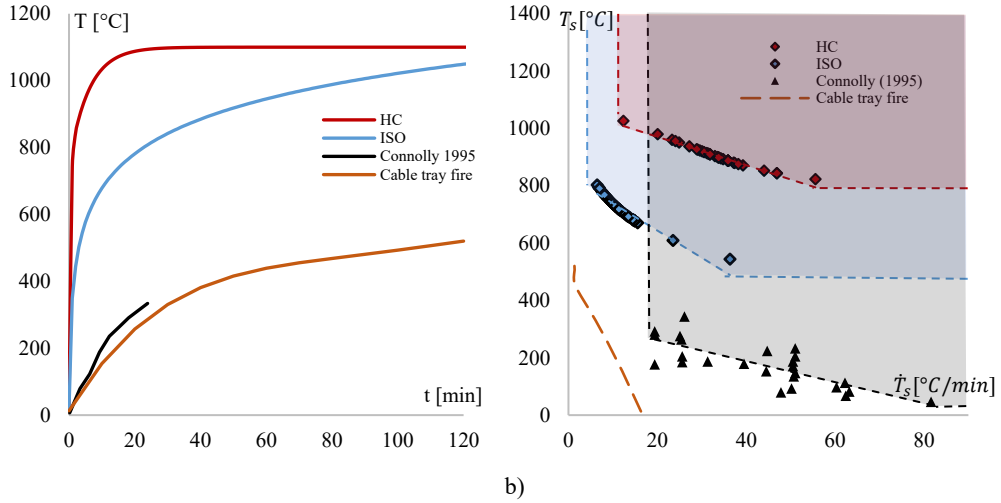


*Figure 81: a) fire curves applied; b) overlay of temperature-heating rate pairs related to fire scenario 1 - Cable tray with experimental results.*

From the Figure 81, it can be observed that the most severe estimated fire scenario for the cavern under examination results in temperature-rise rate pairs (dashed orange line) that do not fall within the critical region where spalling was experimentally observed (regions in grey, blue and red). This already indicates that the extent of this heating curve for the structural elements will not reach the conditions necessary for spalling. In this way, without applying the proposed spalling model, it is possible to state that, given the design fire, spalling cannot occur. Therefore, from the perspective of spalling, it can be concluded that, given the most severe design fire, the maximum damage state that can be configured is *Damage State One (ds1)*. However, in order to assign this damage state, it is necessary to also verify the load-bearing capacity of the structure under fire conditions.

## 5. Fire induced damage states assessment: application on specific underground structure

Below, the verification of the condition associated with *Damage State one (ds0)* is reported.

*Table 11:Verification procedure according to chapter 3.2.1.*

| Maximum membrane and bending forces in fire conditions | | | | | | | |
|---|---|---|---|---|---|---|---|
| $M_{x,max}$ [KNm] | $M_{y,max}$ [KNm] | $M_{xy,max}$ [KNm] | $N_{x,max}$ [KN] | $N_{y,max}$ [KN] | $N_{xy,max}$ [KN] | | |
| 4447 | 4669 | 1375 | 5598 | 3877 | 2343 | | |
| **Verification procedure of *ds0*** | | | | | | | |
| $M_{Ed,fi}$ [KNm] | $N_{Ed,fi}$ [KN] | $A_s = A_s'$ [mm²] | $f_{ck}$ [MPa] | b [mm] | h [mm] | c [mm] | $M_{cr,fi}$ ($N_{Ed,fi}$) [KNm] |
| **4669** | 5598 | 12251 | 35 | 1000 | 1000 | 75 | **7016** |
| $M_{Ed,fi} < M_{cr,fi}(N_{Ed,fi})$ → ***ds0*** | | | | | | | |
| **Level of performance V** | | | | | | | |

As shown in the previous section, the cavern containing ATLAS, defined as UX15, considering the possible natural fire scenarios and the structural characteristics of the cavern, given that the most severe fire is the one derived from the cable tray and that the most heated element is the curved wall defined as wall B, characterized by a thickness of 1 meter, does not suffer any type of damage, neither in terms of spalling nor in terms of erosion of load-bearing capacity. This allows us to affirm that it meets Damage Level 0 and exhibits a Level of performance V.

The natural fire scenarios identified for the cave in this application are localized fires. Depending on the location of the fire load that characterizes each individual scenario, the wall of the cave subjected to the most heating changes. For this reason, below we present, for each fire scenario, the M-N resistance domain of the most heated wall. The same domain is instead reported for each structural element subjected to the ISO curve with and without spalling.

As seen in the discussion presented in the previous chapters, the next step is to define structural reliability in terms of spalling. However, in the specific case under examination, this is not applicable because the proposed reliability model has been calibrated

using results derived from specimens subjected to standard fire curves, ISO and HC. In principle, this does not preclude the application of the model to case studies subjected to natural fire curves, but it is at least necessary that the temperature and heating rate conditions fall within the observation range of the phenomenon. Nevertheless, in order to appreciate the applicability of the proposed reliability model, it will be applied to the case study in the next paragraph under the assumption of a structure subjected to a fire described by the ISO 834 curve.

### 5.1.5 Spalling reliability analysis in case of exposure to the ISO nominal fire

The UX 15 cavern containing ATLAS is characterized, as seen in paragraph 5.1.2, by fire scenarios less severe than the standard one described by the ISO 834 curve. The hypothesis of such a severe fire can therefore be ruled out for two reasons. Firstly, the combustible material inside the cavern and connected to the ATLAS particle detector is minimized (to reduce fire risk). Additionally, the size of the cavern, and thus the compartment, is so large that it significantly reduces the fire load. However, the following is the application of the structural reliability model in terms of spalling, as discussed in paragraph 4.7.

The probability to have spalling initiation in a given time of exposure to the ISO nominal fire, is given by the solving with FORM the Equation (111). The obtained results is showed in Figure 82.

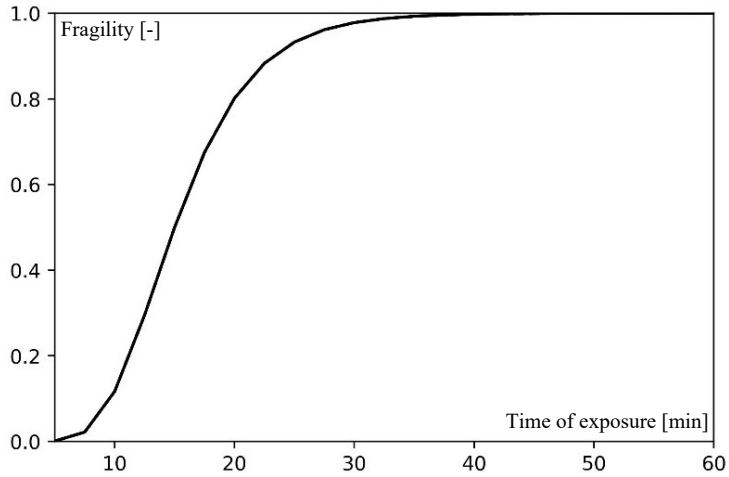


*Figure 82: Fragility curve in terms of initiation spalling time given a set of parameters distributions.*

The probability of having a final spalling depth exceeding a certain threshold in a given time of exposure to the nominal fire is given by solving the bivariate reliability problem mentioned in section 4.7. The obtained results using FORM are depicted in Figure 83.

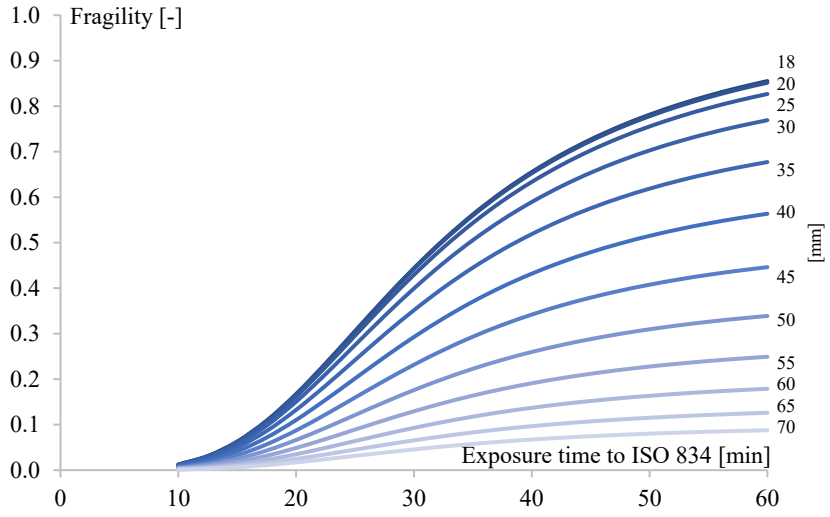


*Figure 83: Fragility curves representing the probability of having a final spalling depth exceeding a certain threshold in each time of exposure to the ISO 834 fire curve.*

In order to apply the proposed reliability procedure, the parameter distributions used are those reported in Table 12.

*Table 12:Verification procedure according to chapter 3.2.1.*

| Parameters | Median M | Standard deviation σ |
|---|---|---|
| $f_c$ [MPa] | 51.56 | 4.00 |
| U [Kg/m³] | 48.00 | 4.80 |
| $\sigma_{ext}$ [MPa] | 4.00 | 0.40 |

The above fragility curves show how, depending on the investigated concrete depth and the fire exposure time, it is possible to determine the probability of spalling occurring, assuming the phenomenon initiates. It is interesting to note that this fragility distribution is specific to the single case study and takes into account a range of parameters that influence the problem. These parameters are not set as constants; instead, a distribution is considered for each to describe its variability. This tool can be used in various ways, such as:

- evaluating the probability that a certain spalling depth will be exceeded given the exposure time;
- conversely, the probability that a certain spalling depth will not occur for given exposure time;
- the probability that spalling will occur between a depth of x and y.

In the case under examination, it can be observed that significant probabilities of spalling occur only for exposure times exceeding 30 minutes, affecting a depth of reinforced concrete section of at most around 40 mm. Given the generous cover of about 75 mm, such a final spalling thickness will not cause significant reductions in structural resistance. It should also be specified that, for spalling to occur, the exposure time to the ISO 834 curve must exceed 10 minutes. This is evident from the horizontal translation characterizing the onset point of the fragility curves relative to the origin of the axes.

In reference to the quantification of damage limit states, it can be observed that in the case under examination subject to the ISO fire curve, the probability of exceeding spalling of a certain depth after a given exposure time is still significant. Damage state 2, described and quantified in paragraph 3.2.3, is characterized by a spalling depth close to the cover thickness. Considering that the ATLAS cavern under examination has a cover thickness of about 75 mm, which, net of the transverse reinforcements, is approximately 40÷45 mm, a probability of spalling occurrence exceeding this depth (40÷45 mm) can be identified. This probability varies with the exposure time and exceeds 0.45÷0.55 for times close to 60 minutes (as shown in Figure 84). Given the non-negligibility of this probability, assuming a maximum spalling depth equal to the maximum cover thickness net of the transverse reinforcements (45 mm), a thermomechanical analysis of the cavern was conducted to evaluate the corresponding damage state and performance level in the event of heating induced by the ISO 834 curve.

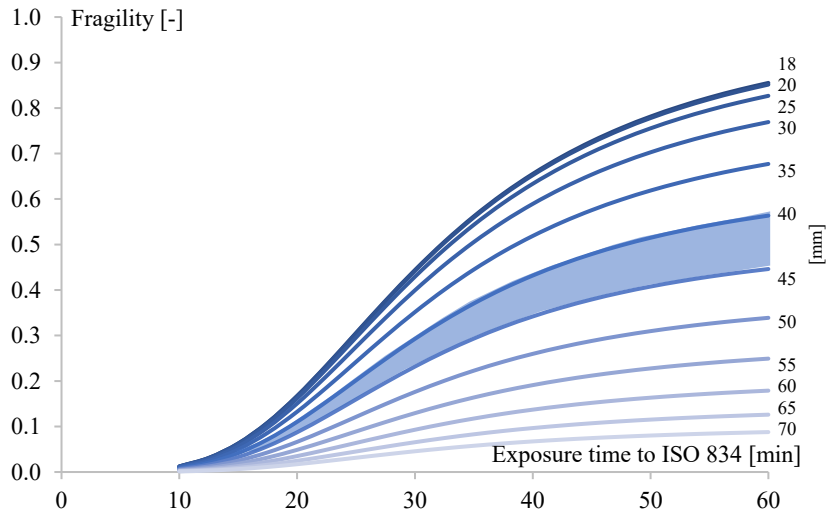


*Figure 84: Fragility curves representing the probability of having a final spalling depth exceeding the concrete cover in each time of exposure to the ISO 834 fire curve according to ds2.*

From the thermomechanical analysis conducted using the dedicated software SAFIR, it was first found that the cavern can avoid structural collapse even after 1 hour of exposure

to the generalized fire described by the ISO 834 curve. Additionally, to understand the effect of spalling on the structural elements, the M-N resistance domains for the main structural elements of the cavern are reported below, distinguishing between the intact sections and the sections reduced by the effect of spalling.

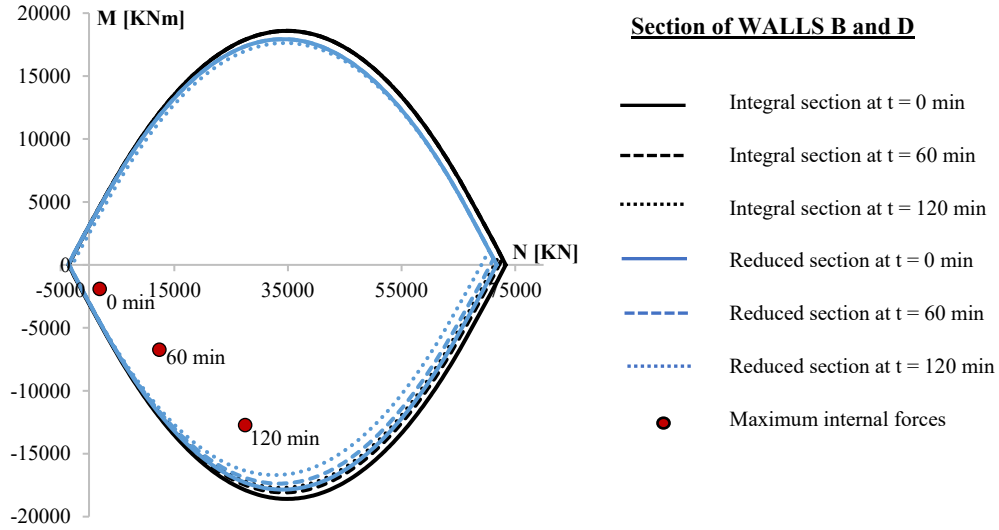


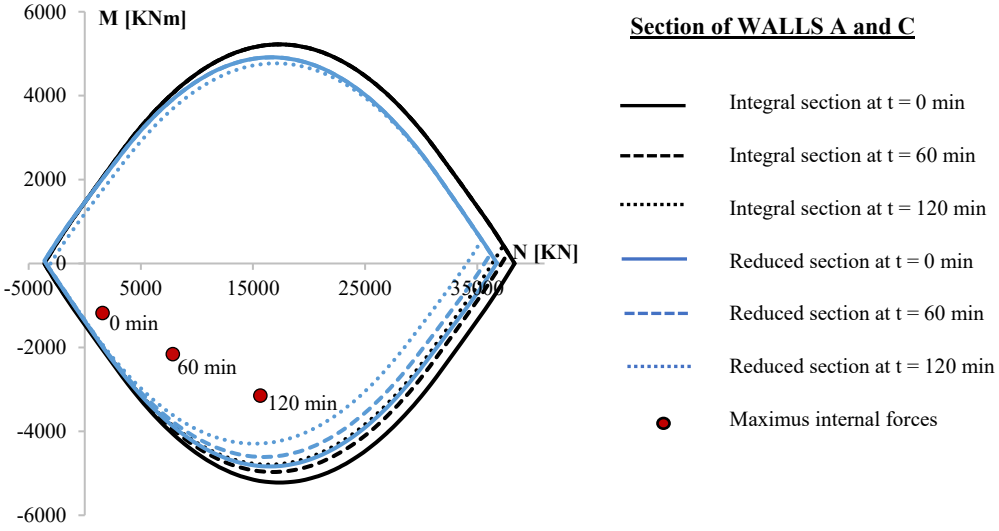

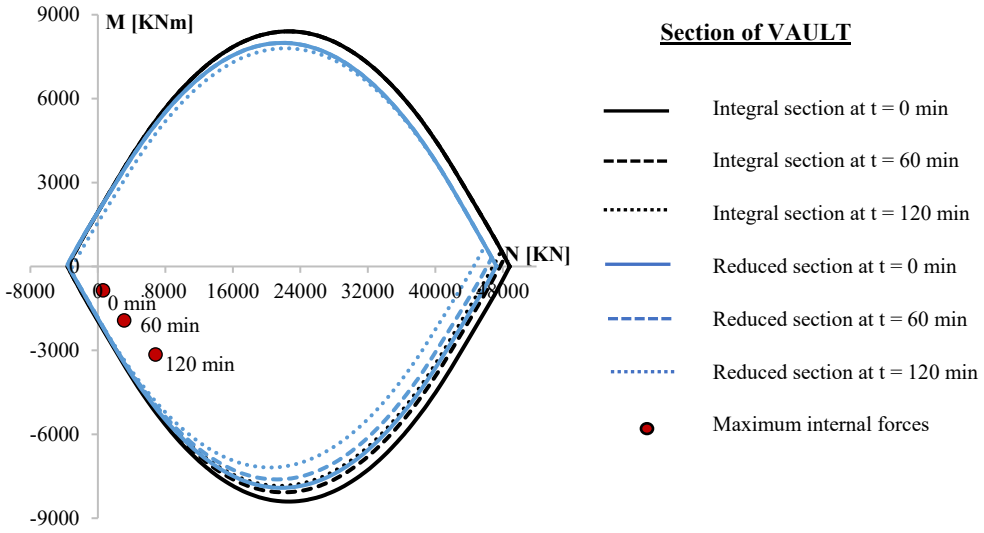


*Figure 85: M-N domains under fire conditions with and without spalling related to the structural elements of the UX15 cavern.*

From the analysis of the domains shown in Figure 85, it can be observed that, despite the considerable size of the structural elements under examination, the erosive effects of high temperatures significantly reduce the load-bearing capacity. Additionally, it is evident that spalling significantly impacts the reduction of the structural resistance of the section and exacerbates the erosive effect of high temperatures. In some cases, it can be observed that, for the same normal force, the flexural strength is reduced by up to 50% due to the combined effect of spalling and high temperatures. It can therefore be concluded that the fire resistance of the structure under examination is still guaranteed even for a fire described by the standard ISO 834 curve for a duration of 2 hours. Indeed, despite the high probability of spalling (as shown by the curves in Figure 84), which significantly reduces the load-bearing capacity of the structural elements, the maximum stresses acting on the structural elements still fall within the plastic resistance limits of the reinforced concrete unit sections that characterize the structural elements.

### 5.1.6 Limitations of the models and methods

The methodology and models proposed in this thesis and applied in the present chapter can, in principle, be applied to other case studies involving underground structures with different purposes. These methodologies are indeed applicable both to tunnels and underground station structures used for railway and metro traffic, as well as to tunnels and underground structures designed for road traffic. The main distinguishing factor between these infrastructures lies in the type of fire they may be subjected to. However, as introduced in paragraph 4.5.2, variations in fire type can significantly affect the reliability of the proposed spalling model, as it has only been calibrated on experimental results based on the ISO834 and HC fire curves. This represents a clear limitation in extending the model's applicability to scenarios with different or more extreme fire conditions, such as fires involving particular materials or the presence of winds that influence heat propagation.

An additional limitation of the spalling model lies in the structural materials considered and their mechanical properties. The model was calibrated using specimens of ordinary reinforced concrete, characterized by a defined range of mechanical and physical properties (see paragraph 4.5.2 for details). However, in modern underground infrastructures, there is a growing use of fibre-reinforced concrete, which, as evidenced by several studies in the literature, exhibits significantly different behaviour under fire conditions, especially regarding spalling. Specifically, the behaviour of fibre-reinforced materials under thermal stress can be more complex to model and requires further experimentation to precisely calibrate the predictions.

To further improve the applicability of the proposed methodology and models, it is crucial to explore new research frontiers, with particular attention to the following aspects:

a) *Diversification of fire curves:* Additional experimental studies are needed on fire curves other than ISO834 and HC, including scenarios with variable thermal loads, fires involving different fuels (such as those derived from plastic or chemical materials), and situations where environmental conditions, such as ventilation or the presence of secondary combustible materials, can significantly alter fire development;

b) *Innovative materials and advanced models:* The growing adoption of fibre-reinforced concrete, as well as other advanced composite materials, requires the development of models that more accurately account for their behaviour under fire conditions. This could include studying the behaviour of concrete reinforced with polymeric, metallic, or hybrid fibres, with particular attention to their resistance to spalling and the changes in mechanical properties during heat exposure;

c) *Modelling thermomechanical behaviour in extreme scenarios:* While current thermomechanical models are generally valid, they may not be sufficiently precise for underground infrastructures exposed to extreme or highly variable fire scenarios. In this context, it would be useful to develop new numerical simulations capable of considering not only extreme thermal conditions but also dynamic stresses that could influence the structural response during a fire;

d) *Integration of probabilistic approaches:* Given the wide variability of parameters that influence the behaviour of underground structures in the event of a fire (such as materials, tunnel geometry, ventilation, fire type, and intensity), it might be beneficial to integrate probabilistic approaches into the proposed models. Such approaches would allow for a more accurate estimation of the likelihood of severe structural damage or collapse, providing a more comprehensive framework for risk management;

e) *Applicability to new types of infrastructure:* In addition to the underground structure examined, related to particle physics research, the methodology could be adapted and validated for other types of infrastructures, such as railway and road tunnels. These contexts present unique challenges in terms of fire risk, and customizing the methodology could allow for a more accurate assessment of structural behaviour in complex scenarios;

In conclusion, while the methodology proposed in this thesis can be considered of general relevance and applicable to various contexts, exploring new research directions, such as those mentioned above, will allow for broader dissemination and applicability.

Chapter 6

# Conclusions and future developments

Underground infrastructures, such as tunnels, are becoming increasingly important in modern society due to their utility in overcoming significant physical obstacles and technological advancements in their construction. The mechanization of excavation and modern lining construction techniques has made their construction more efficient, optimizing both time and costs. Consequently, the safety of these structures is an absolute priority, particularly regarding their behaviour in exceptional situations such as seismic events, explosions, and fires. Among the events that can damage underground structures and compromise their functionality, fire is the most frequent. During a fire, ensuring the fire resistance of tunnel linings is essential to allow evacuation of occupants, the intervention of rescue teams, and the future functionality of the structure in safety. The aim of this thesis is to improve the scientific research on the fire resistance of underground structure linings, addressing some of the regulatory gaps. The thesis io organised in four phases, and the main conclusions are described as follows.

The first phase of this work consisted in the analysis of the state of the art regarding two crucial aspects of structural fire safety: fire modelling and the thermomechanical behaviour of linings. These aspects were examined in both the prescriptive and performance-based approaches. It was possible to study from the scientific literature the developments of the last 50 years concerning the identification of nominal fire curves for studying fire safety in tunnels, such as the hydrocarbon (HCM) standard curve, the RWS

curve or the RABT curve. All these curves derive from experimental data and are applicable for evaluating the fire resistance of underground structures. On the other hand, the main natural fire models present in the scientific literature were also studied. Starting from the simplest natural fire models, such as parametric fire models, more advanced models like CFD modelling, widely used for the fire safety of structures and underground infrastructures, were addressed.

Another aspect of central relevance studied in the scientific literature is the modelling of the thermomechanical behaviour of structures exposed to fire. This is influenced by factors such as the thermal properties of materials, the thermal degradation of their mechanical properties, structural schemes, relative stiffness, load variations, and fire exposure. Significant progress has been made in evaluating fire resistance in buildings both in the scientific literature and in national and international standards such as the Eurocode. To comprehensively assess the structural fire safety of these structures, various modelling approaches can be adopted, ranging from simple methods using tabulated data to more sophisticated methods involving both thermal and mechanical modelling using the Finite Element Method (FEM). Advanced thermomechanical analyses allow the evaluation of structural response under fire conditions, considering the variation of material properties, thermal deformations, and even the effects of concrete spalling. Therefore, advanced analyses are an important and fundamental tool for studying the fire behaviour of underground structures. However, it is noted that greater effort is needed for underground structures due to their high weakness to fires, caused by the high confinement of underground environments. From various analyses of the consequences of real fires in tunnels documented in the literature, different types of damage to linings have emerged. In underground structures subject to fire, the main structural damages observed include widespread cracks in reinforced concrete, large areas subject to the separation of concrete layers (known as spalling), softening of steel reinforcement in structural elements, and, in some cases, even partial collapse of the reinforced concrete lining.

In the first phase, it emerged that regarding fire modelling, significant results are present in the scientific literature for both nominal and natural fires, useful for simulating fires in tunnels. CFD fire models are among the most suitable and allow detailed simulation of fire development through the propagation of flames and hot smoke. However, concerning the evaluation of the thermomechanical behaviour of reinforced concrete tunnel linings, some gaps are present in the scientific literature and regulations, as reported before. Among these, the main ones are the absence of codified performance levels for tunnels under fire conditions and the limited understanding of the effects of fire on linings, such as the spalling phenomenon, and their modelling. Based on these gaps, in the subsequent phases of this work, a method was proposed to define the performance levels of tunnel linings subjected to fire and a probabilistic method to evaluate the effects of spalling in the structural fire analyses, both within a performance-based approach.

The second phase of the work deals with the evaluation of the performance levels of the reinforced concrete linings of underground structures. To define these performance levels, it was necessary to evaluate the damage states. In this phase, it emerged that, depending on the severity of the fire affecting the tunnels, different damage configurations can occur. In fact, in the literature, there are several studies of tunnel post-fire damage, from which it emerged that both minor damages, such as localized and superficial cracks and spalling, and significant damages such as wide and deep cracks, extensive spalling, and collapse of the lining can be observed. These findings led to the definition of 5 different damage states, ranging from no damage (ds0) to collapse (ds4), which were quantified using capacity models, for reinforced concrete structures in fire, already known in the literature and standards. Once the quantification of the damage states was identified, it was then possible to define the performance levels to which these are correlated. Since it is one of the most common phenomena observed post-fire in tunnels, it was essential to introduce several spalling depth thresholds, emphasizing the need of introducing it in the calculations.

To estimate the occurrence or not of shallow and localized cracking, it was necessary to introduce limit thresholds of internal forces based on the tensile strength of concrete and the yielding strength of steel. Then, to evaluate cases where partial or total collapses are recorded, it was necessary to introduce limit thresholds of internal forces, based on the ultimate resistance of reinforced concrete sections, and collapse configuration criteria. The definition and quantification of damage states and related performance levels can allow a systematic approach to the fire resistance design of underground structures, crucial to ensuring safety and functionality during fire events.

The third phase of the work focuses on the study of the spalling phenomenon, given its significant relevance. First, the main parameters influencing the evolution of the phenomenon were studied from the literature, such as the input fire curve, the mechanical and physical properties of concrete, the geometry of the structure, the water content of the concrete, and the field of internal stresses. Subsequently, an extensive literature review was conducted to identify the models developed to simulate the phenomenon, showing the existence of two families of models, macroscopic and microscopic, based on two theories, the theory of stress due to restrained thermal deformation and the theory of stress due to increased pore vapor pressure. The main difference between the two families of models is the scale of observation and modelling of the phenomenon. For structural safety assessment purposes, it is evident that macroscopic models provide faster and more applicable tools to evaluate the depth of the section affected by spalling and the related exposure time. However, few models can achieve this goal, considering most of the involved parameters and the associated degree of uncertainty. Among the various models examined, the one considered most complete (Coupled buckling instability and crack failure spalling analytical model), in terms of parameters used, was studied. To test the studied model, the results of an extensive experimental testing campaign, present in scientific literature, were derived, collecting information on the fires used (ISO 834 and HC), the geometry of the elements, the thermomechanical properties of the materials, the

times, and the spalling depths detected. Applying the model to all the considered samples and comparing the results with the experimental ones, a high discrepancy between them emerged in terms of spalling depth and time. For some samples subjected to the HC fire curve, neither the spalling depth nor the thickness was captured. Based on the defects identified from the model application, a theoretical modification was formulated, leading to a more satisfactory comparison of the results with respect to the previous one, capturing the phenomenon in all cases. However, the extent of the concrete thickness involved in the spalling phenomenon and the time estimated by the modified model are still in disagreement with the experimental evidence.

For this reason, starting from the analytical buckling and cracking relations underlying the model, a new spalling model was proposed. The proposed model is based on the variation of the logical application flow of the underlying relations, the introduction of correlations between the characterizing parameters of the samples, and the optimization of variables throughout the development of a Python code. In particular, the model performs thermal analyses on the structural section (using the SAFIR software) and, by solving the instability and cracking relations underlying the phenomenon, provides the spalling depth, initiation spalling time, and duration of phenomenon for each case study. Applying the model to the samples for which experimental results are available, it shows how the new calculated magnitudes are in greater agreement with the experimental ones, showing a significantly lower bias. However, the presence of randomness in the individual parameters involved still leads to results not perfectly matching the experimental data.

To improve the proposed spalling model and address the uncertainties present in it and in the parameters used, a probabilistic corrective model for deterministic results was developed. This corrective model is based on established theories and general models present in the literature and is calibrated with the experimental results studied and derived in this work. The benchmark between the results of the probabilistically corrected proposed model and the experimental results showed that the model provides results for

spalling depth and time strongly in agreement with the experimental results for both ISO 834 and HC curve samples. The analysis also shows that exposure to the ISO 834 fire curve results in spalling characterized by longer occurrence times and greater depths compared to exposure to the HC fire curve, in accordance with experimental observations. Furthermore, by using a probabilistic spalling model, it was possible to implement a reliability-based approach, defined as FORM, and to obtain fragility curves that allow for assessing the probability of a certain spalling thickness as a function of exposure time to a specific fire curve for a specific structural element. These curves, using probability distributions of the values of the main parameters involved in the spalling phenomenon, enable the evaluation of possible spalling depths as a function of exposure time in a fully probabilistic approach.

The fragility curves in terms of spalling can be a valuable tool for quickly estimating the probability of spalling in existing and new underground structures, guiding design choices, and assessing the potential need for further investigations and analyses. The proposed spalling model thus progresses from a semi-probabilistic to a fully probabilistic model, allowing for the consideration of significant uncertainties related to the spalling phenomenon.

The fourth phase of the thesis describes the application of the proposed methodologies to evaluate damage states, performance levels, and the consequences of spalling phenomena in a particular case study. The application was made to a unique underground structure used for different purposes than common railway and road tunnels. It is a cavern dedicated to nuclear physics studies, housing the ATLAS particle detector, part of CERN, located in Geneva, Switzerland. The representation begins with the study conducted by the Fire Safety Engineering group of the Occupational Health & Safety and Environmental Protection section of the CERN, which involved identifying fire scenarios and deriving natural fire curves based on CFD fire models constructed using FDS software. Knowing the design fires, it was possible to proceed with the thermo-mechanical evaluation of

the cavern by constructing an advanced three-dimensional finite element model composed exclusively of shell elements, with boundary conditions based on the as-built conditions, using the SAFIR software. Once the model was created, thermal analyses were performed on the structural sections in a decoupled manner, differentiating them based on significant changes in fire exposure. The results of thermal analyses conducted on sections exposed to natural fire curves showed that the temperature in the reinforcement bars barely exceeds 100 °C. Therefore, it was possible to determine from the thermal analysis that no collapse occurs as natural fires of modest intensity did not lead to reduction of the structural resistance of the lining. However, given the high degree of redundancy of the studied cavern, the effects of constrained thermal expansions and thermal distortions are not negligible. Therefore, considering the temperature profiles in the structural elements, an advanced mechanical analysis was conducted for each selected natural fire scenario. These analyses confirmed the absence of collapse during the natural fires exposure and allowed understanding of the evolution of stress properties within the cavern's reinforced concrete lining. Following the advanced thermo-mechanical analyses, knowing the temperature and internal forces development during the fire, it was possible to apply the proposed methodology for performance level assessment. This application confirmed that the structure remains untouched and fully functional even after exposure to the identified natural fire scenarios, ensuring a performance level V. This performance level corresponds to “Fire resistance requirements ensuring, at the end of the fire, the maintenance of full operational functionality of the underground space without any type of damage.”

However, to further investigate the thermo-mechanical behaviour of the cavern, an advanced thermo-mechanical analysis using the ISO 834 fire curve was also conducted. This analysis revealed a high probability of spalling throughout the thickness of the concrete cover due to the high temperatures and heating rates of the sections exposed to the fire. Considering this, a mechanical analysis was performed with reduced sections from

the spalling depth, which showed a significant reduction in resistance and considerable increases in internal forces. The resistance reduction is evaluated through the benchmark of reduced M-N resistance domains at different fire exposure minutes. Analysis of these domains reveals that the reduction in resistance of individual structural walls, due to spalling and temperature increases, reaches up to about 50% of the cold resistance. The significant reduction is justified by the fact that, due to spalling and the severity of the ISO 834 curve, the reinforcement steel temperature exceeds 400 °C (the limit after which resistance erosion begins). However, for a thermo-mechanical analysis conducted for a 2-hour exposure to the ISO 834 curve, the structure did not show any collapse. Additionally, analysing the structure subjected to the ISO 834 curve, it was also possible to apply the reliability approach in terms of spalling. The application led to the construction of several fragility curves varying with possible spalling thickness. Each fragility curve describes the variation of the probability of a defined spalling thickness as a function of the fire exposure time described by the ISO curve.

In conclusion, potential future developments to improve the approach proposed in this thesis are possible and the main ones are listed below.

The methodology developed for calculating damage states and performance levels allows for defining, through assignment criteria, the fire resistance verification of tunnel linings with various uses. The proposed methodology has been successfully applied to a unique underground structure. However, to better assess the use of the approach, it could be applied to other underground infrastructures already subjected to fires. Reconstructing past fires and their effects using the models studied in this work provides the expected damage state and performance level. These evaluations can then be compared with directly observed damage described in post-fire investigation reports. This would allow evaluating the reliability of the provided approach and making any necessary improvements.

The proposed deterministic spalling model has been calibrated and studied based on experimental tests conducted on reinforced concrete slab samples subjected to ISO 834 and HC curves. To extend its reliability to natural fire curves with varying heating rates and temperatures, future work could involve collecting experimental data conducted with natural curves. These data are useful for studying potential correlations between parameters (e.g., fire curve, heating rate, water content, material resistance, and external stresses) and for testing any potential limits of model applicability.

Furthermore, analysing samples subjected to natural fire curves with variable temperatures and heating rates could provide a richer and more varied data set to calibrate a new version of the proposed probabilistic spalling model, extending the limits of applicability. Given the increasingly frequent use of fiber-reinforced concretes for tunnel lining construction and the benefits in terms of limiting spalling shown in the literature, the proposed spalling model could be improved in this regard. In particular, the possibility of applying it to reinforced fiber-reinforced concrete structures could be studied by introducing various parameters that account for the type and quantity of fibers, through comparisons with experimental results.

This work can represent a step forward in the study of fire vulnerability in underground environments characterized by reinforced concrete linings. In particular, cross-sectional studies could be undertaken involving industrial entities to evaluate the fire behaviour and damage probability of underground infrastructures used for specific purposes, such as petrochemical industries. Like what was done in the case study presented in this work, using the same approach, it could be possible to estimate the fire vulnerability of structures used for industrial purposes, guiding the choice of interventions aimed at mitigating risks.

# Bibliography

[1] T. E. P. A. T. C. O. T. E. UNION, *DIRECTIVE 2004/54/EC OF THE EUROPEAN PARLIAMENT AND OF THE COUNCIL of 29 April 2004,* 2004.

[2] C. R. (. N. 1303/2014, *concerning the technical specification for interoperability relating to 'safety in railway tunnels' of the rail system of the European Union,* 2014.

[3] E. C. f. Standardization, *Eurocode 2: Design of concrete structures - Part 1-2: General rules - Structural fire design,* European Committee for Standardization, 2008.

[4] A. Sirico, P. Bernardi, R. Cerioni and M. E., "Evaluation of the response of concrete tunnel linings subjected to fire: a three-dimensional approach," in *1° fib Italy YMG Symposium on Concrete and Concrete Structures* , Parma, 2019.

[5] N. Hua, N. Elhami Khorasani and A. Tessari, "Numerical modeling of the fire behavior of reinforced concrete tunnel slabs during heating and cooling," *Engineering Structures,* no. 258, p. 15, 2022.

[6] H. INGASON, "State of the Art of Tunnel Fire Research," *Fire Safety Science,* vol. 9, pp. 33-48, 2009.

[7] W.-K. Chow, H. Ingason, Y. Z. Li, L. Hu and F. Tang, "Fire Safety for Tunnels and Underground Space," *Tunnelling and Underground Space Technology,* 2

Novembre 2022.

[8] *EN 1991-1-2 (2002)-Eurocode 1: Actions on structures - Part 1-2:General actions - Actions on structures exposed to fire,* Brussels, Belgium: CEN, European Committee for Standardization, 2002.

[9] Technical Committee ISO / TC 92 / SC 2, *ISO 834-1:1999 - Fire-resistance tests,* Technical Committee ISO / TC 92 / SC 2, 1999.

[10] N. Taillefer, P. Carlotti, C. Larive, C. Lemerle, R. Avenel and P. Pimienta, "Ten Years of Increased Hydrocarbon Temperature Curves in French Tunnels," 2013.

[11] *Technical fire prevention standards,* Italy: Ministry of the Interior, 2015.

[12] J. Zehfuss and D. Hosser, "A parametric natural fire model for the structural fire design of multi-storey buildings," *Fire Safety Journal,* no. 42, p. 115–126, 2007.

[13] A. PCHELINTSEV, Y. HASEMI, W. TAKASHI and Y. YOKOBAYASHI, "Experimental And Numerical Study On The Behaviour Of A Steel Beam Under Ceiling Exposed To A Localized Fire," *FIRE SAFETY SCIENCE-PROCEEDINGS OF THE FIFTH INTERNATIONAL SYMPOSIUM,* no. 5, pp. 1153-1 164, 1997.

[14] N. Tondini, C. Thauvoye, F. Hanus and O. Vassart, "Development of an analytical model to predict the radiative heat flux to a vertical element due to a localised fire," *Fire Safety Journal,* 2019.

[15] X. Yan and T. Gernay, "Numerical modeling of localized fire exposures on structures using FDS-FEM and simple models," *Engineering Structures,* no. 246,

2024.

[16] B. Waldeck, A Comparison Between FDS and the Multi-Zone Fire Model regarding gas temperatures and visibility in enclosure fires, LTH | LUNDS UNIVERSITET , 2020.

[17] K. Suzuki, K. Harada and T. Tanaka, “A Multi-layer Zone Model For Predicting Fire Behavior In A Single Room,” in *Fire Safety Science 7*, 2003.

[18] K. Suzuki, T. Tanaka, K. Harada and H. Yoshida, “An application of A Multi-layer Zone Model to A Tunnel fire,” in *Fire Safety Science, 6*, 2004.

[19] B. Karlsson and L. Quintiere, “ Application of Nonlinear Dynamics in Studying Flashover Fire in a Small Open Kitchen,” *Enclosure Fire Dynamics,* 2000.

[20] W. Jones, R. Peacock, G. Forney and P. Reneke, *Consolidated Model of Fire Growth and Smoke Transport (Version 6). Technical Reference Guide.,* National Institute of Standards and Technology, 2009.

[21] J.-F. Cadorin and F. J-M, “A tool to design steel elements submitted to compartment fires—OZone V2. Part 1: pre- and post-flashover compartment fire model,” *Fire Safety Journal,* vol. 38, no. 5, pp. 395-427, 2003.

[22] J. Vonneumann and D. R. Richtmyer, “A Method for the Numerical Calculation of Hydrodynamic Shocks,” *Istitute for Advanced Study, princeton, New Jersey - J. Appl. Phys.,* 1950.

[23] F. Harlow and J. Welch, Numerical Calculation of Time-Dependent Viscous

Incompressible Flow of Fluid with Free Surface, The Physics of Fluids, 1965.

[24] Author:, “Fromm, J. E.,” *Numerical method for computing nonlinear, time dependent, buoyant circulation of air in rooms,* vol. 15, no. 3, p. 186–196, 1971.

[25] F. D. S. T. R. G. -. V. 1. M. Model, *McGrattan, Kevin; Hostikka, Simo; Floyd, Jason; McDermott, Randall; Vanella, Marcos; Mueller, Eric,* National Institute of Standards and Technology, 2013.

[26] E. C. F. STANDARDIZATION, *Eurocode 2: Design of concrete structures - Part 1-1: General rules and rules for buildings,* Brussels: BRITISH STANDARD, 2004.

[27] E. C. f. Standardization, *EN 1993-1-2: Eurocode 3: Design of steel structures - Part 1-2: General rules - Structural fire design,* The European Union, 2005.

[28] B. Bresler, R. H. Iding and Z. Nizamuddin, *FIRES-T3 : a computer program for the FIre REsponse of Structures - Thermal Three-dimensional version,* California, 1996.

[29] J. M. Franssen and T. Gernay, “Modeling structures in fire with SAFIR®: Theoretical background and capabilities,” *Journal of Structural Fire Engineering,* 2017.

[30] U. Wickström, *TASEF-2 : A Computer Program for Temperature Analysis of Structures Exposed to Fire,* Lund Institute of Technology, 1979.

[31] S. Melchior, D. Xavier, J. Balša, C. Ranjit Kumar and R. Van Coile, “FIERCE: A COST BENEFIT ANALYSIS FOR TUNNEL FIRE SAFETY,” in *11th*

*International Conference 'Tunnel Safety and Ventilation'*, Graz, 2022.

[32] D. de Silva, M. Andreini, A. Bilotta, S. La Mendola and E. Nigro, "Definition of damage states for concrete tunnel linings subjected to fire action," in *International Fire Safety Symposium IFireSS 2019*, Napoli, 2019.

[33] D. de Silva, M. Andreini, A. Bilotta, G. De Rosa, S. La Mendola, E. Nigro and O. Rios, "Structural safety assessment of concrete tunnel lining subjected to fire," *Fire Safety Journal,* vol. 134, no. 103697, 2022.

[34] C. J. Raymond, *The spalling of concrete in fires - PhD Dissertation thesis,* Birmingham: Ashton University, United Kingdom, 1995.

[35] Barret, "French and other methods of constructing iron floors," *Civil Engineering and Architect's Journal,* vol. XVII, p. 94, 1854.

[36] D. Pardon, P. Pimienta, B.-L. Marie-Jeanne, S. Hameury, N. Pinoteau, B. Moreau, L. D'aloia Schwartzentruber, C. Larive, P. Peyrac and X. Thollard, "In situ concrete spalling risk assessment in tunnel by means of a mobile oil-fired furnace," in *Proceedings of the 6th International Workshop on Concrete Spalling due to Fire Exposure*, Sheffield, United Kingdom, UK, 2019.

[37] M. Guerrieri, S. Fragomeni, C. Sanabria, W. Ming Lee and P. Esteban, "Australian large scale structural fire test facility for concrete tunnel linings," in *Proceedings of the 6th International Workshop on Concrete Spalling due to Fire Exposure*, Sheffield, UK, 2019.

[38] O. Lalu and T. Lennon, "Experimental Investigations into the Spalling of High

Strength Concrete and the Fire Performance of Tunnel Linings," in *6th International Workshop on Concrete Spalling due to Fire Exposure*, Sheffield, UK, 2019.

[39] A. Klimek, S. Hothan and A. Rogge, "Investigation of size effects in concrete spalling," in *Proceedings of the 6th International Workshop on Concrete Spalling due to Fire Exposure*, Sheffield, UK, 2019.

[40] G. A. Khoury, "Effect of fire on concrete and concrete structures," in *Progress in structural engineering and materials*, New York, 2000.

[41] "Fire design of concrete structures – materials, structures and modeling state of art report," Féédéération international du bééton (Bulletin d'information, 38), Lausanne, 2007.

[42] M. Hedayati, M. Sofi, P. A. Mendis and T. Ngo, "A Comprehensive Review of Spalling and Fire Performance of Concrete Members," *Electronic Journal of Structural Engineering,* vol. 15, pp. 8-34, 2015.

[43] L. T. Phan, T. P. Mcallister, J. L. Gross and M. J. Hurley, "NIST Technical Note 1681: Best practice guidelines for structural fire resistance design of concrete and steel buildings," National Institute of Standards and Technology, USA, 2010.

[44] W. Z. Zheng, X. M. Houn, D. S. Shi and M. X. Xu, "Experimental study on concrete spalling in prestressed slabs subjected to fire," *Fire Safety Journal,* vol. 45, p. 283–297, 2010.

[45] N. Taillefer, P. Pimienta and D. Dhima, "Spalling of concrete: A synthesis of

experimental tests on slabs," in *MATEC Web of Conferences*, Marne la Vallée, France, 2013.

[46] C. Maluk, J. Tignard, A. Ridout, T. Clarke and R. Winterberg, "Experimental study on the fire behaviour of fibre reinforced concrete used in tunnel applications," *Fire Safety Journal,* vol. 120, no. 103173, 2021.

[47] L. Boström and R. Jansson, "Self-Compacting Concrete Exposed to Fire," SP Report, Boras, 2008.

[48] L. Fangxia, *Doctoral Thesis: On the prediction of concrete,* Zurich: ETH Library, 2015.

[49] V. Kodur and S. Banerji, "Modeling the fire-induced spalling in concrete structures incorporating hydro-thermo-mechanical stresses," *Cement and Concrete Composites,* no. 117, 2021.

[50] N. Hua, A. Tessari and N. E. Khorasani, "Characterizing damage to a concrete liner during a tunnel fire," *Tunnelling and Underground Space Technology,* vol. 109, no. 103761, 2021.

[51] L. Boström and R. J. McNamee, "Proceedings of the 5th International Workshop on Concrete Spalling due to Fire Exposure," in *RISE Research Institutes of Sweden*, Borås, 2017.

[52] I. Burgess and S. S. Huang, "Proceedings of the 6th International Workshop on Concrete Spalling due to Fire Exposure," in *The University of Sheffield*, Sheffield, United Kingdom, 2019.

[53] M. De Poli, C. B. M. Blom and B. B. G. Lottman, "Concrete spalling failure: a coupled buckling instability and crack failure analytical model," in *Proceedings of the 6th International Workshop on Concrete Spalling due to Fire Exposure*, Sheffield, United Kingdom, 2019.

[54] A. Akhtaruzzaman and P. Sullivan, "Explosive spalling of concrete exposed to high temperature - Concrete Structures Research Report," Imperial College, Great Britain, 1970.

[55] W. 4, *Fire effects and tunnel performance system structural response M43 - Damage to concrete in tunnels after fire exposure - Evaluation report,* UPTUN, 2008.

[56] J.-M. Franssen and T. Gernay, *USER'S MANUAL FOR SAFIR (version 2022) A COMPUTER PROGRAM FOR ANALYSIS OF STRUCTURES SUBJECTED TO FIRE,* Liege, Belgium: University of Liegi, 2022.

[57] B. Lottman, *The spalling mechanism of fire exposed concrete - Doctoral Dissertation,* Rotterdam: Delft University of Technology, 2017.

[58] P. Gardoni, A. Der Kiureghian and K. M. Mosalam, "Probabilistic Capacity Models and Fragility Estimates for Reinforced Concrete Columns based on Experimental Observations," *J. Eng. Mech,* vol. 128, p. 15, 2002.

[59] A. M, G. P, P. S and S. M, "Probabilistic Models for Erosion Parameters and Reliability Analysis of Earth Dams and Levees," Vols. . ASCE-ASME J. Risk Uncertain. Eng. Syst. Part A Civ. Eng. 2. , no. https://doi.org/10.1061/AJRUA6.0000878., 2016.

[60] Y. Zhenlin, “A modified family of power transformations,” *Economics Letters,* vol. 92, no. 1, pp. 14-19, 2006.

[61] B. G.E.P. and C. D.R., “An analysis of transformations,” *J. R. Stat. Soc. Ser.,* vol. 26, p. 211–252, 1964.

[62] R. C. Radhakrishna and T. Helge, Linear Models: Least Squares and Alternatives, Second Edition, New York: Springer , 1999.

[63] R. F. S. G., “A Method of Maximum-likelihood Estimation,” *Journal of the Royal Statistical Society: Series B (Methodological),* vol. 23, no. 2, p. 469–475, 1961.

[64] B. George E.P. and T. George C., Bayesian Inference in Statistical Analysis, New York: Wiley, 1992.

[65] P. Darko, V. H. Patrick, M. Dan, M. Vilhelm, G. Louise, P. Joakim, R. Oriol and L. M. Saverio, “Identification and characterization of design fires and particle emissions to be used in performance-based fire design of nuclear facilities,” *fire and materials,* vol. 45, no. 8, pp. 1008-1024, 2020.

[66] E. C. f. Standardization, *Eurocode 2: Design of concrete structures - Part 1-1: General rules and rules for buildings,* Europe, 2008.

[67] N. Johansson, E. Ronchi, R. Scozzari and M. Fronterrè, “The use of multi-zone modelling for tunnel fires,” *Tunnelling and Undeground Space Technology,* vol. 134, no. 104996, 2023.

[68] CrossrailLtd, “Crossrail Project - youtube channel,” Crossrail Project, 2013.

[Online]. Available: https://www.youtube.com/watch?v=z38JIqGDZVU.

[69] I. F. Academy, “Tunnel fires from 2012 to 2023: Statistics from media reports,” International Fire Academy , 2024. [Online]. Available: https://www.ifa-swiss.ch/en/magazine/detail/tunnel-fires-from-2012-to-2023-statistics-from-media-reports.